DEVELOPING A CAPILLARY ZONE ELECTROPHORESIS PLATFORM WITH TANDEM MASS SPECTROMETRY FOR ANALYSIS OF SULFATED GLYCOSAMINOGLYCAN CARBOHYDRATES

by

MORGAN STICKNEY

(Under the Direction of I. Jonathan Amster)

ABSTRACT

Glycosaminoglycans (GAGs) are long linear polysaccharides with a repeating uronic acid sugar and amino sugar disaccharide backbone that can be heavily modified. These modifications make GAGs highly negatively charged and contribute to GAGs being a major player in many important biological processes. Intact GAGs are typically too long and complex to analyze with mass spectrometry (MS) and completely digested GAG disaccharides provide valuable statistical data but are too short to retain binding motifs. Partially digested GAG chains are the best way to characterize structural modifications that make up binding motifs, but partial digestion often presents samples that are highly complex and full of isomers. Online separation paired with MS is the best way to simplify complex biological GAG samples for tandem MS analysis. Capillary zone electrophoresis separations are designed for highly charged samples like GAGs and separate samples based on their charge to size ratio. Negative electron transfer dissociation is a fast electron-based ion activation technique that works well within online separation time limitations and enables fragmentation and characterization of GAGs without loss of informative sulfo-modifications. A CZE-MS platform and method optimized for GAG separations and

analysis would be a powerful tool for biological research that could enhance our understanding of disease and biological operations.

INDEX WORDS: Sulfated glycosaminoglycan, carbohydrate, orbitrap mass spectrometry, negative electron transfer dissociation, capillary zone electrophoresis

DEVELOPING A CAPILLARY ZONE ELECTROPHORESIS PLATFORM WITH TANDEM MASS SPECTROMETRY FOR ANALYSIS OF SULFATED GLYCOSAMINOGLYCAN CARBOHYDRATES

by

MORGAN STICKNEY

B.S., The University of California in Santa Cruz, 2013

A Dissertation Submitted to the Graduate Faculty of the University of Georgia in Partial Fulfillment of the Requirements for the Degree

DOCTOR OF PHILOSOPHY

ATHENS, GEORGIA

2020

DEVELOPING A CAPILLARY ZONE ELECTROPHORESIS PLATFORM WITH TANDEM MASS SPECTROMETRY FOR ANALYSIS OF SULFATED GLYCOSAMINOGLYCAN CARBOHYDRATES

by

MORGAN STICKNEY

Major Professor: I. Jonathan Amster

Committee: Jeffrey Urbauer
Joshua Sharp

Electronic Version Approved:

Ron Walcott
Interim Dean of the Graduate School
The University of Georgia
May 2020

DEDICATION

For my family. Without you I would not be here.

ACKNOWLEDGEMENTS

I did not do this on my own. Jon Amster taught me all about glycosaminoglycans and was my guide. Patience Sanderson and I learned capillary zone electrophoresis-mass spectrometry together. Jiana Duan wrote the software I used for my work and was a good friend. Franklin Leach helped get NETD up and running on our orbitrap and he was an excellent source of knowledge. Robert J. Linhardt is one of the driving forces behind this research into GAGs. James Xia commercialized the excellent CZE-MS interface we utilized for our research and was always suggesting new experiments. Dennis Philips in the proteomics and mass spectrometry facility lent us his materials, his problem-solving skills, and his sense of humor.

TABLE OF CONTENTS

Page

LIST OF TABLES

LIST OF FIGURES

CHAPTER 1

INTRODUCTION AND LITERATURE REVIEW

1.1 INTRODUCTION TO GLYCOSAMINOGLYCANS

The work presented in this dissertation establishes a platform for online separation of sulfated glycosaminoglycan carbohydrates. Glycosaminoglycans (GAGs) are carbohydrates abundant in most eukaryotes and are involved in many biological processes[1]. GAGs are long linear polysaccharides, up to hundreds of degrees of polymerization, typically attached to a core protein to form a proteoglycan[2]. GAGs are formed by a series of transferase enzymes that extend and modify the carbohydrate chain. GAGs are categorized by repeating disaccharide backbone templates and functionalized by modifications including sulfation, modification of the nitrogen group on the amino sugar, and modification of the stereochemistry of the hexuronic acid[1]. The basic repeating disaccharide backbone is a hexosamine on the reducing end and a uronic acid on the non-reducing end.

Heparin and Heparan sulfate are the most complex variants of the GAG family of polysaccharides. Heparin is produced in connective-tissue type mast cells and has more sulfates per hexosamine than heparan sulfate[3]. HS is produced by most mammalian cells, and located on cell surfaces and in the extracellular matrix[4]. Heparin and heparan sulfate are composed of uronic acid and glucosamine (GlcN) repeating disaccharide subunits[4], and joined by alternating α(1,4) and β(1,4) linkage[1]. The uronic acid of the repeating disaccharide unit can be either L-IdoA or D-GlcA, both of which can be 2-*O* sulfated, however this sulfation pattern is predominantly seen on IdoA (IdoA2S)[3, 5]. The D-(GlcN) can be N-sulfated (GlcNS), N-

acetylated (GlcNAc), or N-hydrated ($GlcNH_2$), all of which can have 6-*O* sulfo-modification, but only the GlcNS can also be 3-*O* sulfated[3, 4, 6-8]. Heparin is a well-known anticoagulant and heparan sulfate is linked to cell growth, angiogenesis, and viral invasion among others[3, 4].

Chondroitin sulfate has a disaccharide backbone composed of N-acetylgalactosamine (GalNAc) and glucuronic acid (GlcA) joined by an alternating β(1,4) and β(1,3) linkage, respectively[1, 6]. Chondroitin sulfate is polymerized into chains hundreds of residues long and is usually composed of hybrid structures containing more than one type of chondroitin disaccharide unit. There are three principal types of chondroitin sulfate, CSA, CSB, also known as dermatan sulfate (DS), and CSC. CSA and CSB are predominantly sulfated at the 4-*O* position of the GalNAc, and CSC has predominantly 6-*O* sulfated GalNAc subunits[1]. Dermatan sulfate (CSB/DS) is composed of repeating disaccharide units containing a GalNAc and an iduronic acid (IdoA) instead of a GlcA residue[1]. GlcA and IdoA differ in C-5 stereochemistry of the carboxyl group. Chondroitin sulfate (CS) is used widely as a medication for osteoarthritis as well as other diseases[9-11]. Dermatan sulfates are the primary GAG in the dermis and are responsible for binding proteins involved in modulation of a broad range of physiological processes[12, 13]. Other patterns of modification, including those with two sulfo-groups per disaccharide, have been reported; CSD has 2-*O* sulfation on the uronic acid and 6-*O* sulfation on the GalNAc, and CSE has 4-*O* and 6-*O* sulfation on the GalNAc[11, 14].

Keratan sulfate has a backbone of N-acetylglucosamine (GlcNAc) and galactose (GalA) joined by an alternating β(1,3) linkage and a β(1,4) linkage respectively. Keratan sulfate has sulfo-modifications at the 6-O position of either monomer and may also be fucosylated. Keratan sulfate has been linked to corneal health as well as cell motility[15].

Hyaluronon has a backbone of N-acetylglucosamine (GlcNAc) and glucuronic acid (GlcA) with a β(1,4) linkage and a β(1,3) linkage respectively. Hyaluronon is the only non-sulfated GAG and has therefore been studied extensively. Hyaluronon is a major component of synovial tissues and has been shown to shield stem cells from growth factor proteins[16, 17].

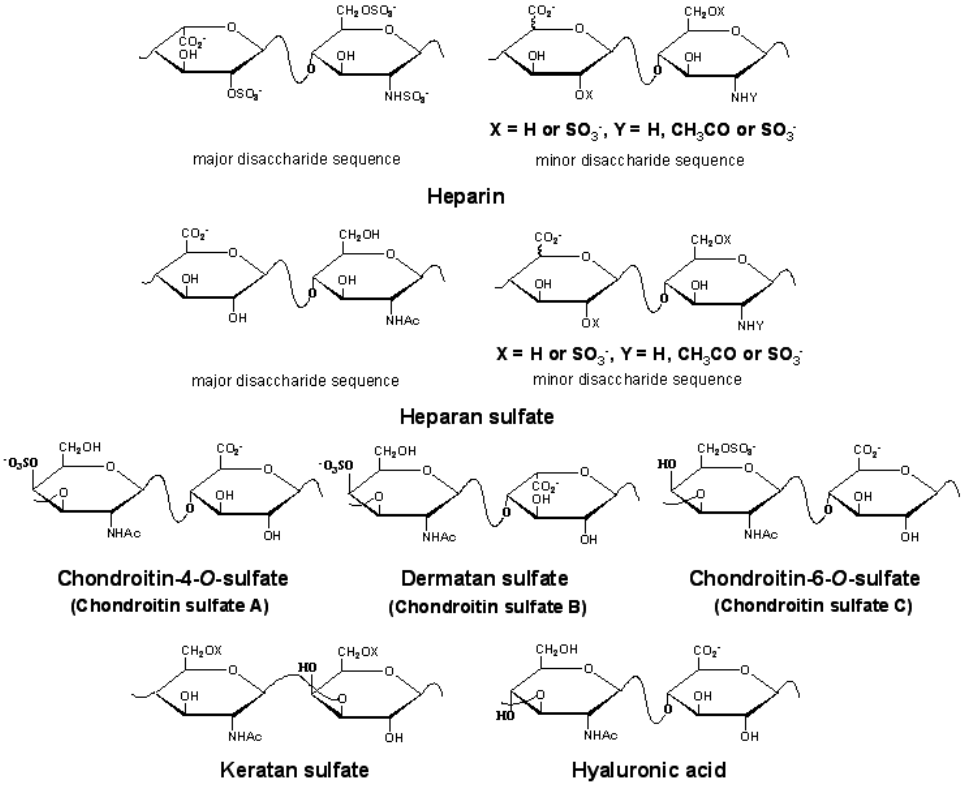

Figure 1.1. A molecular schematic representation of the different GAG classifications including linkages and possible sites of modification.

Modification patterns within GAGs present binding motifs that are specific to proteins and their biological function[8]. This is exemplified by arixtra's role in modulating the antithrombinIII protein which is strongly related to its specific structure, especially the rare 3-O sulfo-modification[7, 18]. This structure-function relationship has increased interest in

characterizing specific GAG structures. However, GAG structural analysis remains a significant analytical challenge[19, 20]. Intact sulfated GAGs are difficult to analyze because they are very large and complex, though the shortest and simplest GAGs, Bikunin and Decorin, have been characterized intact by mass spectrometry[19, 21-23]. The characterization of Bikunin and decorin further cemented that GAGs have conserved modification patterns. Bottom up analysis, where GAGs are completely digested down to their disaccharide constituents offer statistically informative information related to the abundance of each type of modification present but lack full binding motifs as biologically relevant structural motifs are longer than disaccharides, the basic building block of GAGs[24]. Middle out analysis, where GAGs are partially digested down to 4-30 degrees of polymerization, are the best way to keep binding motifs intact but present as complex mixtures that can be difficult to analyze by mass spectrometry. The components of complex mixtures can be isolated and purified offline, but this takes a great deal of time and effort and can still prove inadequate. Furthermore, GAGs are generally only available in small quantities and cannot be overexpressed or amplified like other biopolymers[25].

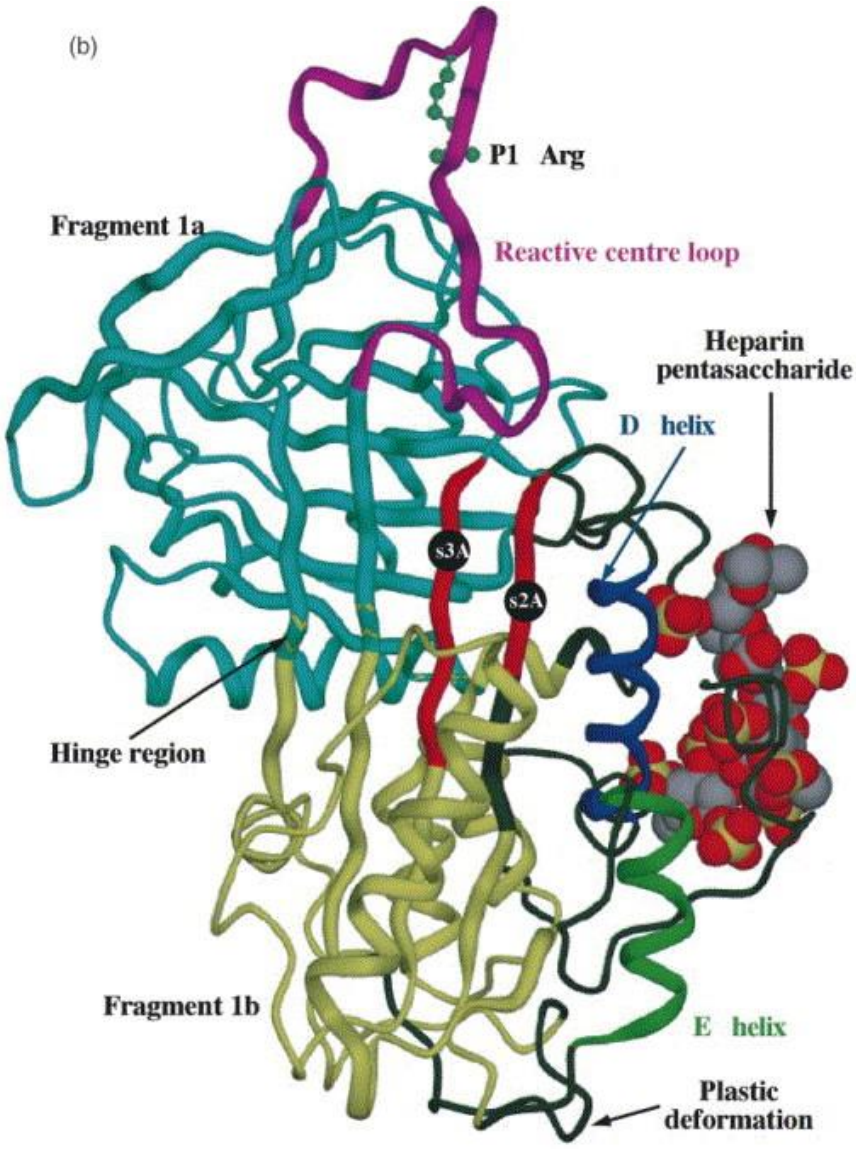

Figure 1.2. Molecular representation of Antithrombin with bound arixtra pentasaccharide.[26]

MS methods have been thoroughly developed for analysis of partially digested GAGs that have been purified and isolated, and bespoke synthetic GAG species. Partially digested GAGs from biological sources present as complex mixtures that are dense and overlapping. Furthermore, many of the developed techniques require expert knowledge in mass spectrometry to perform well. CZE-MS is a platform that can separate and purify the individual components of complex biological GAG mixtures without long and complex purification and isolation techniques.

Methods have been developed to make GAG experiments on the CZE-MS platform easy and widely accessible to the biological sciences at large.

1.2 MASS SPECTROMETRY OF GAGS

FTICR-MS

Mass spectrometry measures the mass to charge (m/z) ratio of gas phase ions. This can be done by scanning through m/z with radio frequencies in a quadrupole mass filter, measuring ion time of flight, or converting ion oscillations using the Fourier transform (FT). Fourier transform is the most accurate way for measuring m/z and is used in Fourier transform ion cyclotron resonance (FTICR) mass spectrometers and orbitrap mass spectrometers.

In FTICR ions are trapped by voltage barriers in an analyzer cell where ions oscillate perpendicular to a uniform magnetic field. The ions oscillate at a velocity based on their m/z value[27, 28]. The charge inherent to the ions produces current on detection plates within the analyzer cell. Current increases on a detection plate as an ion bundle approaches and decreases as an ion bundle moves away, creating a sinusoidal wave. Fourier transform is applied to the sin waves generated this way to transform the time domain sin waves into their constituent frequencies which represent highly accurate m/z values.

Electrostatic Axially Harmonic Orbital Trapping: Orbitrap

The electrostatic axially harmonic orbital trapping mass spectrometer, known as the Orbitrap, was developed by Makarov based on the orbital trapping principle established by

Kingdon[29, 30]. The Mass accuracy and resolving power are comparable to FTICR-MS with low magnetic fields but does not rely on a magnetic field to produce those results. Instead the analyzer is composed of an outer shell electrode and an inner spindle electrode. Ions injected between the electrodes will form rings around the spindle electrode that oscillate back and forth along the spindle with a velocity based on the m/z value. The ring oscillations are measured by the outer electrode as sin waves which are Fourier transformed into accurate m/z values.

The key to an effective orbitrap mass analyzer was the development of the storage device called the C-trap[31-33]. The C-trap is a bent quadrupole that can store ions and cool them down before orthogonally injecting them into the electrostatic fields of the orbitrap analyzer cell.

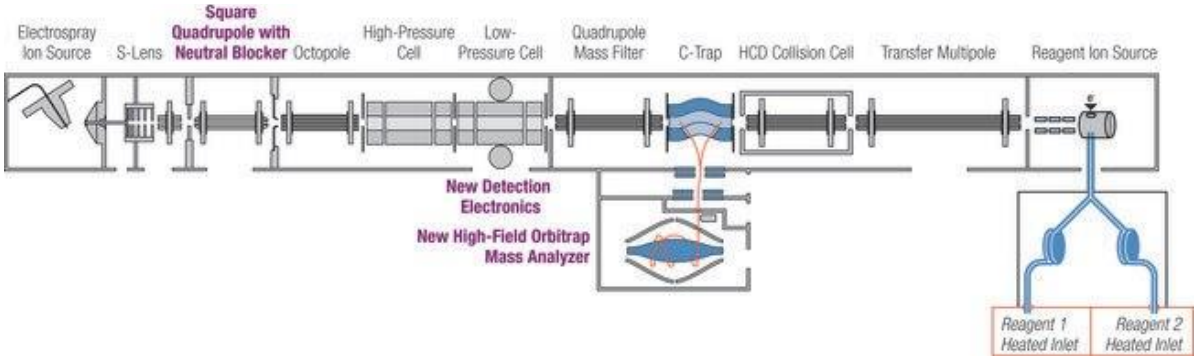

Figure 1.3. A schematic representation of the Orbitrap elite mass spectrometer. Ion trap mass measurements take place in the low-pressure cell at the front of the instrument. Fourier transform measurements take place in the high-field orbitrap mass analyzer in the middle of the schematic. CID takes place in the high-pressure cell near the front and HCD takes place in the HCD collision cell near the back. NETD reagent ions are generated at the reagent ion source at the back and reacted with sample ions in the high-pressure cell before fragments are detected in either the low-pressure cell or the orbitrap mass analyzer.

Structural characterization of GAGs

GAG composition, or more specifically, Polysaccharide length, degree of sulfo-modification, and the number of acetyl groups can be determined by accurate m/z measurements. Therefore, MS analyzers with high resolving power, like FTICR or Orbitrap, are desirable for GAG analysis. However, even high mass accuracy cannot resolve isomeric compounds or determine the exact location of modifications. For complete structural analysis of partially digested GAGs, tandem mass spectrometry fragmentation methods are required.

Domon and Costello developed a nomenclature for the fragments that result from ion activation[34]. B and C fragments are glycosidic cleavages, or cleavages between the sugar rings, that retain information from the non-reducing end of the GAG, while Y and Z fragments are glycosidic cleavages that retain information from the reducing end. B and Y fragments, and C and Z fragments are complimentary; when combined the molecule is made whole again. From glycosidic cleavages the location of a modification can be narrowed down to a sugar ring, but the specific location of the modification cannot be determined. A and X fragments are cross-ring cleavages that retain information from the non-reducing end and the reducing end respectively.

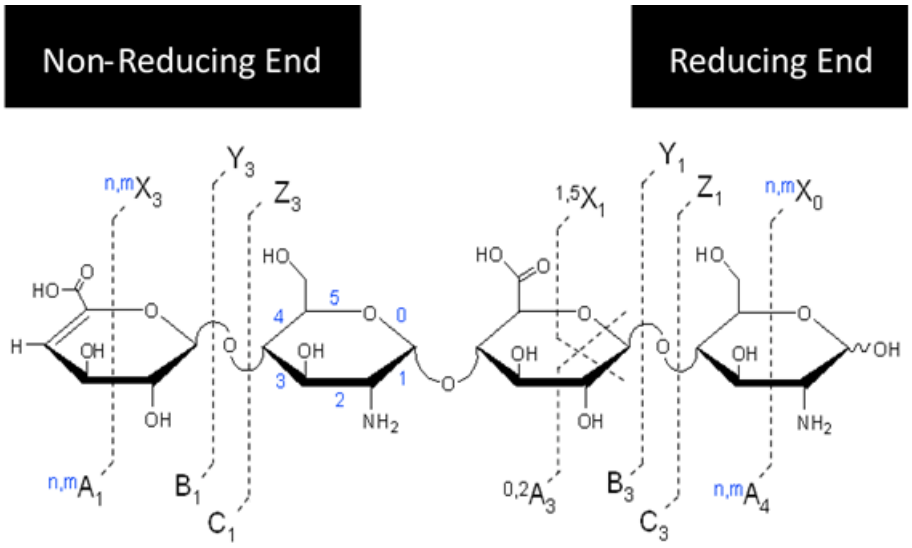

Figure 1.4. A representation of the fragmentation types possible for GAGs. B and C ions represent glycosidic fragments that retain information on the non-reducing end and Y and Z ions represent glycosidic fragments that retain information on the reducing end. A and X fragments are cross-ring fragments that retain information on the non-reducing end and the reducing end respectively. The "n" represents the first carbon bond that a cross-ring fragment breaks and the "m" represents the second.[34]

Electrospray Ionization

Mass spectrometry requires charged particles or ions to produce a reading which can be measured. Originally mass spectrometers used chemical ionization (CI) which produced singly charged ions and was of limited use. In 1989 John Fenn coupled electrospray ionization (ESI) to mass spectrometry to analyze large biomolecules[35]. ESI was later adapted for minute solvent flow rates called nanoelectrospray ionization (nESI) by Matthias Wilm[36]. The advent of ESI saw

the generation of multiply charged ions which quickly lead to ESI as the standard and to increased interest in mass spectrometry.

ESI generates a fine mist of charged particles by passing solution through a strong electric field[37, 38]. A voltage difference between the ESI source and the mass spectrometer inlet pulls and charges the sample molecules. The solvent rapidly evaporates due to heat and dry gas causing a buildup of charge on the sample molecules. ESI is a soft ionization method that can produce multiply charged molecules and keep fragile molecules intact. These features quickly enshrined ESI as the standard method of ionization and to increased interest in mass spectrometry. High charge states produced by ESI are better for both threshold fragmentation and electron-based fragmentation methods[39]. GAGs that are closer to being fully ionized are more stable under threshold activation and more easily fully ionized with Na-H exchange. GAGs with higher charge states have more active sites available for reaction with electrons or reagent ions making electron-based activation methods more efficient.

One of the greatest disadvantages of ESI is ion suppression of the most polar components of a mixture. This disadvantage can be overcome by integrating an online separation technique. ESI is performed under atmospheric conditions and can easily interface with separation techniques like LC, CE, or IM. Salts and detergents ionize much more favorably than most biological molecules and severely reduce sensitivity. Salts and detergents must be removed prior to experimentation or from preparation entirely.

GAGs present as highly anionic molecules due to the carboxyl group on the uronic acid sugar which can easily deprotonate, as well as any sulfo-modification which is also likely to deprotonate. Therefore, MS analysis is most easily accomplished in negative ion mode.

Ion Activation

CID/HCD is the most common and easiest to implement form of ion activation for mass spectrometry. Inside an ion trap a dc potential well causes ions to oscillate back and forth, rapidly colliding with a neutral collision gas and building up thermal energy which will break the molecular bonds. Sulfo-modifications for GAGs are typically the most labile bonds by far as low energy levels will cause a hydrogen rearrangement reaction on the sulfate[40]. Thus, highly sulfated GAGs will only produce sulfate loss when subjected to threshold activation techniques like CID/HCD. Informative fragmentation can be generated from sparsely sulfated GAGs like keratan sulfate, bikunin, and even CS/DS, which can have fully ionized precursors with ESI because sulfate loss pathway will be closed. Sodium counterions can stabilize sulfo-modifications by shutting down the rearrangement pathway that leads to fragmentation by substituting sodium for the operative hydrogen, effectively fully ionizing the precursor. Sodium, however, contaminates mass spectrometers and makes spectra more complex and is generally avoided if possible. CID/HCD will generate b- and y-type fragments in proteins and glycosidic fragments in GAGs, if precursors are fully ionized.

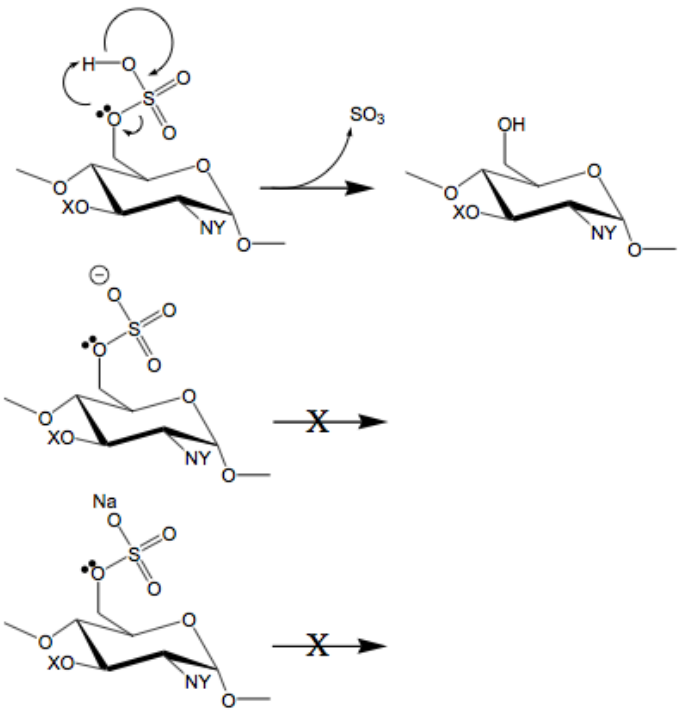

Figure 1.5. Thermal/kinetic energy causes the sulfo-modification to be lost, while ionized sulfate groups or sulfate groups with a metal cation substitution are much more stable[40].

ECD was developed in 1998 by Roman Zubarev and was the first low energy electron-based (~1eV) ion activation method[41]. Low energy electron capture typically works on positively charged ions that can accept electrons. Though, recently Kristina Hakansson has been applying negative ion electron capture dissociation (niECD) to negative mode peptides and glycans[42]. Electrons captured by positively charged molecules can undergo fragmentation from radical rearrangement in a non-ergodic mechanism. This type of fragmentation will lead to c- and z-type fragments in proteins, which are complimentary to the b- and y- type fragments generated by CID. The most common product of ECD is charge state reduction, where an ion captures an electron but does not fragment.

GAGs are highly negatively charged and are therefore not amenable to ECD fragmentation. EDD is the negative ion mode compliment to ECD developed in 2001[43]. Negatively charged ions, like GAGs, when bombarded by moderately high energy electrons (~18eV), can lose an electron to form a radical and undergo rearrangement and fragmentation. EDD ion activation on sulfated GAGs has been extensively researched by the Amster group[44-53]. This type of fragmentation produces glycosidic and cross-ring cleavages without sulfate loss and allows for informative structure characterization. Since the EDD activation pathway does not break the most labile bonds primarily, fully ionized precursors are not necessary to produce informative fragmentation without sulfate loss.

EDD is ill suited for high throughput analysis as it can take seconds of ion accumulation and reaction to produce low intensity fragments. Both ECD and EDD require a direct path from the filament where electrons are generated to the sample. This limits ECD and EDD to expensive FTICR instruments where electrons can be directed towards trapped sample ions in the analyzer cell.

NETD was developed as a reagent ion version of EDD, where an intermediary reagent ion delivers the extra electron to a positively charged sample ion[54, 55]. In NETD a neutral carrier gas, like nitrogen, is heated up to a thermally reactive temperature and then reacted with a reagent ion, like fluoranthene or xenon, which becomes a radical species. The radicalized reagent ions act as an intermediary for delivering electrons to multiply charged sample ions. The reagent ion reacts quickly with the sample of interest, within milliseconds, creating an odd-electron species that undergoes fragmentation which is not based on thermal energy. The NETD ion activation time falls within the time restrictions imposed by online separation techniques. NETD produces both informative glycosidic and cross-ring fragments similar to EDD, also without

fully ionized precursors[55-58]. Franklin Leach demonstrated NETDs ability to produce informative fragmentation on a millisecond time scale making it a good candidate to be paired with separation techniques[57].

NETD can take place within ion traps because reagent ions can be guided by rf voltages unlike electrons. The ion-ion reaction between the reagent and the sample is efficient and fast and can be well controlled. New MS instruments, like the orbitrap, use charge-sign independent trapping (CSIT), where rf voltages are applied in both the radial (quadrupole rods) and axial (end lenses) directions without additional dc offsets to trap sample ion and reagent ions in the linear ion trap at the same time.[54, 59].

Liquid Chromatography

Liquid chromatography (LC) paired with mass spectrometry has become the gold-standard for online separation of biomolecules. There are many forms of LC that have been applied to GAGs, including size exclusion chromatography (SEC), strong anion exchange (SAX), reverse phase ion pairing (RPIP), and hydrophilic interaction liquid chromatography (HILIC). Most LC techniques struggle with the highly anionic nature of GAGs and require preparation either before or after separation to ensure proper separation or prevent contamination of the mass spectrometer.

SEC uses sieves with sized pores to alter the distance molecules moving through the matrix must travel based on their size. SEC separates GAGs over time based on their molecular size. SEC has been used online to separate low molecular weight heparins (LMWH) and dalteparin into distinct chain lengths[60, 61]. However, SEC does not account for isoforms which

are abundant in GAGs and may not perfectly separate GAG chain lengths since GAGs are linear and not globular like the proteins SEC was designed for. For these reasons, SEC is most often used as one step for offline purification and isolation of GAG samples.

SAX uses highly ionic resin to capture sample molecules with an opposite charge and then salt is flushed through to release sample molecules by exchanging with them onto the resin. The use of large amounts of salts make this technique very incompatible with MS due to contamination and ion suppression, though some groups have worked to reduce the abundance of salt after separation[58, 60]. Miller et al. combined SEC and SAX to better separate GAG oligosaccharides based on their size and degree of modification[62].

RPIP uses ion pairing reagents that bind to GAGs and increase their retention to the separation column, improving separation and resolution. Ion pairing reagents are typically organic compounds like di- and tributyl amines[63]. Ion pairing enables high enough spectral resolution to differentiate similar GAG species at the cost of higher sample complexity, reduced ionization efficiency, and reduced fragmentation efficiency[63-66].

HILIC uses a polar stationary phase and a non-polar solvent system that ramps to a more polar solvent to separate sample molecules by their polarity. Typically, the solvent system is acetonitrile ratioed with water which works well with mass spectrometry, and little to no sample preparation is required for GAGs separated by HILIC. HILIC has been used by several groups to analyze a wide range of GAG chain lengths[67-69]. Combined HILIC/LC methods have even been reported to be capable of separating chemically synthesized tetra- and hexasaccharide isomers without permethylation over the course of an hour[70].

LC-MS has difficulty with the highly negative charge of GAGs and separating isomeric compounds abundant in biological GAG mixtures. RPIP was developed to account for the highly anionic nature of GAGs but introduces sample complexity and lowers ionization efficiency. HILIC takes advantage of the polar nature of GAGs but is difficult to perform and fails to separate isomers efficiently on its own.

Ion Mobility Spectrometry (IMS)

IMS separations take place in the gas phase after the sample molecules are electrosprayed. IMS uses electric fields and buffer gases to control the mobility of ions based on their size and shape[71]. Because ion mobility is a gas phase technique separation occurs within milliseconds. Kailemia et al. used high field asymmetric waveform IMS (FAIMS) to separate isobaric GAG mixtures followed by structural characterization by EDD[72]. Gated-trapped IMS (gated TIMS) was used by Wei et al. to separate isomeric highly sulfated GAGs which were analyzed by NETD[73]. IMS is a promising new separation technique for GAGs, but many of the methods are still in development and further experiments with more complex biological mixtures are required for a true evaluation.

Capillary Zone Electrophoresis

Capillary zone electrophoresis (CZE) occurs when one end of a capillary is held at a high voltage and the other end is held at a relatively lower voltage[74]. There are two main forces in a CZE experiment that cause ions to migrate through the capillary. Electrophoretic force (EF) is when charged molecules, or ions, migrate towards the voltage of opposite polarity and away

from the like polarity. When a high voltage is applied to the inlet of the capillary sample ions rapidly concentrate until they are the same resistance as the surrounding background electrolyte and begin to migrate towards the outlet. The concentration of sample this way makes investigation of small amounts of low concentration sample viable. This principle paired with MS makes a powerful separation system for highly charged molecules like GAGs. The second main force, electroosmotic flow (EOF), is when a charged double layer of background electrolyte ions builds up on the inner surface of the capillary and bulk flow is induced. The influence of EOF can be considerable in capillaries with very narrow inner diameters. CZE-MS, then, is well suited to the highly anionic nature of GAGs and separates them based on the size of their electric dipole.

CZE has been used to investigate GAG samples, especially disaccharides, for a long time but suffered from some core issues[20, 75-78]. The background electrolyte, or solvent system for CZE separation must be tailored to fit a specific sample type and to work well with MS. Most BGEs were developed initially for fluorescence-based detection, not MS. Many of the BGEs initially developed to effectively separate GAGs are very salty or have low ionization efficiency which would contaminate and interfere with MS.

Second, the inner surface of bare fused silica capillaries is not well suited for migration of negatively charged ions in CZE experiments. The silica oxide present on the inner surface of BFS capillaries builds up a mobile layer of positively charged particles that flows in the opposite direction of the negatively charged carbohydrate samples of interest, a detrimental EOF[79]. Both temporary and permanent capillary coatings can negate or reverse the electroosmotic flow, but permanent coatings are more reliable and less of a hassle.

The third issue is, CZE requires a high voltage and a complete electrical circuit. A large voltage is applied the BGE container at the inlet of the capillary, but the circuit must be completed at the outlet of the capillary. Originally this was solved by flowing sheath liquid from a secondary reservoir around the capillary outlet to generate electrospray[80]. This would complete the circuit, but also heavily dilute the sample. Many groups have attempted to improve sensitivity by stacking or concentrating the sample in the capillary[81, 82]. Other groups are trying to solve the dilution problem by removing the sheath liquid entirely, by adding an electrode to the outlet of the capillary, but this is difficult to accomplish[83]. Recently, a company has come out with an interface, based on research from the Dovichi group, designed to drastically reduce the dilution factor by limiting the sheath liquid to a nanospray needle[84-87]. The outlet of the capillary is etched by nitric acid to fit more snuggly into the nanospray needle and reduce the mixing volume as much as possible.

This CZE-MS system is tailored to work well for analysis of small quantities of highly negatively charged GAGs.

1.3 DISSERTATION TOPIC: DEVELOPING A CZE-MS PLATFORM FOR GAG ANALYSIS

Partially digested biological GAG samples often present a complex mixture that is difficult to interpret by MS or tandem MS alone. A robust and easy to use separation technique is required to meaningfully advance understanding of GAG structural mechanisms and their role in biological processes. This dissertation details the first steps in developing a CZE-MS platform designed to separate and characterize complex GAG samples. Optimal separation and ionization

conditions for highly negatively charged GAGs were determined using a basic CE instrument and an orbitrap mass analyzer. Then, NETD fragmentation was optimized on GAG tetrasaccharide standards before being used to analyze the components of a complex partially digested GAG pharmaceutical.

1.4 REFERENCES

1. Varki, A.; Cummings, R. D.; Esko, J. D.; Freeze, H. H.; Stanley, P.; Bertozzi, C. R.; Hart, G. W.; Etzler, M. E., *Essentials of Glycobiology*. NY, 2009; Vol. 2.

2. Laremore, T. N.; Zhang, F.; Dordick, J. S.; Liu, J.; Linhardt, R. J., Recent progress and applications in glycosaminoglycan and heparin research. *Current Opinion in Chemical Biology* **2009,** *13* (5), 633-640.

3. Esko, J. D.; Lindahl, U., Molecular diversity of heparan sulfate. *The Journal of Clinical Investigation* **2001,** *108* (2), 169-173.

4. Rabenstein, D. L., Heparin and heparan sulfate: structure and function. *Natural Product Reports* **2002,** *19* (3), 312-331.

5. Sasisekharan, R.; Raman, R.; Prabhakar, V., Glycomics approach to structure-function relationships of glycosaminoglycans. *Annual Review of Biomedical Engineering* **2006,** *8* (1), 181-231.

6. Sugahara, K.; Kitagawa, H., Recent advances in the study of the biosynthesis and functions of sulfated glycosaminoglycans. *Current Opinion in Structural Biology* **2000,** *10* (5), 518-527.

7. Thacker, B. E.; Xu, D.; Lawrence, R.; Esko, J. D., Heparan sulfate 3-O-sulfation: a rare modification in search of a function. *Matrix biology : journal of the International Society for Matrix Biology* **2014,** *35*, 60-72.

8. Xu, D.; Esko, J. D., Demystifying Heparan Sulfate–Protein Interactions. *Annual Review of Biochemistry* **2014,** *83* (1), 129-157.

9. Clegg, D. O.; Reda, D. J.; Harris, C. L.; Klein, M. A.; O'Dell, J. R.; Hooper, M. M.; Bradley, J. D.; Bingham, C. O.; Weisman, M. H.; Jackson, C. G.; Lane, N. E.; Cush, J. J.; Moreland, L. W.; Schumacher, H. R.; Oddis, C. V.; Wolfe, F.; Molitor, J. A.; Yocum, D. E.; Schnitzer, T. J.; Furst, D. E.; Sawitzke, A. D.; Shi, H.; Brandt, K. D.; Moskowitz, R. W.;

Williams, H. J., Glucosamine, Chondroitin Sulfate, and the Two in Combination for Painful Knee Osteoarthritis. *New England Journal of Medicine* **2006,** *354* (8), 795-808.

10. Shen, Y.; Tenney, A. P.; Busch, S. A.; Horn, K. P.; Cuascut, F. X.; Liu, K.; He, Z.; Silver, J.; Flanagan, J. G., PTPσ Is a Receptor for Chondroitin Sulfate Proteoglycan, an Inhibitor of Neural Regeneration. *Science* **2009,** *326* (5952), 592-596.

11. Watanabe, H.; Yamada, Y.; Kimata, K., Roles of Aggrecan, a Large Chondroitin Sulfate Proteoglycan, in Cartilage Structure and Function. *The Journal of Biochemistry* **1998,** *124* (4), 687-693.

12. Penc, S. F.; Pomahac, B.; Winkler, T.; Dorschner, R. A.; Eriksson, E.; Herndon, M.; Gallo, R. L., Dermatan Sulfate Released after Injury Is a Potent Promoter of Fibroblast Growth Factor-2 Function. *Journal of Biological Chemistry* **1998,** *273* (43), 28116-28121.

13. Malmström, A.; Bartolini, B.; Thelin, M. A.; Pacheco, B.; Maccarana, M., Iduronic Acid in Chondroitin/Dermatan Sulfate:Biosynthesis and Biological Function. *Journal of Histochemistry & Cytochemistry* **2012,** *60* (12), 916-925.

14. Zhang, Q.; Du, Y.; Chen, J.; Xu, G.; Yu, T.; Hua, X.; Zhang, J., Investigation of chondroitin sulfate D and chondroitin sulfate E as novel chiral selectors in capillary electrophoresis. *Analytical and Bioanalytical Chemistry* **2014,** *406* (5), 1557-1566.

15. Funderburgh, J. L., MINI REVIEW Keratan sulfate: structure, biosynthesis, and function. *Glycobiology* **2000,** *10* (10), 951-958.

16. LAURENT, T. C.; LAURENT, U. B.; FRASER, J. R. E., The structure and function of hyaluronan: An overview. *Immunology & Cell Biology* **1996,** *74* (2), a1-a7.

17. Monslow, J.; Govindaraju, P.; Puré, E., Hyaluronan – A Functional and Structural Sweet Spot in the Tissue Microenvironment. *Frontiers in Immunology* **2015,** *6* (231).

18. Naimy, H.; Leymarie, N.; Bowman, M. J.; Zaia, J., Characterization of heparin oligosaccharides binding specifically to antithrombin III using mass spectrometry. *Biochemistry* **2008,** *47* (10), 3155-61.

19. Chi, L.; Wolff, J. J.; Laremore, T. N.; Restaino, O. F.; Xie, J.; Schiraldi, C.; Toida, T.; Amster, I. J.; Linhardt, R. J., Structural Analysis of Bikunin Glycosaminoglycan. *Journal of the American Chemical Society* **2008,** *130* (8), 2617-2625.

20. Zamfir, A.; Seidler, D. G.; Kresse, H.; Peter-Katalinić, J., Structural characterization of chondroitin/dermatan sulfate oligosaccharides from bovine aorta by capillary electrophoresis and electrospray ionization quadrupole time-of-flight tandem mass spectrometry. *Rapid Communications in Mass Spectrometry* **2002,** *16* (21), 2015-2024.

21. Ly, M.; Leach, F. E., 3rd; Laremore, T. N.; Toida, T.; Amster, I. J.; Linhardt, R. J., The proteoglycan bikunin has a defined sequence. *Nat. Chem. Biol.* **2011,** *7* (11), 827-33.

22. Duan, J.; Jonathan Amster, I., An Automated, High-Throughput Method for Interpreting the Tandem Mass Spectra of Glycosaminoglycans. *Journal of The American Society for Mass Spectrometry* **2018,** *29* (9), 1802-1811.

23. Yu, Y.; Duan, J.; Leach, F. E.; Toida, T.; Higashi, K.; Zhang, H.; Zhang, F.; Amster, I. J.; Linhardt, R. J., Sequencing the Dermatan Sulfate Chain of Decorin. *Journal of the American Chemical Society* **2017,** *139* (46), 16986-16995.

24. Moure, M. J.; Eletsky, A.; Gao, Q.; Morris, L. C.; Yang, J.-Y.; Chapla, D.; Zhao, Y.; Zong, C.; Amster, I. J.; Moremen, K. W.; Boons, G.-J.; Prestegard, J. H., Paramagnetic Tag for Glycosylation Sites in Glycoproteins: Structural Constraints on Heparan Sulfate Binding to Robo1. *ACS Chemical Biology* **2018,** *13* (9), 2560-2567.

25. Kailemia, M. J.; Ruhaak, L. R.; Lebrilla, C. B.; Amster, I. J., Oligosaccharide Analysis by Mass Spectrometry: A Review of Recent Developments. *Analytical Chemistry* **2014,** *86* (1), 196-212.

26. Whisstock, J. C.; Pike, R. N.; Jin, L.; Skinner, R.; Pei, X. Y.; Carrell, R. W.; Lesk, A. M., Conformational changes in serpins: II. the mechanism of activation of antithrombin by heparin†22Edited by J. Thornton†Paper I in this series is Whisstock et al. (2000). *Journal of Molecular Biology* **2000,** *301* (5), 1287-1305.

27. Abboud, J.-L. M.; Notario, R., FT ICR. Basic Principles and Some Representative Applications. In *Energetics of Stable Molecules and Reactive Intermediates*, Minas da Piedade, M. E., Ed. Springer Netherlands: Dordrecht, 1999; pp 281-302.

28. Barrow, M. P.; Burkitt, W. I.; Derrick, P. J., Principles of Fourier transform ion cyclotron resonance mass spectrometry and its application in structural biology. *Analyst* **2005,** *130* (1), 18-28.

29. Makarov, A., Electrostatic Axially Harmonic Orbital Trapping: A High-Performance Technique of Mass Analysis. *Analytical Chemistry* **2000,** *72* (6), 1156-1162.

30. Kingdon, K. H., A Method for the Neutralization of Electron Space Charge by Positive Ionization at Very Low Gas Pressures. *Physical Review* **1923,** *21* (4), 408-418.

31. Hardman, M.; Makarov, A. A., Interfacing the Orbitrap Mass Analyzer to an Electrospray Ion Source. *Analytical Chemistry* **2003,** *75* (7), 1699-1705.

32. Hu, Q.; Noll, R. J.; Li, H.; Makarov, A.; Hardman, M.; Graham Cooks, R., The Orbitrap: a new mass spectrometer. *Journal of Mass Spectrometry* **2005,** *40* (4), 430-443.

33. Makarov, A.; Denisov, E.; Kholomeev, A.; Balschun, W.; Lange, O.; Strupat, K.; Horning, S., Performance Evaluation of a Hybrid Linear Ion Trap/Orbitrap Mass Spectrometer. *Analytical Chemistry* **2006,** *78* (7), 2113-2120.

34. Domon, B.; Costello, C. E., A systematic nomenclature for carbohydrate fragmentations in FAB-MS/MS spectra of glycoconjugates. *Glycoconjugate Journal* **1988,** *5* (4), 397-409.

35. Fenn, J. B.; Mann, M.; Meng, C. K.; Wong, S. F.; Whitehouse, C. M., Electrospray ionization for mass spectrometry of large biomolecules. *Science* **1989,** *246* (4926), 64.

36. Wilm, M.; Mann, M., Analytical Properties of the Nanoelectrospray Ion Source. *Analytical Chemistry* **1996,** *68* (1), 1-8.

37. Fenn, J. B.; Mann, M.; Meng, C. K.; Wong, S. F.; Whitehouse, C. M., Electrospray ionization–principles and practice. *Mass Spectrometry Reviews* **1990,** *9* (1), 37-70.

38. Wilm, M., Principles of electrospray ionization. *Molecular & cellular proteomics : MCP* **2011,** *10* (7), M111.009407-M111.009407.

39. Siuzdak, G., *The expanding role of mass spectrometry in biotechnology*. Mcc Press: 2006.

40. Zaia, J., Principles of mass spectrometry of glycosaminoglycans. *J Biomacromol Mass Spectrom* **2005,** *1* (1), 3-36.

41. Zubarev, R. A.; Kelleher, N. L.; McLafferty, F. W., Electron Capture Dissociation of Multiply Charged Protein Cations. A Nonergodic Process. *Journal of the American Chemical Society* **1998,** *120* (13), 3265-3266.

42. Hersberger, K. E.; Håkansson, K., Characterization of O-Sulfopeptides by Negative Ion Mode Tandem Mass Spectrometry: Superior Performance of Negative Ion Electron Capture Dissociation. *Analytical Chemistry* **2012,** *84* (15), 6370-6377.

43. Budnik, B. A.; Haselmann, K. F.; Zubarev, R. A., Electron detachment dissociation of peptide di-anions: an electron–hole recombination phenomenon. *Chemical Physics Letters* **2001,** *342* (3), 299-302.

44. Wolff, J. J.; Amster, I. J.; Chi, L.; Linhardt, R. J., Electron detachment dissociation of glycosaminoglycan tetrasaccharides. *J Am Soc Mass Spectrom* **2007,** *18* (2), 234-44.

45. Wolff, J. J.; Chi, L.; Linhardt, R. J.; Amster, I. J., Distinguishing glucuronic from iduronic acid in glycosaminoglycan tetrasaccharides by using electron detachment dissociation. *Analytical chemistry* **2007,** *79* (5), 2015-2022.

46. Leach, F. E.; Wolff, J. J.; Laremore, T. N.; Linhardt, R. J.; Amster, I. J., Evaluation of the experimental parameters which control electron detachment dissociation, and their effect on

the fragmentation efficiency of glycosaminoglycan carbohydrates. *International Journal of Mass Spectrometry* **2008,** *276* (2), 110-115.

47. Wolff, J. J.; Laremore, T. N.; Busch, A. M.; Linhardt, R. J.; Amster, I. J., Electron detachment dissociation of dermatan sulfate oligosaccharides. *J Am Soc Mass Spectrom* **2008,** *19* (2), 294-304.

48. Wolff, J. J.; Laremore, T. N.; Busch, A. M.; Linhardt, R. J.; Amster, I. J., Influence of charge state and sodium cationization on the electron detachment dissociation and infrared multiphoton dissociation of glycosaminoglycan oligosaccharides. *Journal of the American Society for Mass Spectrometry* **2008,** *19* (6), 790-798.

49. Wolff, J. J.; Laremore, T. N.; Leach, F. E.; Linhardt, R. J.; Amster, I. J., Electron Capture Dissociation, Electron Detachment Dissociation and Infrared Multiphoton Dissociation of Sucrose Octasulfate. *European Journal of Mass Spectrometry* **2009,** *15* (2), 275-281.

50. Leach, F. E.; Xiao, Z.; Laremore, T. N.; Linhardt, R. J.; Amster, I. J., Electron detachment dissociation and infrared multiphoton dissociation of heparin tetrasaccharides. *International Journal of Mass Spectrometry* **2011,** *308* (2), 253-259.

51. Oh, H. B.; Leach, F. E.; Arungundram, S.; Al-Mafraji, K.; Venot, A.; Boons, G.-J.; Amster, I. J., Multivariate Analysis of Electron Detachment Dissociation and Infrared Multiphoton Dissociation Mass Spectra of Heparan Sulfate Tetrasaccharides Differing Only in Hexuronic acid Stereochemistry. *Journal of The American Society for Mass Spectrometry* **2011,** *22* (3), 582-590.

52. Leach, F. E.; Arungundram, S.; Al-Mafraji, K.; Venot, A.; Boons, G.-J.; Amster, I. J., Electron detachment dissociation of synthetic heparan sulfate glycosaminoglycan tetrasaccharides varying in degree of sulfation and hexuronic acid stereochemistry. *International Journal of Mass Spectrometry* **2012,** *330-332*, 152-159.

53. Agyekum, I.; Zong, C.; Boons, G.-J.; Amster, I. J., Single Stage Tandem Mass Spectrometry Assignment of the C-5 Uronic Acid Stereochemistry in Heparan Sulfate Tetrasaccharides using Electron Detachment Dissociation. *Journal of The American Society for Mass Spectrometry* **2017**, 1-10.

54. Syka, J. E. P.; Coon, J. J.; Schroeder, M. J.; Shabanowitz, J.; Hunt, D. F., Peptide and protein sequence analysis by electron transfer dissociation mass spectrometry. *Proceedings of the National Academy of Sciences of the United States of America* **2004,** *101* (26), 9528-9533.

55. Wolff, J. J.; Leach, F. E.; Laremore, T. N.; Kaplan, D. A.; Easterling, M. L.; Linhardt, R. J.; Amster, I. J., Negative electron transfer dissociation of glycosaminoglycans. *Analytical chemistry* **2010,** *82* (9), 3460-3466.

56. Leach, F. E.; Wolff, J. J.; Xiao, Z.; Ly, M.; Laremore, T. N.; Arungundram, S.; Al-Mafraji, K.; Venot, A.; Boons, G.-J.; Linhardt, R. J.; Amster, I. J., Negative electron transfer

dissociation Fourier transform mass spectrometry of glycosaminoglycan carbohydrates. *European Journal of Mass Spectrometry (Chichester, England)* **2011,** *17* (2), 167-176.

57. Leach, F. E.; Riley, N. M.; Westphall, M. S.; Coon, J. J.; Amster, I. J., Negative Electron Transfer Dissociation Sequencing of Increasingly Sulfated Glycosaminoglycan Oligosaccharides on an Orbitrap Mass Spectrometer. *Journal of The American Society for Mass Spectrometry* **2017,** *28* (9), 1844-1854.

58. Wu, J.; Wei, J.; Hogan, J. D.; Chopra, P.; Joshi, A.; Lu, W.; Klein, J.; Boons, G.-J.; Lin, C.; Zaia, J., Negative Electron Transfer Dissociation Sequencing of 3-O-Sulfation-Containing Heparan Sulfate Oligosaccharides. *Journal of The American Society for Mass Spectrometry* **2018,** *29* (6), 1262-1272.

59. McAlister, G. C.; Phanstiel, D.; Good, D. M.; Berggren, W. T.; Coon, J. J., Implementation of Electron-Transfer Dissociation on a Hybrid Linear Ion Trap−Orbitrap Mass Spectrometer. *Analytical Chemistry* **2007,** *79* (10), 3525-3534.

60. Zaia, J.; Khatri, K.; Klein, J.; Shao, C.; Sheng, Y.; Viner, R., Complete Molecular Weight Profiling of Low-Molecular Weight Heparins Using Size Exclusion Chromatography-Ion Suppressor-High-Resolution Mass Spectrometry. *Analytical Chemistry* **2016,** *88* (21), 10654-10660.

61. Zhang, Q.; Chen, X.; Zhu, Z.; Zhan, X.; Wu, Y.; Song, L.; Kang, J., Structural Analysis of Low Molecular Weight Heparin by Ultraperformance Size Exclusion Chromatography/Time of Flight Mass Spectrometry and Capillary Zone Electrophoresis. *Analytical Chemistry* **2013,** *85* (3), 1819-1827.

62. Miller, R. L.; Guimond, S. E.; Shivkumar, M.; Blocksidge, J.; Austin, J. A.; Leary, J. A.; Turnbull, J. E., Heparin Isomeric Oligosaccharide Separation Using Volatile Salt Strong Anion Exchange Chromatography. *Analytical Chemistry* **2016,** *88* (23), 11542-11550.

63. Volpi, N.; Linhardt, R. J., High-performance liquid chromatography-mass spectrometry for mapping and sequencing glycosaminoglycan-derived oligosaccharides. *Nat Protoc* **2010,** *5* (6), 993-1004.

64. Guo, Q.; Reinhold, V. N., Advancing MSn spatial resolution and documentation for glycosaminoglycans by sulfate-isotope exchange. *Analytical and bioanalytical chemistry* **2019,** *411* (20), 5033-5045.

65. Du, J. Y.; Chen, L. R.; Liu, S.; Lin, J. H.; Liang, Q. T.; Lyon, M.; Wei, Z., Ion-pairing liquid chromatography with on-line electrospray ion trap mass spectrometry for the structural analysis of N-unsubstituted heparin/heparan sulfate. **2016,** *1028*, 71-76.

66. Doneanu, C. E.; Chen, W.; Gebler, J. C., Analysis of Oligosaccharides Derived from Heparin by Ion-Pair Reversed-Phase Chromatography/Mass Spectrometry. **2009,** *81* (9), 3485-3499.

67. Gill, V. L.; Aich, U.; Rao, S.; Pohl, C.; Zaia, J., Disaccharide Analysis of Glycosaminoglycans Using Hydrophilic Interaction Chromatography and Mass Spectrometry. *Analytical Chemistry* **2013,** *85* (2), 1138-1145.

68. Li, L.; Zhang, F.; Zaia, J.; Linhardt, R. J., Top-Down Approach for the Direct Characterization of Low Molecular Weight Heparins Using LC-FT-MS. *Analytical Chemistry* **2012,** *84* (20), 8822-8829.

69. Antia, I. U.; Mathew, K.; Yagnik, D. R.; Hills, F. A.; Shah, A. J., Analysis of procainamide-derivatised heparan sulphate disaccharides in biological samples using hydrophilic interaction liquid chromatography mass spectrometry. *Analytical and Bioanalytical Chemistry* **2018,** *410* (1), 131-143.

70. Wu, J.; Wei, J.; Chopra, P.; Boons, G.-J.; Lin, C.; Zaia, J., Sequencing Heparan Sulfate Using HILIC LC-NETD-MS/MS. *Analytical Chemistry* **2019,** *91* (18), 11738-11746.

71. Borsdorf, H.; Eiceman, G. A., Ion Mobility Spectrometry: Principles and Applications. *Applied Spectroscopy Reviews* **2006,** *41* (4), 323-375.

72. Muchena J. Kailemia, M. P., Desmond A. Kaplan, Andre Venot,; Geert-Jan Boons, L. L., Robert J. Linhardt, I. Jonathan Amster, High-field asymmetric-waveform ion mobility spectrometry and electron detachment dissociation of isobaric mixtures of glycosaminoglycans. *J. Am. Soc. Mass Spectrom.* **2013**.

73. Wei, J.; Wu, J.; Tang, Y.; Ridgeway, M. E.; Park, M. A.; Costello, C. E.; Zaia, J.; Lin, C., Characterization and Quantification of Highly Sulfated Glycosaminoglycan Isomers by Gated-Trapped Ion Mobility Spectrometry Negative Electron Transfer Dissociation MS/MS. *Analytical Chemistry* **2019,** *91* (4), 2994-3001.

74. Whatley, H., Basic Principles and Modes of Capillary Electrophoresis. In *Clinical and Forensic Applications of Capillary Electrophoresis*, Petersen, J. R.; Mohammad, A. A., Eds. Humana Press: Totowa, NJ, 2001; pp 21-58.

75. Karamanos, N. K.; Hjerpe, A., A survey of methodological challenges for glycosaminoglycan/proteoglycan analysis and structural characterization by capillary electrophoresis. *Electrophoresis* **1998,** *19* (15), 2561-2571.

76. Ruiz-Calero, V.; Moyano, E.; Puignou, L.; Galceran, M. T., Pressure-assisted capillary electrophoresis–electrospray ion trap mass spectrometry for the analysis of heparin depolymerised disaccharides. *Journal of Chromatography A* **2001,** *914* (1), 277-291.

77. Fermas, S.; Gonnet, F.; Varenne, A.; Gareil, P.; Daniel, R., Frontal Analysis Capillary Electrophoresis Hyphenated to Electrospray Ionization Mass Spectrometry for the Characterization of the Antithrombin/Heparin Pentasaccharide Complex. *Analytical Chemistry* **2007,** *79* (13), 4987-4993.

78. Ampofo, S. A., Disaccharide compositional analysis of heparin and heparan sulfate using capillary zone electrophoresis. *Analytical biochemistry* **1991,** *199* (2), 249.

79. Hayes, M. A.; Kheterpal, I.; Ewing, A. G., Effects of buffer pH on electroosmotic flow control by an applied radial voltage for capillary zone electrophoresis. *Anal. Chem.* **1993,** *65* (1), 27-31.

80. Smith, R. D.; Olivares, J. A.; Nguyen, N. T.; Udseth, H. R., Capillary zone electrophoresis-mass spectrometry using an electrospray ionization interface. *Analytical Chemistry* **1988,** *60* (5), 436-441.

81. Albin, M.; Grossman, P. D.; Moring, S. E., Sensitivity enhancement for capillary electrophoresis. *Analytical Chemistry* **1993,** *65* (10), 489A-497A.

82. Osbourn, D. M.; Weiss, D. J.; Lunte, C. E., On-line preconcentration methods for capillary electrophoresis. *Electrophoresis* **2000,** *21* (14), 2768-2779.

83. Zamfir, A.; Seidler, D. G.; Schönherr, E.; Kresse, H.; Peter-Katalinic´, J., On-line sheathless capillary electrophoresis/nanoelectrospray ionization-tandem mass spectrometry for the analysis of glycosaminoglycan oligosaccharides. *Electrophoresis* **2004,** *25* (13), 2010-2016.

84. Wojcik, R.; Dada, O. O.; Sadilek, M.; Dovichi, N. J., Simplified capillary electrophoresis nanospray sheath-flow interface for high efficiency and sensitive peptide analysis. *Rapid Communications in Mass Spectrometry* **2010,** *24* (17), 2554-2560.

85. Sun, L.; Zhu, G.; Zhang, Z.; Mou, S.; Dovichi, N. J., A third-generation electro-kinetically pumped sheath flow nanospray interface with improved stamass spectrometry analysis of complex proteome digests. *Journal of proteome research* **2015,** *14* (5), 2312-2321.

86. Sarver, S. A.; Schiavone, N. M.; Arceo, J.; Peuchen, E. H.; Zhang, Z.; Sun, L.; Dovichi, N. J., Capillary electrophoresis coupled to negative mode electrospray ionization-mass spectrometry using an electrokinetically-pumped nanospray interface with primary amines grafted to the interior of a glass emitter. *Talanta* **2017,** *165*, 522-525.

87. Dovichi, N. J.; Wojcik, R. Sheath-flow electrospray interface. US 9234880 B2. June 3, 2011.

CHAPTER 2

EXPERIMENTAL METHODS

2.1 MATERIALS

BFS capillaries (360 µm o.d. x 50 µm i.d.) were purchased from PolyMicro Technologies (Phoenix, AZ). Borosilicate glass capillaries (1.0 mm o.d. x 0.75 mm i.d.) and pulled coated electrospray emitters (1.0 mm o.d. x 0.75 mm i.d., E-BS-CC1-750-1000-10 µ-B30) were obtained from CMP Scientific (Brooklyn, NY). Coating reagents, dichlorodimethylsilane (DMS, Sigma-Aldrich, St. Louis, MO) and N-(6-aminohexyl)aminomethyltriethoxysilane (AHS, Gelest, Morrisville, PA) were prepared in toluene. Ammonium acetate, water, and methanol were of HPLC grade (Fisher Scientific, Hampton, NH). Diethylamine, sodium hydroxide, concentrated hydrofluoric acid (~48% wt), acetone, and toluene were purchased from Sigma-Aldrich (St. Louis, MO). All solutions were filtered with 0.45 µm syringe filter (Millipore, Temecula, CA) before use.

2.2 GAG SAMPLE PREPARATION

GAG oligosaccharides were prepared by enzymatic depolymerization and purified using strong anion exchange high-pressure liquid chromatography (SAX-HPLC). GlcA-GlcNAc6S-IdoA-GlcNAc6S (GI) and GlcA-GlcNAc6s-GlcA-GlcNAc6S (GG) were chemically synthesized and purified as shown in the literature[1]. Low molecular weight heparin (LMWH), Enoxaparin, was from the USP (Rockville, MD). Low molecular weight heparin (LMWH), Lovenox, was

from Sanofi (Bridgewater, NJ). Enoxaparin and Lovenox were chemically digested with hydrogen peroxide[2].

All samples were diluted in HPLC grade water and desalted with a 3kDa Amicon Ultra centrifugal filter (Millipore, Temecula, CA) prior to separation and mass spectrometry analysis. Although the GAGs have molecular weights below 3 kDa, heparin and heparan sulfate tetrasaccharides and larger chains do not pass through the 3 kDa membrane. The membrane permeability is based on size and shape. GAGs have a linear structure compare to proteins which are often globular, and this makes the GAGs behave as if they have a higher molecular weight for the purposes of the centrifugal filter membrane. Filters were conditioned with water, and the sample was then washed with two filter volumes of water (14,000 x g for 25 min each). Before analysis, GAG samples were diluted to 5 µg/mL and the LMHWs were diluted to 100 µg/mL in water.

2.3 COATINGS

Bare fused silica capillaries were etched with concentrated hydrofluoric acid (HF) at one end to reduce the outer diameter of the capillary for use in the sheath flow CE interface described below. For the etching process, the outlet of the capillary was placed in concentrated HF for 45-60 min. the capillary was then thoroughly washed with water. Etched capillaries were coated with AHS to produce a cation coated capillary and DMS to produce a neutral coated capillary. Coating materials were prepared in toluene with 1% concentration of either AHS or DMS. A BFS capillary was first cleaned and prepared for coating by flushing 0.1 M NaOH, water, methanol, dried acetone, and dried toluene, in series for 30 min each. The capillary was then

coated by flushing the 1% AHS or DMS solution for 1 h. The capillary was then flushed with dried toluene, dried acetone, and methanol, in series for 30 min each to remove excess coating solution. AHS coated capillaries were left to dry and cure for 2 weeks before being equilibrated. Finally, capillaries were equilibrated by flushing background electrolyte (BGE, 25mM ammonium acetate 70% MeOH) through the capillary and applying a high voltage to the capillary for 1 h. Once degradation becomes apparent, BFS capillaries can be easily cleaned by flushing sodium hydroxide for a short time; however, the coatings are stripped in basic conditions and must be reapplied by repeating the coating procedure. Very little coating degradation is observed, and coating reapplication is rarely needed.

The interior surface of sheath flow emitters was covalently modified with solutions that were prepared in dried toluene with 1% concentration of either AHS (cationic surface) or DMS (neutral surface). To clean and prepare the emitter for surface modification, the borosilicate glass capillary was rinsed consecutively with 2 mL each of aqueous 0.1 M NaOH, water, methanol, dried acetone, and dried toluene. The surface of the borosilicate glass capillary was then modified by flushing with 500 µL of 1% AHS or DMS over a 20 min period. The borosilicate glass capillary was then consecutively rinsed with 2 mL of each dried toluene, dried acetone, and methanol. The modified borosilicated glass capillaries were then pulled into emitter with 30 µm orifices using a commercial capillary puller, as described previously.

2.4 INSTRUMENTATION

Experiments were conducted on an Agilent HP 3D capillary electrophoresis instrument (Wilmington, DE). The total length of capillaries used ranged from 50 to 60 cm, and their inner

diameter was 50 µm with a total internal volume of approximately 1 µL. The aqueous GAG sample was injected for 3 s at 950 mbar followed by a BGE injection for 10 s at 10 mbar. The injected volume was approximately 0.1 µL. The ionic strength of the injected sample plug is 2-3 orders of magnitude less than that of the background electrolyte. The sample plug will act as a resistor within the capillary circuit when voltage is applied and cause sample stacking and a sharp sample peak. The inlet of the capillary was placed into a BGE vial for separation. A separation voltage of -30 kV was applied to the inlet of the capillary form most experiments. A separation voltage of -15 kV was used for selected experiments as identified in the results below.

An EMASS-II (CMP Scientific, Brooklyn, NY) CZE-MS interface was used to couple the CE with a Thermo Fischer Scientific Orbitrap Elite mass spectrometer (Bremen, Germany). The etched capillary outlet was nested inside of a glass emitter tip with a 30 µm tip orifice (CMP Scientific, Brooklyn, NY). The etched capillary was positioned 0.3-0.5 mm from the tip of the emitter orifice to create a mixing volume of approximately 15 nL, and the emitter tip was filled with sheath liquid (SL, 25 mM ammonium acetate 70% MeOH) from a reservoir vial. An external power supply provided a nano-electrospray (nESI) voltage ranging from -1.6 to -1.9 kV to the sheath liquid and thus the emitter. 2mM NaOH was added to the sheath liquid (SL) to generate sodiated sample peaks

MS detection was performed in negative ion mode. Prior to CZE-MS experiments, a semi-automatic optimization of source parameters was performed using sucrose octasulfate to improve sensitivity of sulfated GAGs and reduce sulfate loss during MS analysis. The Orbitrap Elite was scanned from m/z 150-2000 for GAG oligosaccharides with a specified resolution of 120,000.

2.5 NEGATIVE ELECTRON TRANSFER DISSOCIATION

Fluoranthene radical cation produced by electron ionization was used as the reagent ion for NETD experiments. Ion-ion reactions took place inside the ion trap quadrupole of the Orbitrap Elite mass spectrometery. Analyte ions generated by nESI after CZE separation are accumulated in the ion trap and reacted with fluoranthene reagent ions generated by a chemical ionization source (CI) in a module at the back end of the instrument. 110 ms activation times were used for doubly charged tetrasaccharides and triply charged hexasaccharides. 50 ms activation times were used for triply charged tetrasaccharides. Emission current was set to 75 µA and electron energy was set to -70 V. Experiments were manually optimized. Preliminary CZE-MS were acquired to identify potential precursor ions, followed by individual NETD tandem experiments for each precursor, and then methods were used that split spectra acquisition evenly between MS and NETD MS2 of a single selected precursor. A data dependent method was designed to apply NETD fragmentation to the two most intense m/z in the MS1 throughout the electropherogram, excluding the BGE peaks, and used to asses LMWH samples.

2.6 REFERENCES

1. Linhardt, R. J.; Gunay, N. S., Production and chemical processing of low molecular weight heparins. *Semin. Thromb. Hemost.* **1999,** *25,* 5-16.

2. Guerrini, M.; Rudd, T. R.; Mauri, L.; Macchi, E.; Fareed, J.; Yates, E. A.; Naggi, A.; Torri, G., Differentiation of Generic Enoxaparins Marketed in the United States by Employing NMR and Multivariate Analysis. *Analytical Chemistry* **2015,** *87* (16), 8275-8283.

CHAPTER 3

HEPARIN/HEPARAN SULFATE ANALYSIS BY COVALENTLY MODIFIED REVERSE POLARITY CAPILLARY ZONE ELECTROPHORESIS-MASS SPECTROMETRY

Stickney, M.; Sanderson, P.; Amster, I. J. 2018. J. Chromatogr. A, 1545, 75-83.

Accepted by J. Chromatogr. A. Reprinted here with permission of the publisher.

3.1 ABSTRACT

Reverse polarity capillary zone electrophoresis coupled to negative ion mode mass spectrometry (CZE-MS) is shown to be an effective and sensitive tool for analysis of glycosaminoglycan mixtures. Covalent modification of the inner wall of the separation capillary with neutral or cationic reagents produces a stable and durable surface that provides reproducible separations. By combining CZE-MS with a cation-coated capillary and a nano sheath flow interface, a rapid and reliable method has been developed for the analysis of sulfated oligosaccharides from dp4 to dp12. Several glycosaminoglycan (GAG) mixtures have been separated and detected by mass spectrometry. The mixtures were selected to test the capability of this approach to resolve subtle differences in structure, such as sulfo-modification position and epimeric variation of the uronic acid. The system was applied to a complex mixture of heparin/heparan sulfate oligosaccharides varying in chain length from dp3 to dp12 and more than 80 molecular compositions were identified by accurate mass measurement.

3.2 INTRODUCTION

Sulfated glycosaminoglycan (GAG) carbohydrates are linear, acidic polysaccharide chains that are abundant on the surface of mammalian cells[1]. Several biological processes, such as developmental and disease functions, are impacted by GAGs within the body through protein-binding interactions[2-4]. The biosynthesis of GAG chains is a non-template driven process, facilitated by a number of enzymatic steps (elongation, deacetylation, sulfo-modification, epimerization) that do not go to completion, resulting in highly heterogeneous and complex mixtures[5]. There are several classes of GAGs that are defined by their linkage pattern and amino

sugar (N-acetyl glucosamine (GlcNAc) orN -acetyl galactosamine (GalNAc)), with heparin and heparan sulfate as the most structurally diverse. Heparin and heparan sulfate consist of a repeating disaccharide unit of an N-acetyl glucosamine linked (1←4) to a hexuronic acid sugar. The GlcNAc can be modified by deacetylation and N-sulfo modification, and it can also have sulfo-modification at the 6-O- or 3-O-position. The hexuronic acid sugar can exist as one of two epimers: glucuronic acid (GlcA) or iduronic acid (IdoA) with sulfo-modification commonly at the 2-O-position of IdoA but infrequently at the 2-O-position of GlcA[6]. The structural assignment of GAG chains is a significant analytical challenge and has been the target of several researchers[7-14]. Although full-length sulfated GAGs have been analyzed in top-down fashion by mass spectrometry[15, 16], the typical approach is to partially digest polysaccharides to oligosaccharide mixtures of moderate length (typically disaccharide to decasaccharide) to enable characterization. The structural analysis of sulfated GAGs can be accomplished using mass spectrometry, which has the advantages of high sensitivity and selectivity for structural characterization[10, 12, 13, 17, 18]. The complexity of these digest mixtures makes prior separation (on-line or off-line) desirable to facilitate analysis. Approaches for separating GAGs include high performance liquid chromatography (HPLC), hydrophilic interaction liquid chromatography (HILIC), and capillary zone electrophoresis (CZE). HPLC is an umbrella term that contains several different techniques based on the chosen column. Size exclusion (SEC), strong anion exchange (SAX), reversed phase ion pairing (RPIP), and graphitized carbon chromatography (GCC) are techniques that have been coupled to mass spectrometry for GAG analysis[19-22]. However, these techniques have disadvantages in comparison to CZE-MS. SEC and SAX utilize reagent cations at elevated concentrations that lead to ion suppression if not removed before MS analysis[23]. RPIP-LC-MS can lead to mass spectrometer contamination and may undermine

system performance. HILIC uses a polar stationary phase and mobile phases much like those used in reverse-phase separations, making it more compatible for GAG separations and MS analysis[24, 25]. Unfortunately, HILIC separations resolve components mostly by their degree of polymerization (dp), and do not provide much resolution for isomers[14, 16]. GCC offers adsorption based separation with very stable graphite columns allowing a multitude of conditions to be implemented, such as high temperatures, variable pH, and low salt content[19, 26, 27]. Previous work using HPLC and HILIC demonstrated the ability to separate GAGs up to dp14[20, 28]. Because of the highly ionic nature of sulfated GAG chains, CZE is a well-suited separation technique for this biomolecule class. Anionic biomolecules, such as oligonucleotides and metabolites, have been analyzed using CZE-MS for several years[29-33]. Despite this advantage, CZE-MS analysis of GAG oligosaccharides remains an under-developed approach. Much of the early GAG CZE literature focuses on normal mode polarity where a positive potential is applied to the capillary[34-36]. Using normal polarity, CZE separation of chondroitin sulfate, hyaluronic acid, keratan sulfate, heparan sulfate, and heparin; ranging from disaccharide to oligosaccharide length (up to dp20) has been demonstrated[37]. However, normal polarity is not well suited to the acidic nature of highly sulfated GAGs and generally leads to longer migration times (except with specific electrolytes) and low resolution[35, 36, 38]. Most of this work has been performed with optical detection and structural features cannot be assigned without the use of standards. Replacement of UV absorbance with MS detection is a logical progression; however, the electrolytes used during UV detection experiments are non-volatile and often incompatible with MS limiting the number of well understood electrolytes that can be employed[39-41]. The optimal CZE-MS configuration for GAG oligosaccharide analysis is reverse polarity with negative mode ionization. In reverse polarity CZE, a negative potential is applied to the capillary inlet, generating an electrophoretic

force which migrates negatively charged GAGs in the direction of the mass spectrometer. By using reverse polarity, the migration times of GAGs will decrease, and the sample peaks become narrower, improving resolution. A recent application of CZE-MS to GAGs has used reverse polarity CZE and negative mode MS detection[42]. This work focused on disaccharides and demonstrated fast and complete separations. Researchers have started to tackle larger oligosaccharides, which retain structural information, in an attempt to solve specific biological problems[37] and investigate common pharmaceuticals[43]. In addition to the electrophoretic force (EF), ions are also subject to an electroosmotic force (EOF). The EOF is driven by the bulk movement of solvated counterions near the inner surface of the capillary. With a conventional bare fused silica (BFS) capillary, the inner surface of the capillary presents silanol groups to the solution within the capillary. At neutral pH, the silanol groups are ionized, resulting in a negatively charged static layer which attracts cations from the background electrolyte (BGE) to create a positively charged mobile layer[44, 45]. With reverse polarity CZE in a BFS capillary, the EOF opposes the EF and results in longer migration times, peak broadening, and may cause some less ionized components to migrate away from the MS interface and not be detected. Modification of the surface of the fused silica capillary can alter its properties and either turn off EOF by creating a neutral surface or make a static positively-charged surface, which produces an EOF that moves in the same direction as the EF, thus reduces the migration time of the analytes[46, 47]. Prior work used dynamic coatings to create positive charge at the capillary inner surface[48, 49]. These are simple to implement, but the stability of such non-covalent coatings is an issue that can be improved upon. The present work focuses on the separation and detection of GAG oligosaccharide mixtures using reverse polarity CZE-MS. We have examined neutral and cation coated separation capillaries, using covalent modifications that are durable and stable.

These were tested and compared to BFS capillaries to optimize separation parameters for GAGs. Baseline characterization of each coating was performed with binary mixtures of typical modifications in GAGs. The optimized conditions were used to examine a complex mixture of GAG oligosaccharides with up to 12 saccharide subunits. Although demonstrated on a high-resolution MS system, the described methodology is amenable to most MS instrumentation.

3.3 EXPERIMENTAL

Materials

BFS capillaries (360 μm o.d. x 50 μm i.d.) were purchased from PolyMicro Technologies (Phoenix, AZ), and coated electrospray emitters (1.0 mm OD x 0.75 mm ID, E-BSCC1-750-1000-10μ-B30) were obtained from CMP Scientific (Brooklyn, NY). Coating reagents, dichlorodimethylsilane (DMS, Sigma-Aldrich, St. Louis, MO) and N-(6- aminohexyl) aminomethyltriethoxysilane (AHS, Gelest, Morrisville, PA) were prepared in toluene at 1% concentration. Ammonium acetate, formic acid, water, and methanol were HPLC grade (Fisher Scientific, Hampton, NH). Diethylamine, sodium hydroxide, concentrated hydrofluoric acid (~48% wt), acetone, and toluene were purchased from Sigma-Aldrich (St. Louis, MO). All solutions were filtered with 0.45 μm syringe filter (Millipore, Temecula, CA) before use.

GAG Standards

GAG oligosaccharides were prepared by enzymatic depolymerization and purified using strong anion exchange high-pressure liquid chromatography (SAX-HPLC) for samples 1–6 as

shown in Table 1[50]. Epimer pair heparan sulfate tetrasaccharides (Table 1, samples 7 GlcA-GlcNAc6S-IdoA-GlcNAc6S (GI) and 8 GlcA-GlcNAc6S-GlcA-GlcNAc6S (GG)) were chemically synthesized and purified as described in the literature[51]. Low molecular weight heparin, Enoxaparin, was from the USP (Rockville, MD). All samples were desalted with a 3 kDa Amicon Ultra centrifugal filter (Millipore, Temecula, CA) prior to separation and mass spectrometry analysis. Although the GAGs have molecular weights below 3kDa, heparan sulfate tetrasaccharides and larger chains do not pass through the 3kDa membrane. The membrane permeability is based on size and shape. GAGs have a linear structure compared to proteins which are often globular, and this makes GAGs behave as though they have a higher molecular weight to the centrifugal filter membrane. Filters were conditioned with water, and the sample was then washed with two filter volumes of water (14,000 × g for 25 min each). Before analysis, GAG samples were diluted to 5 µg/mL in water.

Table 1. GAG tetrasaccharide standards used in this study.

Tetrasaccharides	Structure Name	Molecular Weight (Da)	Structure
1	ΔUA2S-GlcNS6S-IdoA2S-GlcNS6S	1153.9427	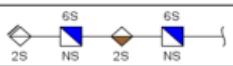
2	ΔUA2S-GlcNS6S-IdoA-GlcNAc6S	1036.0396	
3	ΔUA2S-GlcNS6S-IdoA-GlcNAc	914.0722	
4	ΔUA2S-GlcNS-IdoA-GlcNS6S	994.029	
5	ΔUA2S-GlcNS6S-IdoA2S-GlcNS	1073.9859	
6	ΔUA2S-GlcNS6S-IdoA-GlcNS6S	1073.9859	
7	GlcA-GlcNAc6S-IdoA-GlcNAc6S	936.1471	
8	GlcA-GlcNAc6S-GlcA-GlcNAc6S	936.1471	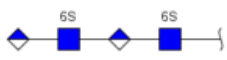

Coatings

Bare fused silica capillaries were etched with concentrated hydrofluoric acid (HF) at the distil end to reduce the outer diameter of the capillary for use in the sheath flow CE interface described below. For the etching process, the outlet of the capillary was placed in concentrated HF for 45–60 min. The capillary tip was then washed with copious amounts of water. The etched capillaries were coated with AHS to render a cation coated capillary and DMS for a neutral coated capillary. Coating solutions were prepared in toluene with 1% concentration of either AHS or DMS. To clean and prepare for coating, the capillary was rinsed with 0.1 M NaOH, water, methanol, dry acetone, and dry toluene, respectively, for 30 min each. The capillary was then coated by flowing 1% AHS or DMS for 1 h. The capillary was consecutively flushed with dry toluene, dry acetone, and methanol for 30 min to remove excess coating solution after coating. Finally, the capillary was equilibrated with background electrolyte buffer (BGE, 25 mM ammonium acetate 70% MeOH) for 1 h. Once degradation becomes apparent, BFS capillaries can be easily cleaned by flushing sodium hydroxide for a short time; however, the coatings are stripped in basic conditions and must be reapplied by repeating the coating procedure. In some experiments, 0.1–1% formic acid (FA) or 0.02– 0.1% diethylamine (DEA) was added to the BGE.

Instrumentation

Experiments were conducted on an Agilent HP 3D capillary electrophoresis instrument (Wilmington, DE). The total length of the capillary ranged from 52–54 cm, and its inner diameter was 50 μm with a volume of approximately 1 μL. The aqueous GAG sample was

injected for 3 s at 950 mbar followed by a BGE injection for 10 s at 10 mbar. The injected volume was 0.1 μL. The ionic strength of the injected sample plug is 2–3 orders of magnitude less than that of the background electrolyte, so sample stacking is expected under these conditions and provides a sharp sample front. The capillary was then placed into a BGE vial for separation. A separation voltage of -30 kV was applied to the capillary for most experiments. A separation voltage of −15 kV was used for selected experiments as identified in the results below. An EMASS-II (CMP Scientific, Brooklyn, NY) CE-MS interface was employed to couple the CE with a Thermo Scientific Velos Orbitrap Elite mass spectrometer (Bremen, Germany)[42, 52, 53]. The etched capillary outlet was nested inside of a cation coated glass emitter tip with a 30 μm tip orifice (CMP Scientific, Brooklyn, NY). The etched capillary was positioned 0.3–0.5 mm from the tip of the emitter orifice to create a mixing volume of ca. 15 nL, and the emitter tip was filled with sheath liquid (SL, 25 mM ammonium acetate 70% MeOH). An external power supply provided a nano-electrospray (nESI) voltage ranging from −1.7 to −1.85 kV to the emitter. MS detection was performed in negative ion mode. Prior to CZE-MS experiments, a semi-automatic optimization of source parameters was performed using sucrose octasulfate to improve sensitivity of sulfated GAGs and reduce sulfate loss during MS analysis. The Orbitrap was scanned from m/z 150–2000 for GAG oligosaccharides with a specified resolution of 120,000. Optimal conditions resulted when the S-lens RF level, multipole 00 offset, and lens 0 were set at 6 %, 7.20 V, and 8.50 V, respectively.

3.4 RESULTS AND DISCUSSION

In capillary zone electrophoresis of mixtures, EF provides component separation due to differences in their mobilities. In contrast, EOF causes an analyte-independent migration of all components. The magnitude and direction of the EOF with respect to the EF depends upon the chemical nature of the separation capillary's inner surface. In an uncoated BFS capillary, with a background electrolyte solution (BGE) of 25 mM ammonium acetate (pH = 7.5) in 70% methanol, a static layer of negatively-charged silanol groups are presented at the inner wall of the capillary. These interact with the BGE to create a mobile layer of solvated positive ions. With reverse-polarity CZE, this mobile layer is attracted by the negative potential at the entrance of the separation capillary. This creates an EOF that opposes the EF for negatively charged analytes. In the case of highly-charged GAG oligosaccharide anions, the EF is greater than the EOF, so sample migrates toward the mass spectrometer interface. However, with EOF moving in the opposite direction, sample migration through the BFS capillary is slowed and results in increased migration times.

We have examined coated capillaries that either eliminate the EOF or reverse it so that it aligns with the EF to optimize the separation of GAG oligosaccharides. After optimization, migration time and peak widths are reduced while the peak capacity remains the same compared to prior work with BFS capillaries. Two different coatings, dichlorodimethylsilane (DMS) and *N*-(6-aminohexyl) aminomethyltriethoxysilane (AHS), were examined. Fig. 1 compares the direction of EF and EOF for BFS, with that of capillaries with neutral (DMS) and cationic (AHS) coatings that were examined for this study.

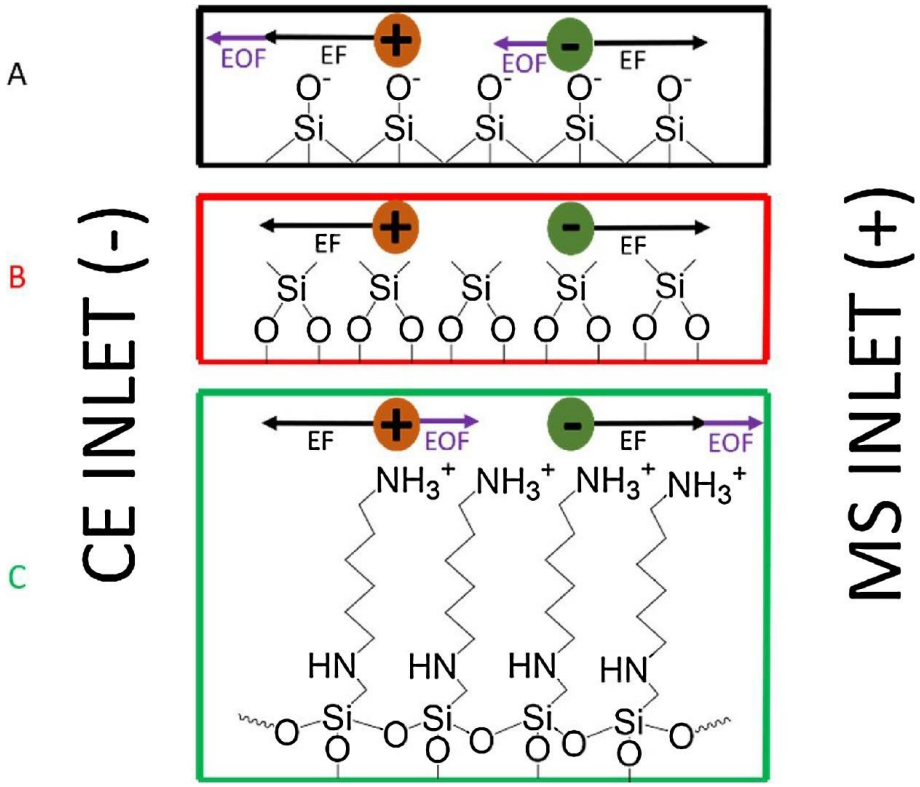

Figure 3.1. Diagram depicting the forces of the electroosmotic flow (EOF) and electrophoretic forces (EF) that act on analytes during a CZE-MS experiment with three different inner capillary sufaces: (A) Bare fused silica (BFS), (B) DMS coated, and (C) AHS coated.

For DMS and AHS capillaries, the reagent forms a covalent ether linkage to silica at the surface of the inner wall of the capillary and produces a durable and stable layer. These fused silica surface modifications have been used by others for nanoparticle modification, protein immobilization supports, and other applications[54-56]. Non-covalent coating methods (also known as dynamic coating) are easier to implement than covalent coating, but the coating can dissociate from the inner surface over time. In our hands, when bovine serum albumin (BSA) is utilized as a non-covalent coating, a cation surface is produced on the inner surface of the capillary but is unstable over time and often leads to plug formation within the capillary as the coating degrades. As shown in Fig. 2, the covalently linked coatings are more durable than the BSA-coated

capillaries. After 81 run iterations on a BSA capillary, degradation of the BSA coating caused plug formation and prevented further trials. The AHS and DMS coated capillaries are found to be quite stable, and the coating hydrolyzes slowly under the separation conditions with a very modest change in migration time from run to run. Furthermore, they do not lead to column plugging, and therefore can be refreshed by reapplication of the coating. In contrast, the BSA-coated capillaries often become plugged by desorbed protein after several runs.

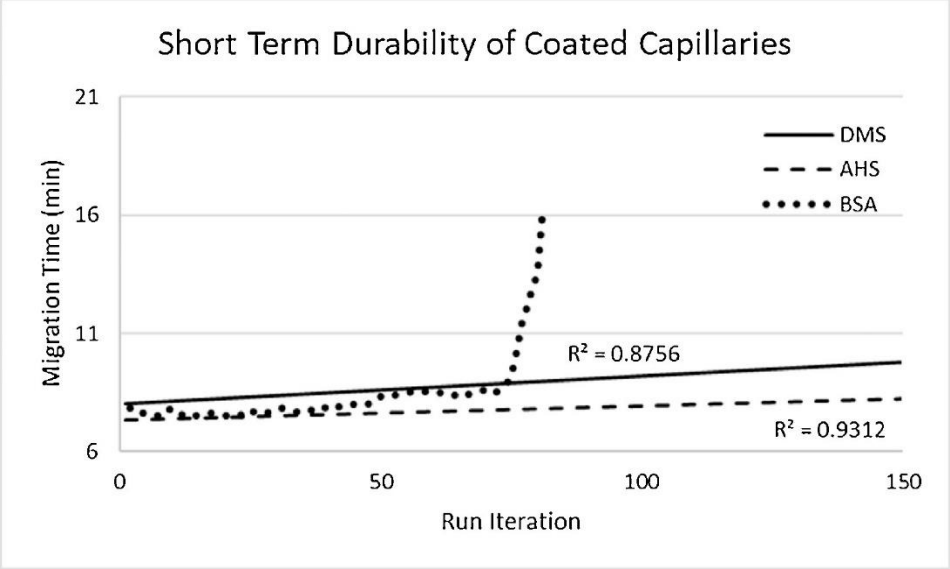

Figure 3.2. Short term durability of neutral (DMS, solid line) and cation (AHS, dashed line; BSA, circle dashed line) coated capillaries shown using sample 1 across 150 iterations. The BSA trial was terminated after 81 iterations due to coating failure.

With a DMS-coated capillary, silanols are capped by neutral methyl groups. This eliminates the EOF in normal and reverse polarity and analytes migrate only under the influence of EF. For negatively charged analytes under reverse-polarity conditions, the sample is expected to migrate through the capillary faster than in an uncoated BFS capillary. The AHS coated capillary will have an EOF that aligns with the EF for negatively charged analytes in reverse-

polarity CZE and should exhibit even faster migration. Multiple amino silane reagents were considered, such as 3-aminopropyltriethoxysilane and *N*-(2-aminoethyl)-3-aminopropyltriethoxysilane. However, AHS was shown to be the most stable coating reagent because its chain length prevents hydrolysis by self-cyclization[54]. Short term durability tests demonstrated that covalent coatings are stable in optimized conditions (Fig. 2), but long-term use showed signs of degradation in DMS-coated capillaries. Both coatings degrade in high pH conditions (pH > 12).

Tetrasaccharide standards that contain common variations in GAG structure were used to test the efficacy of the coatings. A mixture of tetrasaccharides that differ in the number of sulfate modifications, ranging from 3 to 6 (samples 1–3), was analyzed first. Fig. 3 compares the CZE migration profiles (base peak chromatogram) for this GAG tetrasaccharide mixture obtained with BFS, DMS, and AHS coatings on capillaries of similar length and identical experimental conditions. Sample 1 migrates through all of the capillaries first due to the higher number of sulfates present (six) compared to samples 2 and 3 with four and three sulfates, respectively. As expected from the EOF behavior described above, the compounds migrate most rapidly with the AHS capillary and slowest with a BFS capillary. The peaks are narrowest with the AHS capillary, as longitudinal diffusion of a sample band increases linearly with its migration time. For sample 1, the peak widths at 50% peak height (FWHM) were 1.14, 0.49, and 0.2 min for BFS, DMS, and AHS capillaries, respectively. With a decrease in peak width, the sensitivity (limit of detection of 50 ng/mL) was improved using the AHS capillary and optimized experimental conditions. Shortened migration and reduced peak width were achieved with reverse polarity CZE on a cation coated capillary.

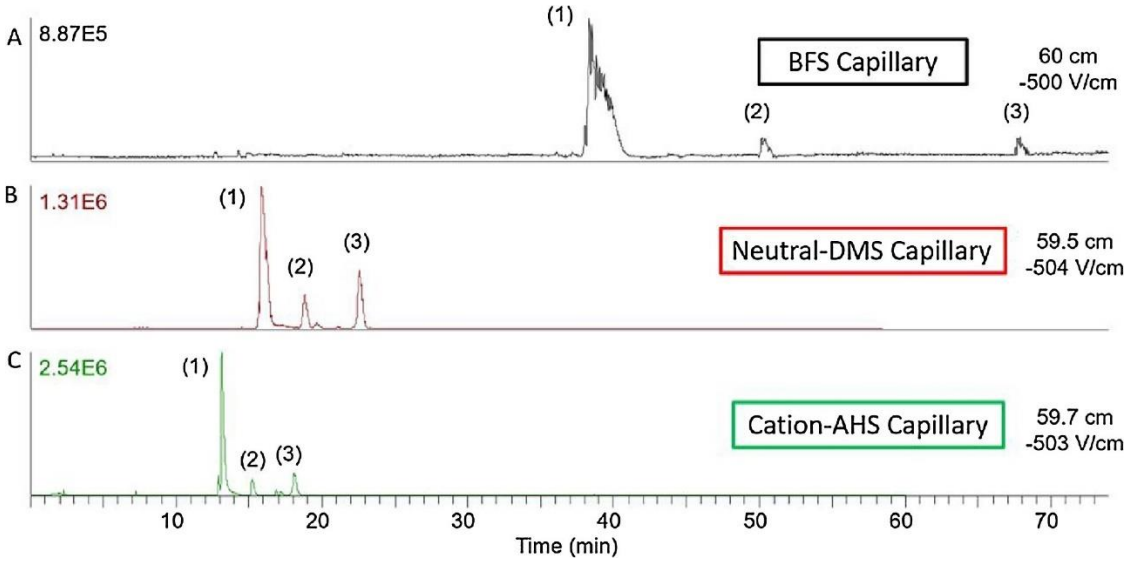

Figure 3.3. Electropherogram comparison of migration times based on different capillary coatings. Samples (1), (2), and (3) are tetrasaccharides with different numbers of sulfates. Sample (1) contains six sulfates, (2) has four sulfates, and (3) has three sulfates. Significant improvement in migration time and peak width is observed with neutral (DMS) and cation coated (AHS) capillaries.

Next, compounds that contain single point variations in structure and produced mixtures of increasing separation difficulty were analyzed. Two GAG tetrasaccharides with different amino modifications, samples 4 and 2 (Table 1), were investigated. These tetrasaccharides have the same number of sulfate modifications, but one has an *N*-sulfo modification on the fourth residue; whereas, the other tetrasaccharide contains an *N*-acetyl group. Using reverse polarity CZE-MS on an AHS capillary, these tetrasaccharides are baseline separated in less than 20 min with approximately 2.5 min between the peaks. The FWHM for the peaks are 13.8 s (sample 4) and 15 s (sample 2). When compared with the DMS and BFS capillaries, the FWHM for the AHS capillary was reduced by a factor of two (DMS) or three (BFS). The two components of

this mixture differ in composition by (*O*-sulfo + *N*-acetyl) versus (OH + *N*-sulfo), evidenced by the 42 Da difference in their mass spectra, shown in panels B and C of Fig. 4.

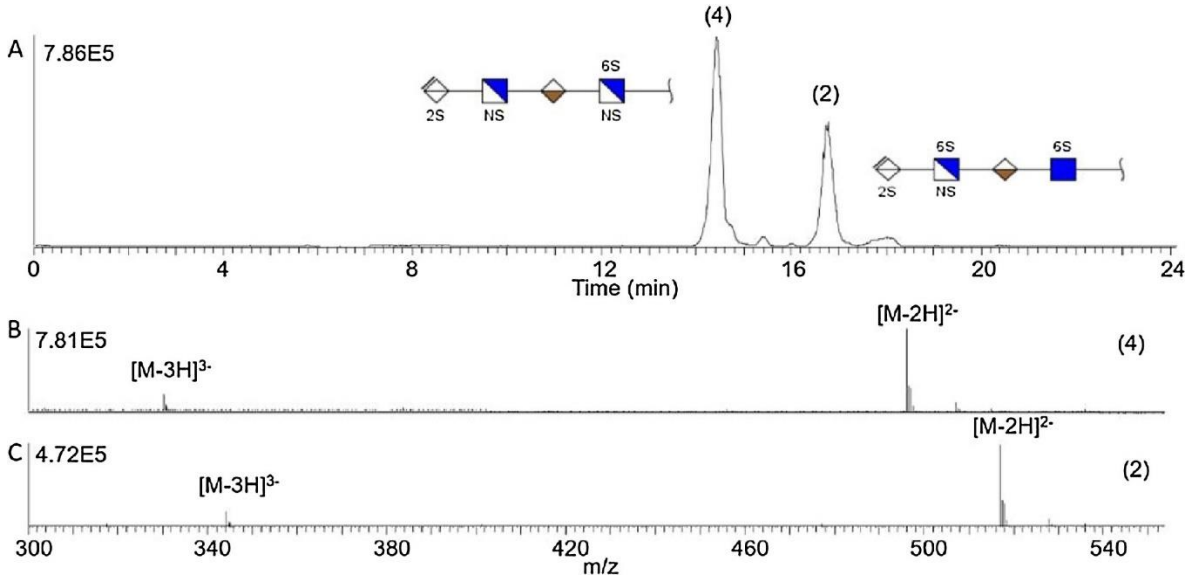

Figure 3.4. A) Baseline separation of tetrasaccharide mixture containing samples 4 and 2 with different amino modifications. Mass spectrum of sample 4 (B) and 2 (C) showing the mass difference due to amino modification.

A more challenging test are the isomeric tetrasaccharides, samples 5 and 6. The analyte structures are closely related and vary only in the position of one of the five sulfate modifications. Fig. 5 shows the separation of this isomer pair (samples 5 and 6) using an AHS coated capillary, with baseline separation of the peaks. As these are positional isomers, their mass spectra are identical, and exhibit double, triple, and quadruple-charged molecular ions, as shown in the lower panel of Fig. 5, for sample 5.

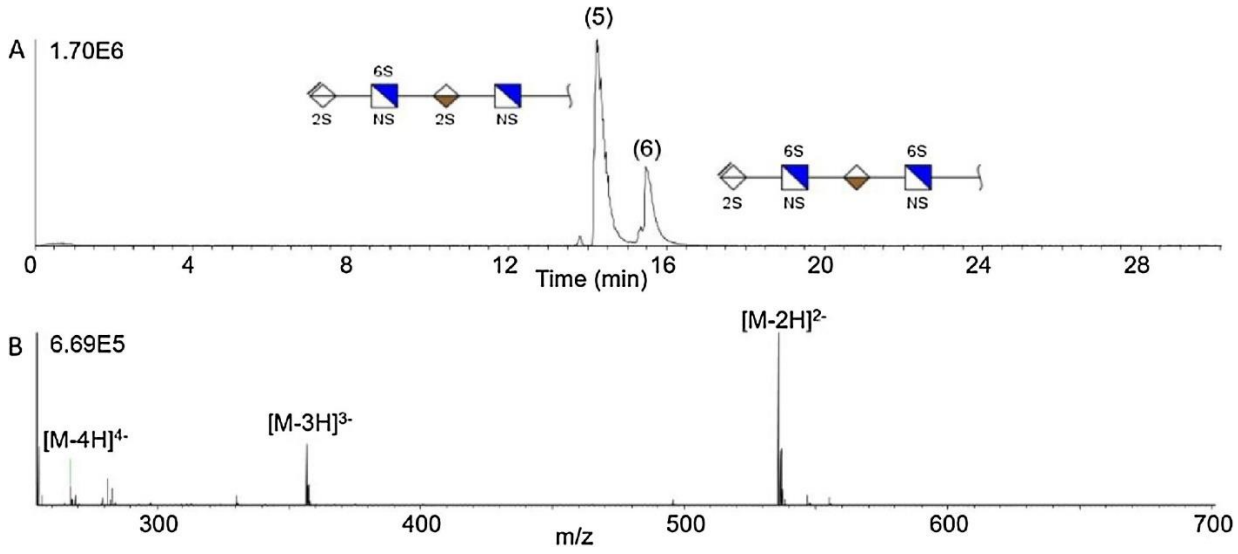

Figure 3.5. (A) Baseline CZE separation of a tetrasaccharide mixture on AHS capillary. Sample 5 and 6 are isomers with the same number of sulfate groups and exact mass but differ in sulfate position on the last two sugar residues. (B) Mass spectrum of sample 5 demonstrating the observed charge state distribution.

The most challenging analysis that often arises in GAG characterization using MS is the differentiation of stereoisomeric compounds arising from epimerization of uronic acids (GlcA vs. IdoA). We examined such a mixture of epimers, and the results are shown in Fig. 6, for samples 7 (GI) and 8 (GG). These GAG tetrasaccharides vary only by the C-5 stereochemistry of the uronic acid near the reducing end. With reverse polarity CZE-MS on an AHS capillary, the two epimers are well separated. The early migrating peak, GI, exhibits a distinct shoulder. A similar result was found using differential ion mobility of these same compounds and was attributed to anomeric nature of the reducing end[57]. The rate of mutarotation of the anomeric carbon is slow compared to the migration time in CZE, so this is a plausible cause of the extra peak in the sample. The lower panel in Fig. 6 shows the mass spectrum of GI which is identical to that of

GG (spectrum not shown). Since these are stereoisomers, all of the peaks in the electropherogram, including the shoulder, produce similar ESI mass spectra.

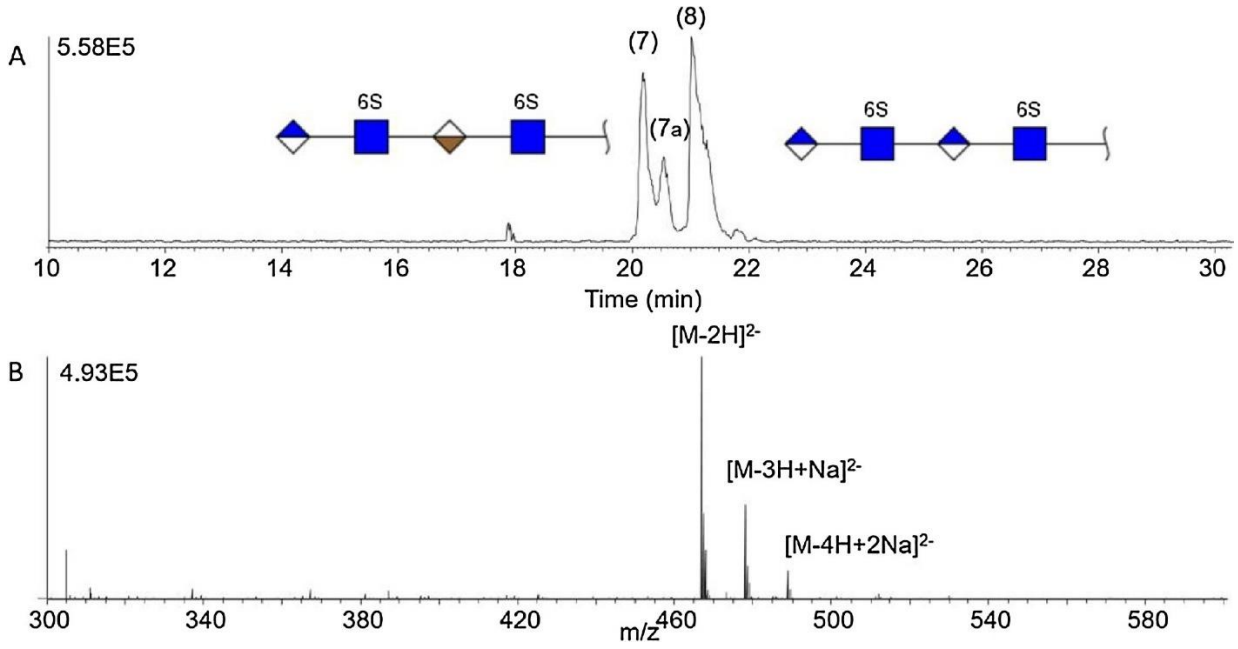

Figure 3.6. Baseline separation of a stereoisomer mixture (samples 7 and 8) on AHS capillary. Sample 7 migrates first followed by sample 8. The peak labeled 7a is attributed to an anomeric form of sample 7.

Enoxaparin, a pharmaceutical product produced by alkaline depolymerization of heparin into low molecular weight components, was also analyzed using reverse polarity CZE and negative ion mode mass spectrometry. Others have analyzed Enoxaparin using on-line separations and mass spectrometry detection[14, 23, 58-60]. This sample is known to be a complex mixture of oligosaccharides varying in degree of polymerization (dp) from dp 3 to dp 20. Fig. 7A shows an ESI mass spectrum of the sample without any prior separation, demonstrating the

innate complexity of this sample. Base peak electropherograms obtained using BFS, DMS, and AHS capillaries are shown Fig. 7B. Enoxaparin migrates more quickly through the capillary on the cation coated capillary (AHS) compared to the neutral and uncoated capillaries.

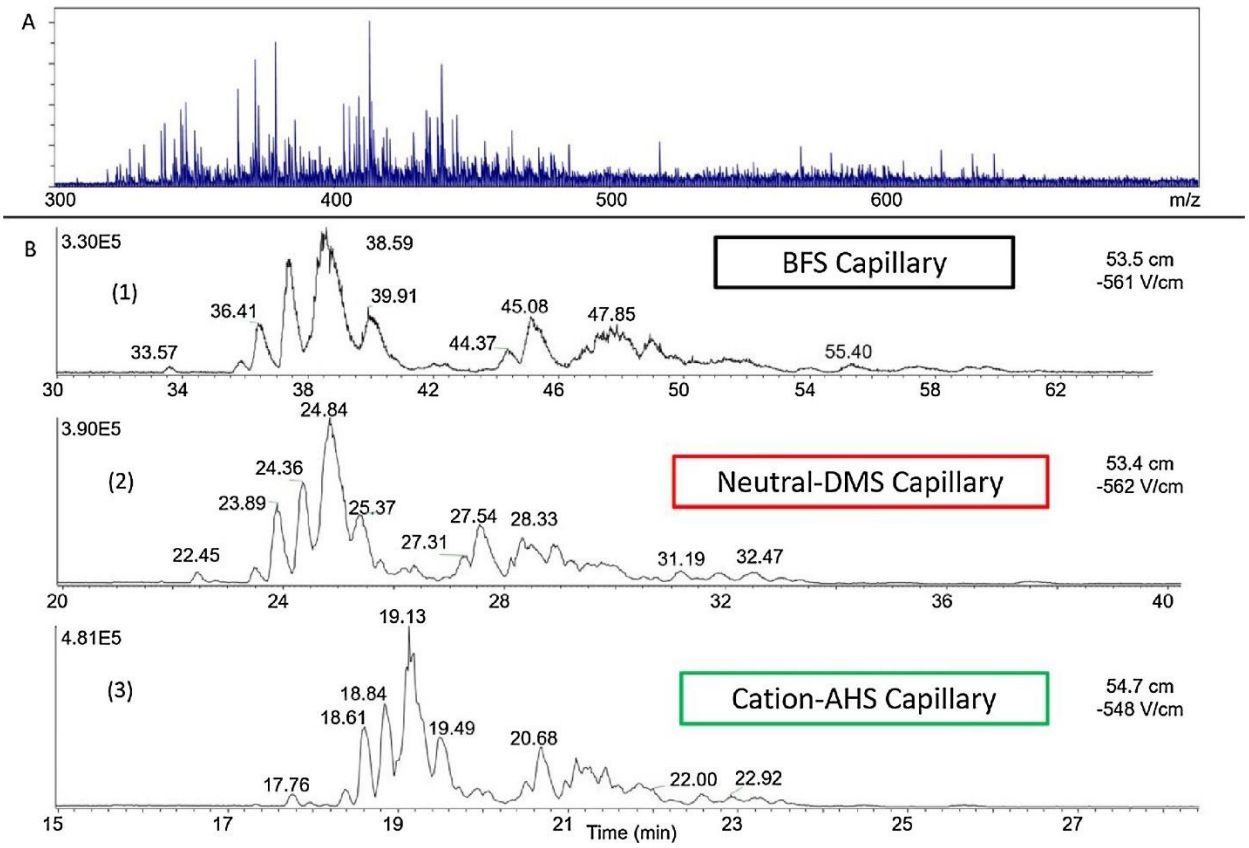

Figure 3.7. A) Mass spectrum of Enoxaparin (LMWH) without separation. B) separation windows of Enoxaparin on uncoated and coated capillaries: (1) BFS, (2) DMS, and (3) AHS with migration times decreasing from 1 to 3. The presented migration time window varies between panels 1-3 to enable comparison.

Although the migration time decreases for the coated capillaries, peaks are not lost. The peaks become narrower when using coated capillaries, as shown previously with the tetrasaccharide mixtures, but they exhibit the same features as the BFS separation. This is a highly complex mixture, and we do not obtain baseline separation of all components.

Nevertheless, the mass spectra obtained at any time point is highly simplified compared to the unseparated sample, and we can evaluate the components that are present. Oligosaccharides ranging from dp 3 to dp 12 were detected with a range of 4–17 sulfo groups present on the GAGs. The neutral masses extend from 753 to 3301 Da with less than 3.5 ppm error for the assigned compositions. Shorter oligosaccharides migrate through the capillary first and the GAG chain length increases over the migration period. The majority of the chains were dp 4 to dp 8 which is expected for the Enoxaparin mixture. Toward the end of the separation, dp 10 to dp 12 are observed in low intensity.

Sodium and ammonia adducts were also assigned for approximately half of the compositions. Sodium adducts are expected because Enoxaparin is manufactured as a sodium salt. The appearance of ammonia adducts can be explained by the choice of an ammonium acetate BGE. A supplemental list of all 83 unique compositions that were identified using the AHS capillary is included (Supp. Table 1).

While optimizing conditions for reverse polarity CZE with negative ionization mode MS, the use of background electrolyte solution (BGE) additives was explored. The role of pH can play a vital part in the extent of separation achieved based on the applied coating. EOF is directly influenced by the pH range of the BGE on capillaries that have a charge on the inner surface of the capillary. The neutral DMS capillary will not be affected by the pH of the BGE because the EOF is eliminated.

Formic acid (FA) and diethylamine (DEA) were used to adjust the pH to lower and higher values during separation, respectively. These reagents were selected for their volatility, which makes them compatible with on-line CZE-MS analysis. Acetic acid and formic acid were both tested as an additive to the BGE and sheath liquid. Using formic acid reduced the amount of

chemical background in the MS which improved the signal to noise ratio compared to acetic acid. Table 2 shows the effect of different BGE additives on the pH of the BGE. Without any additive, a BGE consisting of 25 mM ammonium acetate in 70% MeOH has a pH of 7.5. By adding FA to a concentration of 0.5%, the pH is reduced to 4.2. Conversely, with addition of 0.4% DEA into the BGE, the pH increases to 10.1.

Table 2. Effect of BGE additive on pH.

BGE Additive	pH
0.5% FA	4.2
0.4% FA	4.3
0.3% FA	4.6
0.2% FA	4.8
0.1% FA	5.3
None	7.5
0.05% DEA	8.3
0.1% DEA	8.8
0.2% DEA	9.3
0.3% DEA	9.9
0.4% DEA	10.1

BGE: 25 mM ammonium acetate 70% MeOH.

For the AHS cation coated capillary, increasing the pH of the BGE reduces ionization of the modified surface of the capillary, reduces EOF, and results in longer migration times. In Fig. 8, a mixture of tetrasaccharides containing an increasing number of sulfate groups, ranging from 3 to 6 sulfate groups (samples 1–3, and 6), is separated using 25 mM ammonium acetate in 70% MeOH with the addition of FA in the top electropherogram and DEA in the bottom electropherogram. The middle electropherogram is the separation in normal BGE without any

pH adjustment. FA reduces the migration time and suppresses sodium adducts in the mass spectrum but does not affect the observed charge state. It also decreases the peak width in the electropherogram. The FWHM for sample 1 is reduced to 16 s using 0.1% FA compared to a FWHM of 22 s without any additive. In contrast, DEA increases migration times and the charge states of the ions of interest in the mass spectrum. As one would expect, DEA increases the peak width. For samples that migrate slower through the capillary, the peak widths increase. Peak broadening is diminished for samples that migrate faster through the capillary. Comparison of sample 1 with or without DEA, the FWHM slightly increases from 21 to 22 s. However, for samples 2 and 3, the FWHM changed from 30 to 85.2 s and 22–28 s with the addition of 0.05% DEA, respectively. Overall, lower pH decreases migration time, while, higher pH increases migration time on an AHS cation coated capillary.

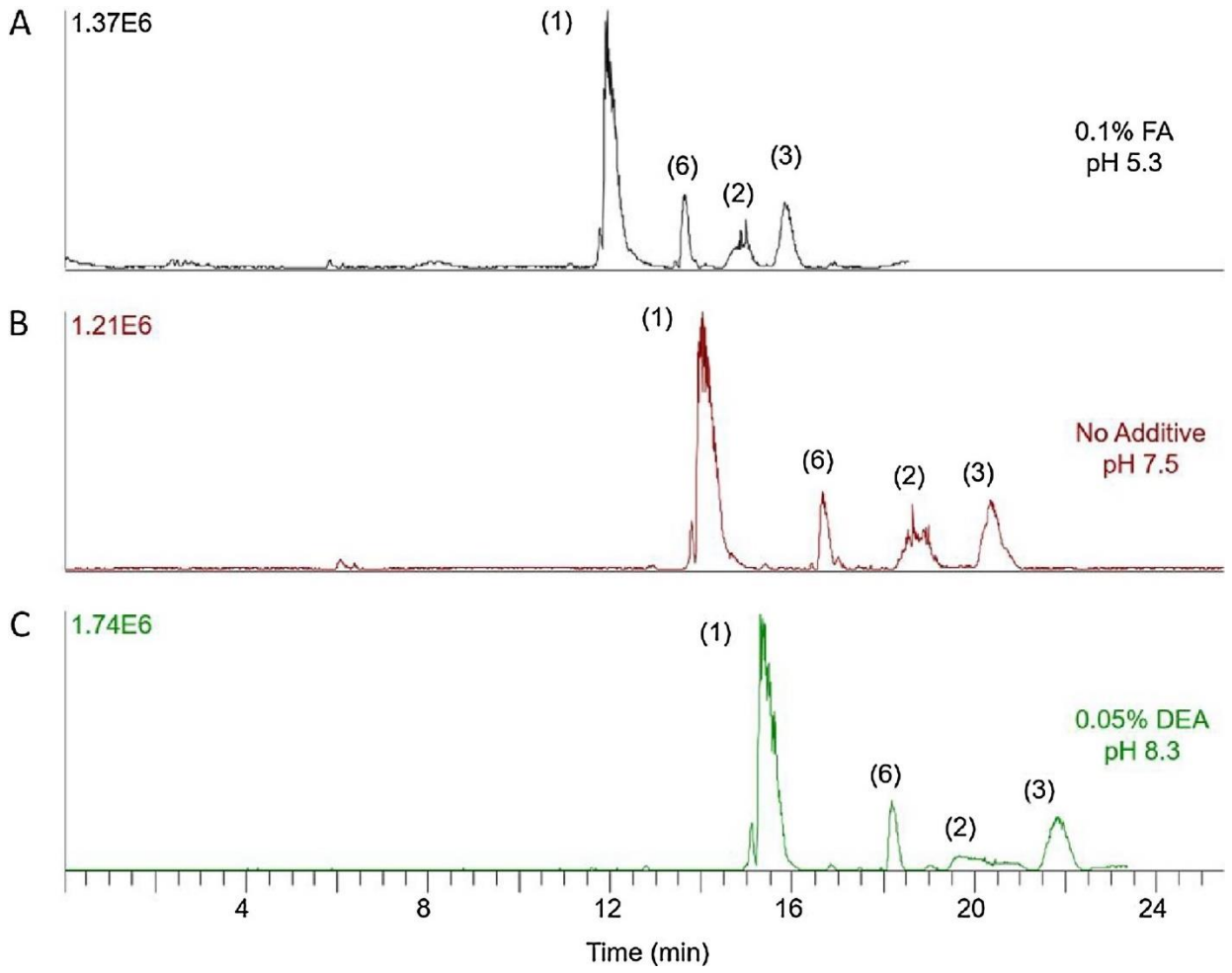

Figure 3.8. Effect of additives on four tetrasaccharide standards with an increasing number of sulfates (samples 1-3 and 6) through and AHS coated capillary. The pH of BGE in AHS coated capillaries modulates migration time. Lower pH, from addition of formic acid, leads to faster migration, and higher pH, from diethylamine, leads to slower migration.

3.5 CONCLUSIONS

In this work, the advantages of using different coated capillaries with reverse polarity CZE-MS separations were demonstrated on oligosaccharide mixtures larger than disaccharides. Standard uncoated, neutral coated, and cation coated capillaries were investigated to determine suitable CZE-MS conditions for sulfated glycosaminoglycans.

Covalently coated capillaries were implemented through simple chemical reactions with silane reagents.

Using a cation coated capillary, structurally similar sulfated GAG oligosaccharides and complex mixtures were separated and analyzed with CZE-MS in a fast and reproducible manner. Positional isomers and stereoisomer tetrasaccharides were baseline separated. Although Enoxaparin was not baseline separated, the mass spectra were significantly simplified and would facilitate tandem mass spectrometry of the various components in this mixture. By incorporating a covalent cation coating, the migration time and peak widths were reduced while increasing the analytically useful lifetime of the separation capillary. Through the use of additives, the charge state distribution and migration time can be altered based on pH of the BGE. Future work will extend this method to incorporate tandem mass spectrometry for online sequence analysis of sulfated GAGs.

3.6 REFERENCES

1. Varki, A., Biological roles of glycans. *Glycobiology* **2017,** *27* (1), 3-49.

2. Afratis, N.; Gialeli, C.; Nikitovic, D.; Tsegenidis, T.; Karousou, E.; Theocharis, A. D.; Pavão, M. S.; Tzanakakis, G. N.; Karamanos, N. K., Glycosaminoglycans: key players in cancer cell biology and treatment. *The FEBS Journal* **2012,** *279* (7), 1177-1197.

3. Barbucci, R.; Magnani, A.; Lamponi, S.; Albanese, A., Chemistry and biology of glycosaminoglycans in blood coagulation. *Polymers for Advanced Technologies* **1996,** *7* (8), 675-685.

4. Sasisekharan, R.; Shriver, Z.; Venkataraman, G.; Narayanasami, U., Roles of heparan-sulphate glycosaminoglycans in cancer. *Nature Reviews Cancer* **2002,** *2* (7), 521-528.

5. Varki, A.; Cummings, R. D.; Esko, J. D.; Freeze, H. H.; Stanley, P.; Bertozzi, C. R.; Hart, G. W.; Etzler, M. E., *Essentials of Glycobiology*. NY, 2009; Vol. 2.

6. Xiao, Z.; Zhao, W.; Yang, B.; Zhang, Z.; Guan, H.; Linhardt, R. J., Heparinase 1 selectivity for the 3,6-di-O-sulfo-2-deoxy-2-sulfamido-α-D-glucopyranose (1,4) 2-O-sulfo-α-L-idopyranosyluronic acid (GlcNS3S6S-IdoA2S) linkages. *Glycobiology* **2010,** *21* (1), 13-22.

7. Wolff, J. J.; Laremore, T. N.; Busch, A. M.; Linhardt, R. J.; Amster, I. J., Electron detachment dissociation of dermatan sulfate oligosaccharides. *J Am Soc Mass Spectrom* **2008,** *19* (2), 294-304.

8. Wolff, J. J.; Amster, I. J.; Chi, L.; Linhardt, R. J., Electron detachment dissociation of glycosaminoglycan tetrasaccharides. *J Am Soc Mass Spectrom* **2007,** *18* (2), 234-44.

9. Leach, F. E.; Wolff, J. J.; Xiao, Z.; Ly, M.; Laremore, T. N.; Arungundram, S.; Al-Mafraji, K.; Venot, A.; Boons, G.-J.; Linhardt, R. J.; Amster, I. J., Negative electron transfer dissociation Fourier transform mass spectrometry of glycosaminoglycan carbohydrates. *European Journal of Mass Spectrometry (Chichester, England)* **2011,** *17* (2), 167-176.

10. Laremore, T. N.; Leach, F. E.; Solakyildirim, K.; Amster, I. J.; Linhardt, R. J., Glycosaminoglycan Characterization by Electrospray Ionization Mass Spectrometry Including Fourier Transform Mass Spectrometry. *Methods in enzymology* **2010,** *478*, 79-108.

11. Bielik, A. M.; Zaia, J., Multistage tandem mass spectrometry of chondroitin sulfate and dermatan sulfate. *Int J Mass Spectrom* **2011,** *305* (2-3), 131-137.

12. Zaia, J.; Costello, C. E., Compositional Analysis of Glycosaminoglycans by Electrospray Mass Spectrometry. *Analytical Chemistry* **2001,** *73* (2), 233-239.

13. Zaia, J.; Costello, C. E., Tandem Mass Spectrometry of Sulfated Heparin-Like Glycosaminoglycan Oligosaccharides. *Analytical Chemistry* **2003,** *75* (10), 2445-2455.

14. Li, G.; Steppich, J.; Wang, Z.; Sun, Y.; Xue, C.; Linhardt, R. J.; Li, L., Bottom-Up Low Molecular Weight Heparin Analysis Using Liquid Chromatography-Fourier Transform Mass Spectrometry for Extensive Characterization. *Analytical Chemistry* **2014,** *86* (13), 6626-6632.

15. Ly, M.; Leach Iii, F. E.; Laremore, T. N.; Toida, T.; Amster, I. J.; Linhardt, R. J., The proteoglycan bikunin has a defined sequence. *Nature Chemical Biology* **2011,** *7*, 827.

16. Li, L.; Zhang, F.; Zaia, J.; Linhardt, R. J., Top-Down Approach for the Direct Characterization of Low Molecular Weight Heparins Using LC-FT-MS. *Analytical Chemistry* **2012,** *84* (20), 8822-8829.

17. Chi, L.; Amster, J.; Linhardt, R. J., Mass Spectrometry for the Analysis of Highly Charged Sulfated Carbohydrates. *Current Analytical Chemistry* **2005,** *1* (3), 223-240.

18. Laremore, T. N.; Zhang, F.; Dordick, J. S.; Liu, J.; Linhardt, R. J., Recent progress and applications in glycosaminoglycan and heparin research. *Current Opinion in Chemical Biology* **2009,** *13* (5), 633-640.

19. Zaia, J., On-line separations combined with MS for analysis of glycosaminoglycans. *Mass Spectrometry Reviews* **2009,** *28* (2), 254-272.

20. Volpi, N.; Galeotti, F.; Yang, B.; Linhardt, R. J., Analysis of glycosaminoglycan-derived, precolumn, 2-aminoacridone–labeled disaccharides with LC-fluorescence and LC-MS detection. *Nat Protoc* **2014,** *9*, 541.

21. Huang, Y.; Shi, X.; Yu, X.; Leymarie, N.; Staples, G. O.; Yin, H.; Killeen, K.; Zaia, J., Improved liquid chromatography-MS/MS of heparan sulfate oligosaccharides via chip-based pulsed makeup flow. *Anal Chem* **2011,** *83* (21), 8222-9.

22. Huang, R.; Liu, J.; Sharp, J. S., An Approach for Separation and Complete Structural Sequencing of Heparin/Heparan Sulfate-like Oligosaccharides. *Analytical Chemistry* **2013,** *85* (12), 5787-5795.

23. Zaia, J.; Khatri, K.; Klein, J.; Shao, C.; Sheng, Y.; Viner, R., Complete Molecular Weight Profiling of Low-Molecular Weight Heparins Using Size Exclusion Chromatography-Ion Suppressor-High-Resolution Mass Spectrometry. *Analytical Chemistry* **2016,** *88* (21), 10654-10660.

24. Gill, V. L.; Aich, U.; Rao, S.; Pohl, C.; Zaia, J., Disaccharide Analysis of Glycosaminoglycans Using Hydrophilic Interaction Chromatography and Mass Spectrometry. *Analytical Chemistry* **2013,** *85* (2), 1138-1145.

25. Buszewski, B.; Noga, S., Hydrophilic interaction liquid chromatography (HILIC)--a powerful separation technique. *Analytical and bioanalytical chemistry* **2012,** *402* (1), 231-247.

26. Pereira, L., Porous Graphitic Carbon as a Stationary Phase in HPLC: Theory and Applications. *Journal of Liquid Chromatography & Related Technologies* **2008,** *31* (11-12), 1687-1731.

27. Ruhaak, L. R.; Deelder, A. M.; Wuhrer, M., Oligosaccharide analysis by graphitized carbon liquid chromatography-mass spectrometry. *Anal. Bioanal. Chem.* **2009,** *394* (1), 163-74.

28. Karlsson, N. G.; Schulz, B. L.; Packer, N. H.; Whitelock, J. M., Use of graphitised carbon negative ion LC–MS to analyse enzymatically digested glycosaminoglycans. *Journal of Chromatography B* **2005,** *824* (1), 139-147.

29. Durney, B. C.; Crihfield, C. L.; Holland, L. A., Capillary electrophoresis applied to DNA: determining and harnessing sequence and structure to advance bioanalyses (2009-2014). *Analytical and bioanalytical chemistry* **2015,** *407* (23), 6923-6938.

30. Soga, T.; Igarashi, K.; Ito, C.; Mizobuchi, K.; Zimmermann, H.-P.; Tomita, M., Metabolomic Profiling of Anionic Metabolites by Capillary Electrophoresis Mass Spectrometry. *Analytical Chemistry* **2009,** *81* (15), 6165-6174.

31. Hirayama, A.; Wakayama, M.; Soga, T., Metabolome analysis based on capillary electrophoresis-mass spectrometry. *TrAC Trends in Analytical Chemistry* **2014,** *61*, 215-222.

32. Karabiber, F.; McGinnis, J. L.; Favorov, O. V.; Weeks, K. M., QuShape: rapid, accurate, and best-practices quantification of nucleic acid probing information, resolved by capillary electrophoresis. *RNA* **2013,** *19* (1), 63-73.

33. Heller, C.; Slater, G. W.; Mayer, P.; Dovichi, N.; Pinto, D.; Viovy, J.-L.; Drouin, G., Free-solution electrophoresis of DNA. *Journal of Chromatography A* **1998,** *806* (1), 113-121.

34. Prabhakar, V.; Capila, I.; Sasisekharan, R., The Structural Elucidation of Glycosaminoglycans. In *Glycomics: Methods and Protocols*, Packer, N. H.; Karlsson, N. G., Eds. Humana Press: Totowa, NJ, 2009; pp 147-156.

35. Volpi, N.; Maccari, F.; Linhardt, R. J., Capillary electrophoresis of complex natural polysaccharides. *Electrophoresis* **2008,** *29* (15), 3095-3106.

36. Campa, C.; Coslovi, A.; Flamigni, A.; Rossi, M., Overview on advances in capillary electrophoresis-mass spectrometry of carbohydrates: A tabulated review. *Electrophoresis* **2006,** *27* (11), 2027-2050.

37. Zamfir, A. D., Applications of capillary electrophoresis electrospray ionization mass spectrometry in glycosaminoglycan analysis. *Electrophoresis* **2016,** *37* (7-8), 973-986.

38. Sun, X., Capillary electrophoresis–mass spectrometry for the analysis of heparin oligosaccharides and low molecular weight heparin. *Analytical chemistry* **2016,** *88* (3), 1937.

39. Ampofo, S. A., Disaccharide compositional analysis of heparin and heparan sulfate using capillary zone electrophoresis. *Analytical biochemistry* **1991,** *199* (2), 249.

40. Mitropoulou, T. N.; Lamari, F.; Syrokou, A.; Hjerpe, A.; Karamanos, N. K., Identification of oligomeric domains within dermatan sulfate chains using differential enzymic treatments, derivatization with 2-aminoacridone and capillary electrophoresis. *Electrophorsis* **2001,** *22* (12), 2458-2463.

41. Toida, T.; Linhardt, R. J., Detection of glycosaminoglycans as a copper (II) complex in capillary electrophoresis. *Electrophoresis* **1996,** *17* (2), 341-346.

42. Lin, L.; Liu, X.; Zhang, F.; Chi, L.; Amster, I. J.; Leach, F. E.; Xia, Q.; Linhardt, R. J., Analysis of heparin oligosaccharides by capillary electrophoresis-negative-ion electrospray ionization mass spectrometry. *Anal. Bioanal. Chem.* **2017,** *409* (2), 411-420.

43. Lin, L.; Liu, X.; Zhang, F.; Chi, L.; Amster, I. J.; Leach, F. E.; Xia, Q.; Linhardt, R. J., Analysis of heparin oligosaccharides by capillary electrophoresis–negative-ion electrospray ionization mass spectrometry. *Analytical and Bioanalytical Chemistry* **2017,** *409* (2), 411-420.

44. Shintani, H., *Handbook of capillary electrophoresis applications*. Springer Science & Business Media: 2012.

45. Kuhn, R.; Hoffstetter-Kuhn, S., *Capillary electrophoresis: principles and practice*. Springer Science & Business Media: 2013.

46. Whatley, H., Basic Principles and Modes of Capillary Electrophoresis. In *Clinical and Forensic Applications of Capillary Electrophoresis*, Petersen, J. R.; Mohammad, A. A., Eds. Humana Press: Totowa, NJ, 2001; pp 21-58.

47. Grossman, P. D.; Colburn, J. C., *Capillary electrophoresis: Theory and practice*. Academic Press: 2012.

48. Man, Y.; Lv, X.; Iqbal, J.; Jia, F.; Xiao, P.; Hasan, M.; Li, Q.; Dai, R.; Geng, L.; Qing, H.; Deng, Y., Adsorptive BSA Coating Method for CE to Separate Basic Proteins. *Chromatographia* **2013,** *76* (1), 59-65.

49. Chang, W. W.; Hobson, C.; Bomberger, D. C.; Schneider, L. V., Rapid separation of protein isoforms by capillary zone electrophoresis with new dynamic coatings. *Electrophoresis* **2005,** *26* (11), 2179-2186.

50. Singh, A.; Kett, W. C.; Severin, I. C.; Agyekum, I.; Duan, J.; Amster, I. J.; Proudfoot, A. E. I.; Coombe, D. R.; Woods, R. J., The Interaction of Heparin Tetrasaccharides with Chemokine CCL5 Is Modulated by Sulfation Pattern and pH. *The Journal of Biological Chemistry* **2015,** *290* (25), 15421-15436.

51. Arungundram, S.; Al-Mafraji, K.; Asong, J.; Leach, F. E.; Amster, I. J.; Venot, A.; Turnbull, J. E.; Boons, G.-J., Modular Synthesis of Heparan Sulfate Oligosaccharides for Structure−Activity Relationship Studies. *Journal of the American Chemical Society* **2009,** *131* (47), 17394-17405.

52. Sun, L.; Zhu, G.; Zhao, Y.; Yan, X.; Mou, S.; Dovichi, N. J., Ultrasensitive and Fast Bottom-up Analysis of Femtogram Amounts of Complex Proteome Digests. *Angewandte Chemie International Edition* **2013,** *52* (51), 13661-13664.

53. Sun, L.; Zhu, G.; Zhang, Z.; Mou, S.; Dovichi, N. J., Third-Generation Electrokinetically Pumped Sheath-Flow Nanospray Interface with Improved Stability and Sensitivity for Automated Capillary Zone Electrophoresis–Mass Spectrometry Analysis of Complex Proteome Digests. *J. Proteome Res.* **2015,** *14* (5), 2312-2321.

54. Zhu, M.; Lerum, M. Z.; Chen, W., How to prepare reproducible, homogeneous, and hydrolytically stable aminosilane-derived layers on silica. *Langmuir* **2011,** *28* (1), 416-423.

55. Liu, X.; Xing, J.; Guan, Y.; Shan, G.; Liu, H., Synthesis of amino-silane modified superparamagnetic silica supports and their use for protein immobilization. *Colloids and Surfaces A: Physicochemical and Engineering Aspects* **2004,** *238* (1-3), 127-131.

56. Kneuer, C.; Sameti, M.; Haltner, E. G.; Schiestel, T.; Schirra, H.; Schmidt, H.; Lehr, C.-M., Silica nanoparticles modified with aminosilanes as carriers for plasmid DNA. *International journal of pharmaceutics* **2000,** *196* (2), 257-261.

57. Muchena J. Kailemia, M. P., Desmond A. Kaplan, Andre Venot,; Geert-Jan Boons, L. L., Robert J. Linhardt, I. Jonathan Amster, High-field asymmetric-waveform ion mobility spectrometry and electron detachment dissociation of isobaric mixtures of glycosaminoglycans. *J. Am. Soc. Mass Spectrom.* **2013**.

58. Galeotti, F.; Volpi, N., Online Reverse Phase-High-Performance Liquid Chromatography-Fluorescence Detection-Electrospray Ionization-Mass Spectrometry Separation and Characterization of Heparan Sulfate, Heparin, and Low-Molecular Weight-Heparin Disaccharides Derivatized with 2-Aminoacridone. *Analytical Chemistry* **2011,** *83* (17), 6770-6777.

59. Li, D.; Chi, L.; Jin, L.; Xu, X.; Du, X.; Ji, S.; Chi, L., Mapping of low molecular weight heparins using reversed phase ion pair liquid chromatography–mass spectrometry. *Carbohydr. Polym.* **2014,** *99*, 339-344.

60. Sun, X.; Sheng, A.; Liu, X.; Shi, F.; Jin, L.; Xie, S.; Zhang, F.; Linhardt, R. J.; Chi, L., Comprehensive Identification and Quantitation of Basic Building Blocks for Low-Molecular Weight Heparin. *Analytical Chemistry* **2016,** *88* (15), 7738-7744.

3.7 SUPPLEMENTAL DATA

Table ST3.1. GAG oligomer compositions identified by CE-MS of Enoxaparin

Neutral Mass	Composition	Error (ppm)
753.01	dp3_3S	2.74
771.02	dp3_3S	3.06
832.96	dp3_4S	1.25
836.01	dp3_4S	3.37
850.97	dp3_4S	2.77
854.94	dp3_4S_Na	1.03
915.97	dp3_5S	2.39
937.95	dp3_5S_Na	2.90
994.03	dp4_4S	1.87
995.92	dp3_6S	2.27
1012.95	dp3_6S_NH3	-1.50
1055.98	dp4_5S (-H2O)	1.50
1073.99	dp4_5S	1.71
1092.00	dp4_5S	2.42
1095.97	dp4_5S_Na	2.50
1153.94	dp4_6S	1.84
1170.97	dp4_6S_NH3	-1.06
1171.95	dp4_6S	0.60
1251.91	dp4_7S	1.93
1268.94	dp4_7S_NH3	-1.02
1329.98	dp5_6S	1.37
1347.00	dp5_6S_NH3	-0.77
1347.99	dp5_6S	1.76
1375.04	dp5_6S_Nac	2.41

1409.93	dp5_7S	2.09
1412.98	dp5_7S	2.04
1426.96	dp5_7S_NH3	0.04
1427.95	dp5_7S	2.55
1443.99	dp5_7S_NH3	-2.71
1453.10	dp6_5S_Nac	2.86
1491.05	dp6_6S	2.25
1492.94	dp5_8S	2.88
1533.06	dp6_6S_Nac	2.22
1571.00	dp6_7S	-0.09
1572.90	dp5_9S	2.78
1588.03	dp6_7S_NH3	-1.28
1589.01	dp6_7S	2.56
1589.92	dp5_9S_NH3	0.29
1606.95	dp5_9S_2NH3	-2.08
1613.01	dp6_7S_Nac	2.14
1630.04	dp6_7S_Nac_NH3	-2.05
1647.06	dp6_7S_Nac_2NH3	-5.25
1650.96	dp6_8S	1.12
1667.99	dp6_8S_NH3	-0.16
1668.97	dp6_8S	1.72
1685.01	dp6_8S_2NH3	-3.06
1730.92	dp6_9S	1.94
1747.94	dp6_9S_NH3	-0.11
1748.93	dp6_9S	2.20
1764.97	dp6_9S_2NH3	-2.22
1765.96	dp6_9S_NH3	0.06

1782.98	dp6_9S_2NH3	-1.31
1826.99	dp7_8S	2.02
1906.95	dp7_9S	2.07
1923.98	dp7_9S_NH3	0.11
1950.12	dp8_7S_Nac	1.96
1986.91	dp7_10S	3.30
1988.06	dp8_8S	1.01
2003.93	dp7_10S_NH3	-0.14
2020.96	dp7_10S_2NH3	-1.44
2030.07	dp8_8S_Nac	0.73
2050.01	dp7_9S_3NAc_NH3	-0.19
2067.04	dp7_9S_3NAc_2NH3	-1.54
2127.06	dp8_9S_Nac_NH3	0.45
2144.08	dp8_9S_Nac_2NH3	-2.32
2147.98	dp8_10S	2.20
2165.00	dp8_10S_NH3	0.28
2182.03	dp8_10S_2NH3	-2.27
2207.01	dp8_10S_Nac_NH3	0.46
2224.04	dp8_10S_Nac_2NH3	-0.23
2227.93	dp8_11S	1.69
2244.96	dp8_11S_NH3	0.70
2261.99	dp8_11S_2NH3	-0.54
2307.89	dp8_12S	1.30
2325.90	dp8_12S	3.40
2341.94	dp8_12S_2NH3	-2.45
2377.99	dp8_10S_2Na	1.42
2775.04	dp9_12S_5NAc_2Na_2NH3	0.44

2804.91	dp10_14S	2.77
2839.95	dp10_14S_NH3	3.15
2855.00	dp9_13S_5NAc_2Na_2NH3	0.45
2971.99	dp10_13S_4NAc_2Na_NH3	1.03
3301.92	dp12_16S	2.21

CHAPTER 4

INVESTIGATION OF ELECTROSPRAY FOR A CAPILLARY ELECTROPHORESIS-MASS SPECTROMETRY INTERFACE IN REVERSE POLARITY AND NEGATIVE ION MODE

Stickney, M.; Amster, I. J. 2019. Eur. J. Mass. Spectrom. 25 (1), 157-163

Accepted by Eur. J. Mass. Spectrom. Reprinted here with permission of the publisher.

4.1 ABSTRACT

Capillary zone electrophoresis (CZE) paired with mass spectrometry (MS) is a powerful analytical technique for examining mixtures of ionic analytes. This study examines the mechanics of the electrospray process for a sheath flow CZE-MS interface under reverse polarity negative ionization conditions. Liquid flow in a sheath flow nano-electrospray CZE-MS interface is driven by two mechanisms: Electroosmotic flow (EOF) and electrospray nebulization. The contribution of these two processes to the overall flow of solution to the electrospray tip is influenced by the surface coatings of the sheath flow emitter tip and by the solvent composition. We have investigated the application of this interface to the reverse polarity separation of glycosaminoglycans and find that the role of EOF is far less than has been reported previously, and the electrospray process itself is the largest contributor to the flow of the sheath liquid.

4.2 INTRODUCTION

The online combination of capillary zone electrophoresis and mass spectrometry (CZE-MS) provides powerful capabilities for the analysis of mixtures of ionic species that are not readily examined by more conventional hyphenated approaches such as liquid chromatography and mass spectrometry (LC-MS) [1, 2]. Recently our laboratory demonstrated the effectiveness of CZE-MS for analyzing glycosaminoglycans (GAGs), a family of sulfated carbohydrates that are difficult to analyze by LC-MS [3]. A commercial sheath flow CZE-MS interface provided the means to implement nano-electrospray with a low dilution factor and minimal sample consumption, while providing ample resolution of closely related isomers.

Sulfated carbohydrates exist as negative ions in solution, and thus require reverse polarity for the CZE separation and negative mode ionization for the mass spectrometry detection. Under these conditions, standard bare fused silica separation capillaries are subject to electroosmotic flow (EOF) that opposes the migration of negative ions, adversely affecting the separation time and resolution for GAGs. Our prior work showed that by modifying the surface of the separation capillary to make it neutral or cationic, shorter separation times could be achieved while maintaining good peak resolution for this class of compounds [3]. In a similar fashion, we modified the surface of the glass capillary that forms the emitter of the sheath interface, with the goal of making a cationic surface that would provide a sufficient EOF to sustain stable electrospray. The sheath flow CZE-MS interface has been reported by others to function by the electrokinetic pumping of the sheath liquid by EOF in the emitter tip [4-6]. We were surprised to find that neutral coated, or even unmodified bare glass capillaries (with an anionic surface) would function well with reverse polarity CZE and negative ionization mass spectrometry. The present study is motivated by the desire for a better understanding of the sheath flow interface, and the mechanism of liquid flow necessary for electrospray ionization.

The sheath flow CZE-MS interface is something of a hybrid between a traditional ESI interface and a nano-ESI interface [7-11], as it uses no desolvation gas, has no backing pressure, and has a moderately sized orifice of 30 μm. Liquid from a reservoir is introduced to a bare glass emitter sheath that surrounds the exit of the separation capillary, and which is pulled to a fine tip that functions as an electrospray ionization emitter. As the analyte exits the separation capillary, it mixes with the sheath liquid in a nanoliter volume and then exits through an orifice as it undergoes electrospray, at the entrance of a mass spectrometer [12].

There are two mechanisms that are responsible for the flow of sheath liquid through the interface: electroosmotic flow (EOF) and electrospray-driven liquid flow [7-13]. EOF is liquid flow caused by the movement of the solvated mobile ions in the electrical double layer present at the inner surface of a glass capillary, and which acts as a nanoscale pump. The ESI-driven flow is created by the aerosolization of solvent at the tip of the emitter. Here we explore the contributions of these forces in reverse polarity CZE and negative ionization mass spectrometry experiments. We use a highly negatively charged glycosaminoglycan sample for this investigation. Cationic and neutral modifications of the inside surface of the bare glass emitter that surrounds the end of the separation capillary were utilized to ascertain the importance of EOF to the performance of the sheath flow CZE-MS interface under reverse polarity conditions.

4.3 EXPERIMENTAL

Materials

Bare fused silica (BFS) capillary for CZE (360 µm o.d. x 50 µm i.d.) was purchased from PolyMicro Technologies (Phoenix, AZ), borosilicate glass capillaries (1.0 mm OD x 0.75 mm ID) and pulled coated electrospray emitters (1.0 mm OD x 0.75 mm ID) were obtained from CMP scientific (Brooklyn, NY). Coating reagents, dichlorodimethylsilane (DMS, Sigma-Aldrich, St. Louis, MO) and N-(6-aminohexyl)aminomethyltriethoxysilane (AHS, Gelest, Morrisville, PA) were prepared in toluene. Ammonium acetate, water, and methanol were of HPLC grade (Fisher Scientific, Hampton, NH). Sodium hydroxide, acetone, and toluene were purchased from Sigma-Aldrich (St. Louis, MO). Ammonium hydroxide and acetic acid were purchased from Avantor (Allentown, PA).

Heparan sulfate GAG sample

The GAG tetrasaccharide sample was prepared by enzymatic depolymerization of heparan sulfate and purified using strong anion exchange high-pressure liquid chromatography (SAX-HPLC), using methods described previously [14, 15]. The sample was desalted with a 3 kDa Amicon Ultra centrifugal filter (Millipore, Temecula, CA) prior to separation and mass spectrometry analysis. Filters were conditioned with water, and the sample was then washed with two filter volumes of water (14,000 x g for 25 min each). Before analysis, GAG samples were diluted to 5 µg/mL in water. The heparan sulfate sample used in this study, referred to as HS1, has been characterized previously [16], and its structure has been assigned as ΔHexA(2S)-GlcNS(6S)-HexA-GlcNS(6S). Its structure is shown in **Figure 4.1**.

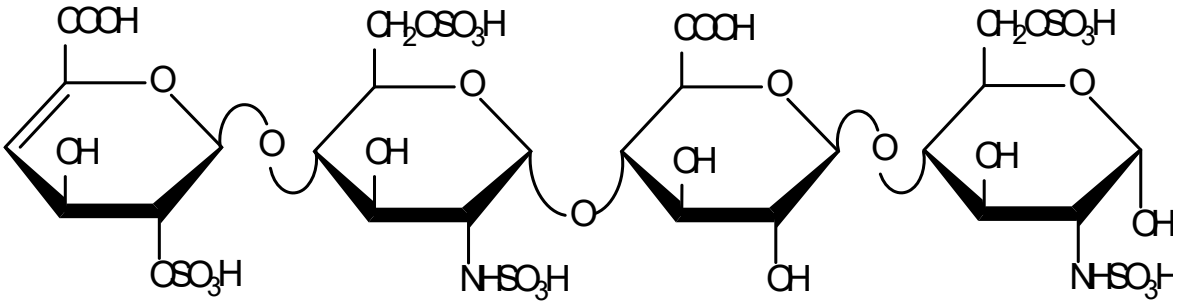

Figure 4.1. Chemical structure diagram of heparan sulfate sample 1 (HS1). This heparan sulfate tetrasaccharide has five sulfo-modifications, making it highly negatively charged.

Emitter Surface Modification

The interior surface of the sheath flow emitter was covalently modified using solutions that were prepared in toluene with 1% concentration of either DMS (neutral surface) or AHS (cationic surface). To clean and prepare the emitter for surface modification, the borosilicate

glass capillary was rinsed consecutively with 2 mL each of aqueous 0.1 M NaOH, water, methanol, dry acetone, and dry toluene. The surface of the borosilicate glass capillary was then modified by flushing with 500 µL of 1% DMS or AHS over a 20 min period. The borosilicate glass capillary was then consecutively rinsed with 2mL of each dry toluene, dry acetone, and methanol. The modified borosilicate glass capillaries were then processed into emitters with 30 µm orifices using a commercial capillary puller, as described previously[17]. For all experiments, the separation capillary was modified with AHS as described in our previous paper [3].

Instrumentation

Separations were conducted with an Agilent HP 3D capillary electrophoresis instrument (Wilmington, DE). A long bare fused silica capillary was used for CZE of GAG analyte, and its inner surface was modified with AHS to speed up analyte migration. The total length of the capillary ranged from 58-60 cm, and its inner diameter was 50 µm with an internal volume of approximately 1 µL. 25 mM ammonium acetate was used as both the background electrolyte (BGE) and the sheath liquid (SL) for reverse polarity experiments. The aqueous GAG sample (HS1) was injected for 3 s at 950 mbar followed by a background electrolyte (BGE) injection for 10 s at 10 mbar. The injected volume was 0.1 µL. The ionic strength of the injected sample plug is 2-3 orders of magnitude less than that of the background electrolyte, and sample stacking is expected under these conditions and provides a sharp sample front [2]. The entrance end of the capillary was then placed into a vial of BGE prior to separation. A voltage of -30 kV was applied to the capillary to drive the separation for all experiments.

An EMASS-II (CMP Scientific, Brooklyn, NY) CZE-MS interface was employed to couple the CZE with a Thermo Scientific Velos Orbitrap Elite mass spectrometer (Bremen, Germany). A separation capillary with a beveled outlet was nested inside a glass emitter sheath with a 0.75

mm inner diameter and a 30 µm tip orifice (CMP Scientific, Brooklyn, NY). The etched end of the capillary was positioned 0.3-0.5 mm from the tip of the sheath emitter orifice to create a mixing volume of ca. 1-5 nL and the emitter tip was filled with sheath liquid (SL), at a concentration of 25 mM ammonium acetate 50-70% MeOH. An external power supply provided a voltage of -1.9 kV to the sheath liquid reservoir via a platinum wire, which produces electrospray at the emitter tip. MS detection was performed in negative ion mode. Prior to CZE-MS experiments, a semi-automatic optimization of source parameters was performed using sucrose octasulfate to improve sensitivity of sulfated GAGs and reduce sulfate loss during MS analysis. The Orbitrap was scanned from m/z 150-2000 for GAG oligosaccharides with a specified resolution of 120,000.

4.4 RESULTS AND DISCUSSION

Figure 4.2 shows a schematic of the nanoflow sheath CZE-MS interface developed by Dovichi and Wojcik, and used for these studies [18]. For reverse polarity CZE-MS experiments 25mM ammonium acetate in 70:30 MeOH:H_2O was used for both the BGE and the SL. A large negative voltage (-30kV) is applied to the BGE vial at the inlet of the separation capillary and a relatively smaller negative voltage (-1.9kV) is applied to the reservoir of the sheath liquid (SL) near the outlet of the separation capillary. The potential applied to the SL serves two purposes. It completes an electrical circuit through the separation capillary by contact of the SL and the BGE near the emitter tip which drives analyte migration through the separation capillary. It also drives the electrospray process by creating a difference in electric potential between the sheath liquid near the emitter and the small potential (-0.33 kV) at the entrance of the mass spectrometer. A Taylor cone forms, and electrospray of the analyte is achieved when the electric potential

difference is large enough to overcome the surface tension of the solvent. Dilution is reduced, and sensitivity is maximized by placing the outlet of the separation capillary in close contact to the orifice of the sheath emitter, producing a mixing volume that is less than 1 nL.

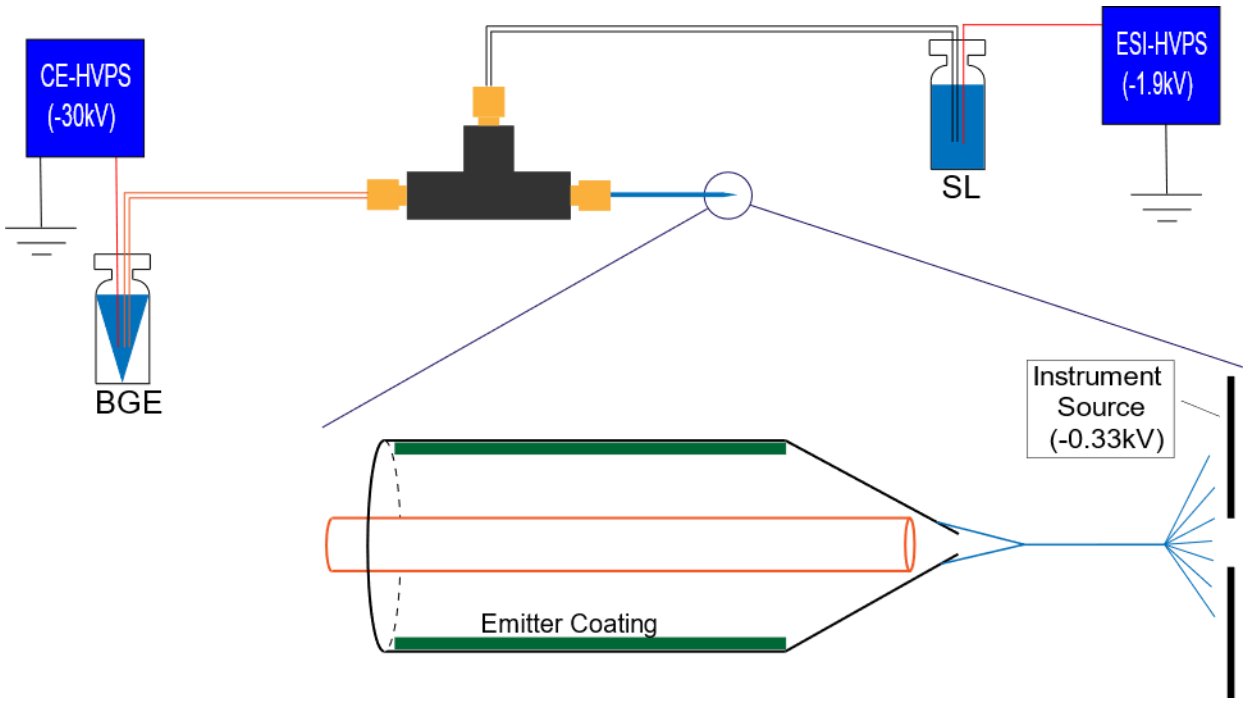

Figure 4.2. Schematic of the CZE-MS sheath flow interface. Background electrolyte (BGE) and sheath liquid (SL) are 25 mM ammonium acetate in 70:30 MeOH:H_2O. The separation capillary makes a snug fit with the emitter sheath and establishes a small mixing volume (ca. 200 pL) where BGE and SL meet and complete the electrical circuit. The electric potential difference between the sheath liquid in the emitter and the detector source forms a Taylor cone and electrospray. Covalent modification of the inner surface used to control EOF in the emitter sheath is represented by the green; it is destroyed in the tip by the pulling process.

The flow of the sheath liquid must be sufficient to sustain a stable electrospray, as the flow rate of the liquid exiting the separation capillary is too small to serve this purpose by itself. The inventors of this interface describe the driving force for sheath flow as electrokinetic in nature, resulting from the electroosmotic flow of SL within the emitter [4, 18]. Under normal polarity conditions (positive voltages for CZE and for the SL), a bare glass surface, with its negatively charged surface, would be expected to provide an EOF that moves the sheath liquid from its reservoir toward the emitter tip. Under reverse-polarity conditions (negative voltages for both CZE and the SL), the EOF will reverse in direction, and oppose the desired flow necessary for electrospray ionization. Previous work using reverse-polarity for negatively charged analytes has employed a cation-modified surface on the emitter, which reversed the direction of the EOF, so that it moved toward the emitter tip [5]. Not considered previously was the flow of the SL due to the electrospray process. In the absence of EOF, liquid is drawn through the emitter as the solution is nebulized by ESI. This may be sufficient to overcome EOF even when it flows in the wrong direction. We have made a series of measurements to better understand the relative magnitudes of these forces (EOF versus ESI-driven flow). We were motivated to examine whether or not it was necessary to alter the surface of the emitter in order to make reverse polarity separations. Modifying the surface adds extra complexity to the experiment. This modification process must be accomplished before the emitter is pulled to a fine tip, and heating during this process is certain to damage the modification in an indeterminate portion of the capillary. Also, delamination of the modified surface can occur, leading to a reduced lifetime from plugging of the emitter.

The interior surface of the borosilicate glass emitters was covalently modified to control EOF. We used the same agents for modifying the surface of the emitter as we had previously

used for modifying the separation capillary [3]. We use a cationic reagent (AHS) to reverse EOF and a neutral reagent (DMS) to nullify EOF. Our cation reagent (AHS) is similar to material described by others [5], but has a longer linker to make a more stable and longer-lasting covalent modification. The heat generated pulling the emitter tip is thought to destroy the surface modification in its narrow, conical region, but the extent of this region is poorly characterized.

Figure 4.3 shows the measured average rate of consumption of sheath liquid from the reservoir for each type of inner surface. The volume of the sheath liquid in its reservoir was measured before and after 10 h of use, and the difference in volume over that time is the rate of consumption. Under these reverse polarity conditions, the consumption of SL is found to be similar between all three types of inner surface. The cation-coated surface shows a modestly larger consumption, suggesting that the EOF contributed fractionally to the overall sheath flow for this surface. The neutral-coated and bare glass surface show nearly identical consumption, suggesting that the EOF of the bare glass surface is small compared to the overall sheath flow under the experimental conditions employed. Furthermore, the flow rate of the interface is low, on the order of 10 µL/h, as expected for nanospray conditions.

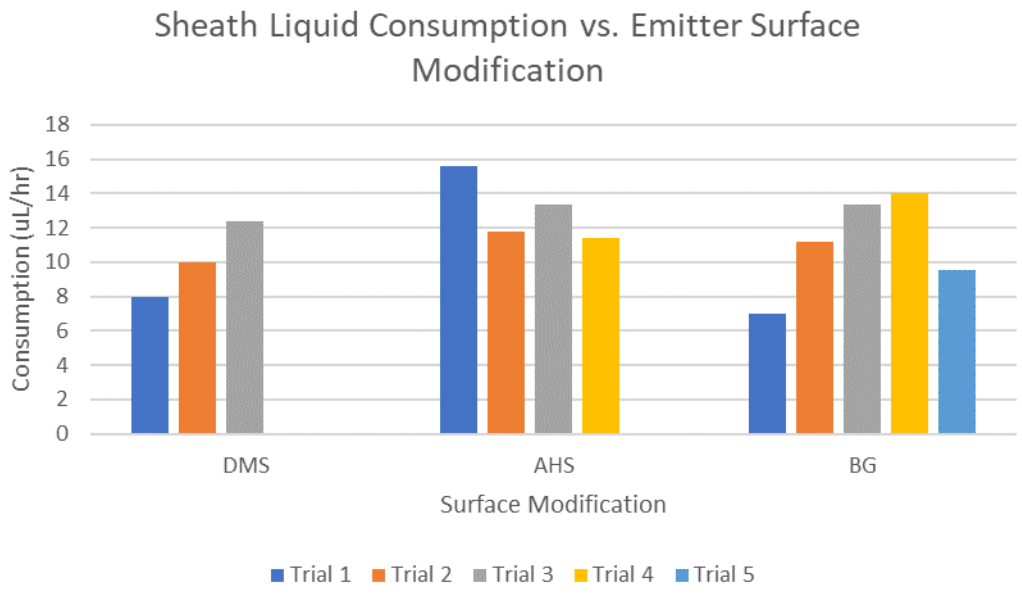

Figure 4.3. Comparison of sheath liquid consumption rates between three types of emitter sheath inner surface; DMS (neutral), AHS (cationic), and bare glass surface (BG) (anionic). DMS (neutral) nullifies EOF, AHS (cationic) provides an EOF toward the emitter tip, and BG (anionic) produces an EOF that opposes the sample flow toward the emitter tip.

Prior studies of heparan sulfate tetramers show that under reverse polarity conditions, with 25 mM ammonium acetate in 70:30 MeOH:H_2O as the BGE and SL, adversarial EOF will double CZE migration times compared to favorable EOF [3]. This suggests that EOF is a relevant and influential factor under these solvent conditions. The emitter is borosilicate glass and presents the same inner surface as the separation capillary, but the EOF is weaker because of the much larger diameter of the emitter compared to the separation capillary (750 µm versus 50 µm). A heparan sulfate tetrasaccharide sample, denoted as HS1 and seen in **Figure 4.3**, was used to test ESI and its stability when using emitters with different surface modifications. **Figure 4.4** and **Table 3** demonstrate that, unlike the separation capillary, modifying the surface of the emitter has no observable effect on the migration time, peak shape, or mass spectrum of HS1. The force

of EOF under these conditions is negligible compared to the ESI force and has no influence on the outcome of the experiment.

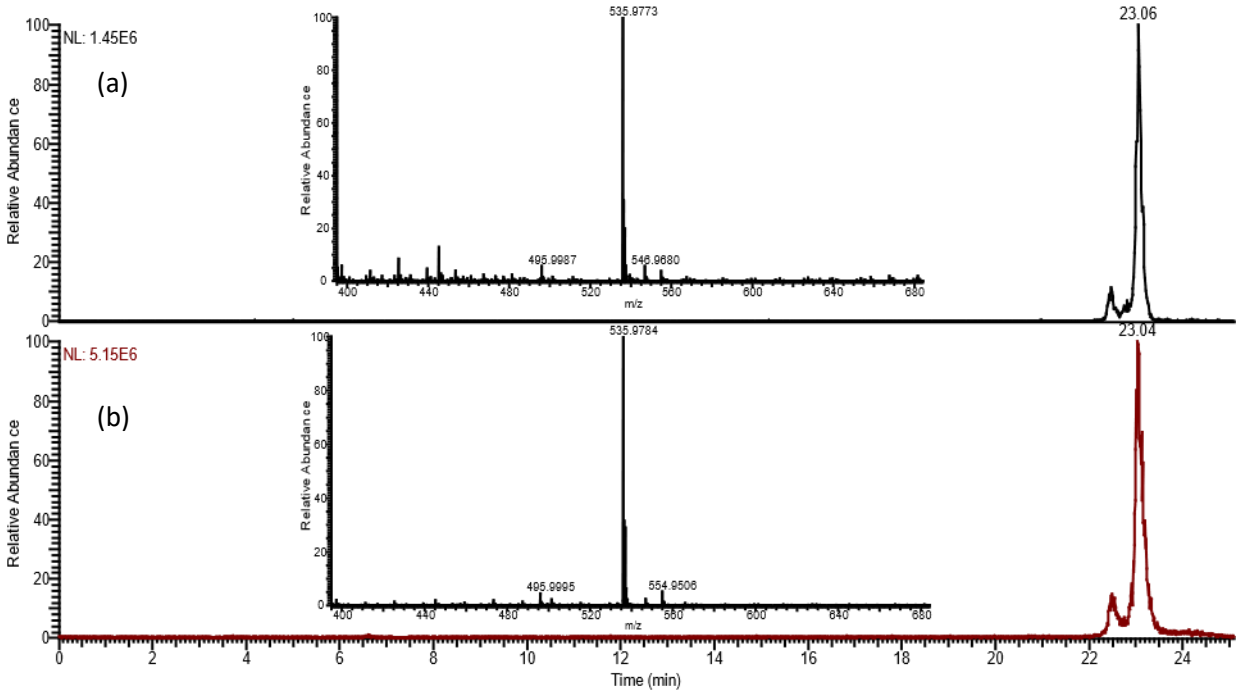

Figure 4.4. CZE-MS measurement of HS1 comparing cationic and anionic emitter inner surfaces. An AHS modified separation capillary was used in tandem with a (a) AHS (cationic surface) coated emitter and (b) uncoated glass (anionic surface) emitter. Mass spectra are shown as insets to the electropherograms, and were acquired for the major feature at 23 min migration time.

Table 3. Comparison of migration times and peak widths for CZE-MS of a glycosaminoglycan tetrasaccharide, with different emitter sheath coated surfaces: AHS (cationic), DMS (neutral), and BFS (anionic)

Emitter type	Migration time (min)	FWHM (s)
AHS	21.41	0.18
	21.33	0.19
	21.16	0.21
	12.19	0.19
	21.11	0.21
	21.04	0.22
AHS avg.	21.21	0.20
DMS	21.76	0.17
	21.33	0.21
	21.00	0.19
	21.08	0.20
	21.16	0.22
	21.25	0.20
DMS avg.	21.26	0.20
BFS	21.28	0.19
	21.20	0.16
	21.20	0.21
	21.04	0.17
	20.93	0.18
	20.72	0.18
BFS avg.	21.06	0.18

Note: The same AHS-modified separation capillary was used for all measurements.

While the direction of EOF is controlled by the surface of the emitter, the magnitude of EOF can be manipulated by the content of the solvent. Varying the organic composition of the solvent will influence the degree of ionization of the silanol groups on the surface of a bare glass emitter, and therefore the number of ions in the electrical double layer. Highly organic solvent systems, like the one used here to effectively separate GAGs, reduces the degree of ionization of the silanol groups, reducing the mobile ions in the double layer, and reducing the EOF. Increasing the aqueous concentration will have the opposite effect, leading to an increase in the EOF.

Figure 4.5 shows the difference in electrospray between a sheath liquid that has 70:30 MeOH:H_2O (**Figure 4.5(a)**) and one that has 50:50 MeOH:H_2O (**Figure 4.5(b) & 4.5(c)**). By increasing the ratio of water vs. organic in the solvent, the double layer increases in size and the magnitude of EOF is expected to increase. This results in unstable electrospray at lower organic concentration for uncoated bare glass emitters, where the EOF is counter to electrospray flow. This exhibits itself as signal dropout observed across the peak in the mobility plot in **Figure 4.5b**. Conversely, AHS emitters, which have EOF with the same direction as the electrospray flow, are found to function normally at higher aqueous concentration, as can be seen in **Figure 4.5c**. These data suggest the EOF increases with a 50% organic/50% aqueous solution to a magnitude that is comparable to the electrospray driven flow.

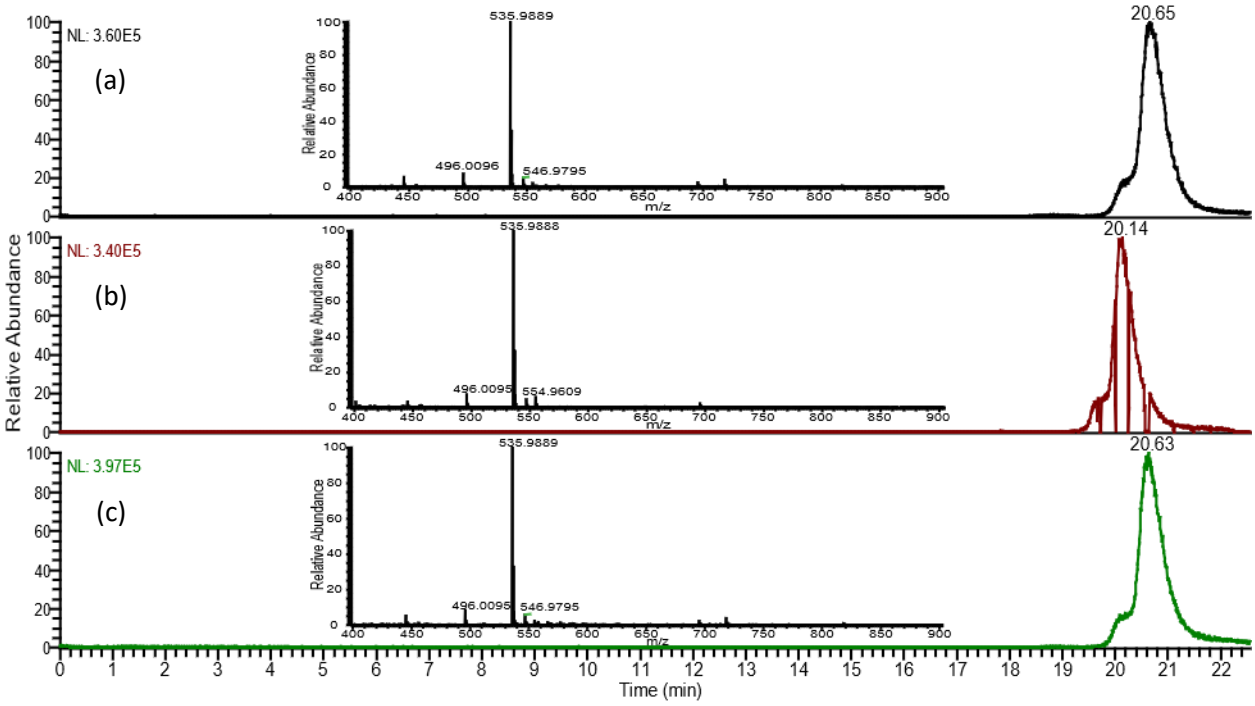

Figure 4.5. CZE-MS electropherograms and mass spectra (inset) for HS1, obtained with different solvent organic concentrations. HS1 in (a) 70:30 MeOH:H_2O BGE and SL with a bare

glass emitter, (b) 50:50 MeOH:H_2O BGe and SL with a bare glass emitter, and (c) 50:50 MeOH:H_2O BGE and SL with a AHS coated emitter. The separation capillary had an AHS modified surface for all three measurements.

Altering the pH of the solvent also changes the magnitude of EOF through changes in the degree of ionization of the surface silanols for bare glass emitters [2, 19]. A higher, more basic, pH, from adding ammonium hydroxide, ionizes a larger proportion of the silanol groups present on the inner surface of an uncoated glass emitter and increases the EOF that opposes the electrospray flow in a reverse polarity CZE experiment. However, solvents with higher pH show no disruption to ESI, and electrospray still works even when detrimental EOF is purposefully applied to the system. Favorable EOF is not necessary for this interface to function properly because the ESI force is robust.

4.5 CONCLUSIONS

Collectively, the data presented here show that the accepted mechanism of EOF-driven flow for the sheath liquid in the CZE-MS interface does not apply under all experimental conditions[6]. The separation of GAG oligomers by capillary zone electrophoresis is optimal at relatively high concentration of organic solvent (70%). While EOF is still significant in the separation capillary with a solvent of this composition, in the sheath flow interface, EOF is small compared to the flow driven by the electrospray itself. At lower organic concentration, the EOF in the sheath interface increases enough to be a concern, but this is not an optimal solvent composition for the separation, and thus is not relevant. Surface modified CZE-MS emitters are expensive, are unstable at high alkaline concentrations (pH 10 or higher), and have more limited lifespans than

unmodified emitters. Thus, it is significant that an emitter with an unmodified surface can be implemented for reverse polarity separations. If coated emitters are required, then covalently bound coatings are best because they are stable and effective[3].

4.6 REFERENCES

1. Smith, R. D.; Olivares, J. A.; Nguyen, N. T.; Udseth, H. R., Capillary zone electrophoresis-mass spectrometry using an electrospray ionization interface. *Anal. Chem.* **1988,** *60* (5), 436-441.

2. Whatley, H., Basic Principles and Modes of Capillary Electrophoresis. In *Clinical and Forensic Applications of Capillary Electrophoresis*, Petersen, J. R.; Mohammad, A. A., Eds. Humana Press: Totowa, NJ, 2001; pp 21-58.

3. Sanderson, P.; Stickney, M.; Leach, F. E.; Xia, Q.; Yu, Y.; Zhang, F.; Linhardt, R. J.; Amster, I. J., Heparin/heparan sulfate analysis by covalently modified reverse polarity capillary zone electrophoresis-mass spectrometry. *J. Chromatogr. A* **2018,** *1545*, 75-83.

4. Sun, L.; Zhu, G.; Zhang, Z.; Mou, S.; Dovichi, N. J., Third-Generation Electrokinetically Pumped Sheath-Flow Nanospray Interface with Improved Stability and Sensitivity for Automated Capillary Zone Electrophoresis–Mass Spectrometry Analysis of Complex Proteome Digests. *J. Proteome Res.* **2015,** *14* (5), 2312-2321.

5. Sarver, S. A.; Schiavone, N. M.; Arceo, J.; Peuchen, E. H.; Zhang, Z.; Sun, L.; Dovichi, N. J., Capillary electrophoresis coupled to negative mode electrospray ionization-mass spectrometry using an electrokinetically-pumped nanospray interface with primary amines grafted to the interior of a glass emitter. *Talanta* **2017,** *165*, 522-525.

6. Wojcik, R.; Dada, O. O.; Sadilek, M.; Dovichi, N. J., Simplified capillary electrophoresis nanospray sheath-flow interface for high efficiency and sensitive peptide analysis. *Rapid Communications in Mass Spectrometry* **2010,** *24* (17), 2554-2560.

7. Kebarle, P.; Tang, L., From ions in solution to ions in the gas phase - the mechanism of electrospray mass spectrometry. *Anal. Chem.* **1993,** *65* (22), 972A-986A.

8. Wilm, M. S.; Mann, M., Electrospray and Taylor-Cone theory, Dole's beam of macromolecules at last? *Int. J. Mass Spectrom. Ion Processes* **1994,** *136* (2), 167-180.

9. Olumee, Z.; Callahan, J. H.; Vertes, A., Droplet Dynamics Changes in Electrostatic Sprays of Methanol−Water Mixtures. *J. Phys. Chem. A* **1998,** *102* (46), 9154-9160.

10. Yamashita, M.; Fenn, J. B., Electrospray ion source. Another variation on the free-jet theme. *J. Phys. Chem.* **1984,** *88* (20), 4451-4459.

11. Wilm, M.; Mann, M., Analytical Properties of the Nanoelectrospray Ion Source. *Anal. Chem.* **1996,** *68* (1), 1-8.

12. Pozniak, B. P.; Cole, R. B., Current measurements within the electrospray emitter. *J. Am. Soc. Mass Spectrom.* **2007,** *18* (4), 737-748.

13. Höcker, O.; Montealegre, C.; Neusüß, C., Characterization of a nanoflow sheath liquid interface and comparison to a sheath liquid and a sheathless porous-tip interface for CE-ESI-MS in positive and negative ionization. *Anal. Bioanal. Chem.* **2018,** *410* (21), 5265-5275.

14. Linhardt, R. J.; Gunay, N. S., Production and chemical processing of low molecular weight heparins. *Semin. Thromb. Hemostasis* **1999,** *25*, 5-16.

15. Laremore, T. N.; Ly, M.; Solakyildirim, K.; Zagorevski, D. V.; Linhardt, R. J., High-resolution preparative separation of glycosaminoglycan oligosaccharides by polyacrylamide gel electrophoresis. *Analytical Biochemistry* **2010,** *401* (2), 236-241.

16. Singh, A.; Kett, W. C.; Severin, I. C.; Agyekum, I.; Duan, J.; Amster, I. J.; Proudfoot, A. E.; Coombe, D. R.; Woods, R. J., The Interaction of Heparin Tetrasaccharides with Chemokine CCL5 Is Modulated by Sulfation Pattern and pH. *J Biol Chem* **2015,** *290* (25), 15421-36.

17. Oesterle, A., *Pipette Cookbook*. Rev. F ed.; Sutter Instrument Company: Novato, CA, 2018; p 108.

18. Dovichi, N. J.; Wojcik, R. Sheath-flow electrospray interface. US 9234880 B2. June 3, 2011.

19. Hayes, M. A.; Kheterpal, I.; Ewing, A. G., Effects of buffer pH on electroosmotic flow control by an applied radial voltage for capillary zone electrophoresis. *Anal. Chem.* **1993,** *65* (1), 27-31.

CHAPTER 5

ONLINE CAPILLARY ZONE ELECTROPHORESIS NEGATIVE ELECTRON TRANSFER DISSOCIATION TANDEM MASS SPECTROMETRY OF GLYCOSAMINOGLYCAN MIXTURES

Stickney, M.; Amster, I. J. 2019. *Int. J. Mass. Spectrom*. 445, 116209.

Accepted by Int. J. Mass. Spectrom. Reprinted here with permission of the publisher.

5.1. ABSTRACT

Glycosaminoglycans (GAGs) are important biological molecules that are highly anionic and occur in nature as complex mixtures. A platform that combines capillary zone electrophoresis (CZE) separations with mass spectrometry (MS) and gas-phase sequencing by using negative electron transfer dissociation (NETD) is shown to be efficacious for the structural analysis of GAG mixtures. CZE is a separation method well suited to the highly negatively charged nature of GAGs. NETD is an electron-based ion activation method that enables the generation of informative fragments with retention of the labile sulfate half-ester modification that determine specific GAG function. Here we combine for the first time NETD and CZE for assigning the structures of GAG oligomers present in mixtures. The speed of ion activation by NETD is found to couple well with the narrow peaks resulting from CZE migration. The platform was optimized with mixtures of GAG tetrasaccharide standards. The potential of the platform is demonstrated by the analysis of enoxaparin, a complex mixture of low molecular weight heparins, which was separated by CZE within 30 minutes and characterized by NETD MS/MS in one online experiment. 37 unique molecular compositions have been identified in enoxaparin using CZE-MS and 9 structures have been assigned with CZE-NETD-MS/MS.

5.2. INTRODUCTION

Sulfated glycosaminoglycan (GAG) carbohydrates serve a wide array of biological functions that are modulated by their structural modifications [1-5]. For example, heparin's pharmaceutical efficacy as an anti-blood clotting agent is tied to a well-defined pattern of sulfation in a pentasaccharide sequence, and binds the protein antithrombin III (ATIII) with high

specificity [6, 7]. Determining GAG-protein binding interactions that rely on specific GAG sequence motifs is nontrivial and currently requires considerable effort and sample. There is considerable interest in developing sensitive and rapid analytical methods to enable the identification of biologically active GAG sequences. Sulfated GAG carbohydrates are challenging targets for analysis due to variability in chain length as well as degree and placement of modifications. These structural variations are a result of their biosynthesis through a series of enzymatic reactions that do not go to completion and lead to highly heterogeneous carbohydrate chains of high molecular weight [8, 9]. The most complex and highly modified GAG is heparin/heparan sulfate (Hep/HS), which consists of a repeating disaccharide unit of a glucosamine, which can be modified with up to three sulfo-modifications, and a uronic acid, which can host one sulfo-modification. Additional complexity results from the epimerization of the carboxyl group on C5 of the uronic acid [10, 11]. The occurrence of carboxyl groups and the sulfo-modifications on GAGs also makes them highly anionic.

The structural characterization of GAG oligomers by mass spectrometry has shown great promise in recent years. Tandem mass spectrometry techniques such as sodium-hydrogen exchange for threshold activation and electron based activation techniques like electron detachment dissociation (EDD) have made structural assignment of the labile sulfo-half-ester modification possible [12, 13]. Native GAG polysaccharides are too long and complex for typical top down analysis and significant effort is required to characterize even the shortest and least complex intact GAG chains [14, 15]. Bottom up approaches where polysaccharides are digested to disaccharides simplify characterization of base constituents but any knowledge of extended sequence is lost [16-19]. Typically, a small segment of 4-12 monosaccharides in a chain is required

for protein binding, and a quasi-bottom up approach where polysaccharides are partially digested is highly amenable to mass spectrometry-based analysis.

Partial digestion of GAG polysaccharides leads to complex mixtures of isomers and variable chain lengths that overlap in mass-to-charge that are difficult, if not impossible, to differentiate by MS alone. Liquid chromatography mass spectrometry (LC-MS) is not well suited to the separation of GAGs [20-22]. Reverse phase ion-pairing (RPIP) LC-MS has been utilized to investigate disaccharide mixtures and low molecular weight heparin (LMWH) mixtures, like enoxaparin, but requires specific ion pairing reagents that add spectral complexity and suppress signal [19, 23-25]. Hydrophilic interaction chromatography (HILIC) LC-MS can be applied to the separation of polar molecules such as GAGs and is well suited for the separation of complex N-glycans by size and degree of modification, but less useful for separating isomers [17, 26, 27].

Capillary zone electrophoresis (CZE) is an ideal technique for the separation of GAG polysaccharide mixtures because the separation mechanism acts upon the charge and shape of a molecule. Not only can CZE resolve structures that differ in mass, such as those that differ in amino modification, but CZE has been utilized to resolve positional isomers as well as enantiomers with baseline resolution [28]. CZE has been under investigation for some time because of its powerful and robust mechanism that separates molecules based on their size, shape, and charge [18, 29-34]. A new commercial interface has made sheathed CZE paired with MS (CZE-MS) more sensitive by lowering the dilution factor associated with these interfaces, providing the capability for nanospray [35]. This feature of the interface is especially useful because it allows for injection and detection of nanoliter sample volumes, making it compatible with the limited amount of a GAG sample when it is isolated from a natural source. CZE-MS has proven very

effective at separating purified HS disaccharides, purified HS tetrasaccharides, and low molecular weight heparin pharmaceuticals [28, 36].

CZE-MS analysis has recently been used to assign the degree of polymerization, sulfo-modification, and to show the presence of isomers [28]. In order to determine specific sites of modification and assign structural motifs for GAG oligomers tandem MS is necessary. Threshold activation methods such as collision induced dissociation (CID/HCD) are well matched with the CZE peak widths (tens of seconds) but are sub-optimal due to their propensity to decompose labile sulfo-modifications [16]. These can be stabilized by forming sodium adducts, or direct deprotonation of the sulfate [12, 13]. During CZE-MS, NaOH can be added to the sheath liquid of the interface to exchange ionizable protons with sodium cations but this results in added experimental and spectral complexity, and reduced sensitivity. The direct deprotonation of all sulfo-groups to generate higher charge state precursors for ion activation would be ideal, but it is difficult to achieve, particularly when employing CZE for online separations.

Electron activation techniques, specifically electron detachment dissociation (EDD), have previously been shown to provide highly informative fragmentation of GAGs [13, 37-39]. However, the duty cycle for this approach is too slow for the narrow (~30 s) peaks generated by CZE separations as several seconds are required for external accumulation and electron irradiation due to poor conversion efficiencies. Fewer than 10 EDD spectra can be generated and averaged together under these constraints. Alternatively, negative electron transfer dissociation (NETD), the negative ion compliment to electron transfer dissociation (ETD), can provide electron activation through comparatively fast ion-ion interactions [40-42] on the order of ~50-100 ms. NETD has previously been implemented to characterize highly purified and synthetic GAG samples from dp4 to dp10 and up to 8 sulfo-modifications [43-46].

Although CE-MS has been previously shown to effectively separate GAG oligomers and provide compositional data, this approach has not been combined with tandem mass spectrometry for structure assignment. The current work provides the first data for CE-MS/MS of GAGs. We show NETD to be a compatible activation technique for sequencing GAGs that have been separated by CZE-MS [28]. The rationale for this combination is that NETD is much more rapid than EDD, while yielding many of the same products, and so is well suited for GAG mixture analysis. The CZE-MS/MS NETD technique was optimized with mixtures of naturally occurring and synthetic GAG tetrasaccharides, and then applied to enoxaparin, a complex low molecular weight heparin mixture.

5.3. EXPERIMENTAL

Materials

Bare fused silica (BFS) capillary for CZE (360 µm o.d. × 50 µm i.d.) was purchased from PolyMicro Technologies (Phoenix, AZ), borosilicate glass capillaries (1.0 mm OD × 0.75 mm i.d.) and pulled coated electrospray emitters (1.0 mm OD × 0.75 mm i.d.) were obtained from CMP scientific (Brooklyn, NY). Coating reagent N-(6-aminohexyl) aminomethyltriethoxysilane (AHS, Gelest, Morrisville, PA) was prepared in toluene. Ammonium acetate, water, and methanol were of HPLC grade (Fisher Scientific, Hampton, NH). Sodium hydroxide, acetone, toluene, and fluoranthene were purchased from Sigma-Aldrich (St. Louis, MO).

GAG Samples

GAG tetrasaccharide samples were prepared by enzymatic depolymerization of heparan sulfate and purified using strong anion exchange high-pressure liquid chromatography (SAX-HPLC), using methods described previously [8, 36]. Epimer pair heparan sulfate tetrasaccharides were chemically synthesized and purified as described in the literature [47]. Low molecular weight heparin, enoxaparin, was purchased from USP (Rockville, MD). All samples were desalted with 3 kDa Amicon Ultra centrifugal filter (Millipore, Temecula, CA) prior to CZE separation and mass spectrometry analysis. Filters were conditioned with water, and the sample washed with two filter volumes of HPLC grade water (14,000 × g for 25 min each). Before analysis, GAG samples were diluted to 50 µg/mL in water, and enoxaparin was diluted to 0.1 mg/mL in water.

Instrumentation

CZE separations were conducted with an Agilent HP 3D capillary electrophoresis instrument (Wilmington, DE). A bare fused silica capillary was used for CZE of GAG analyte, and its inner surface was modified with AHS to reduce observed analyte migration times. The total length of the capillary ranged from 58-60 cm, and its inner diameter was 50 µm with an internal volume of approximately 1 µL. Ammonium acetate (25 mM) was used as both the background electrolyte (BGE) and the sheath liquid (SL) for reverse polarity experiments. Aqueous GAG samples were injected for 3 s at 950 mbar followed by a background electrolyte (BGE) injection for 10 s at 10 mbar. The injected volume was 0.1 nL. The ionic strength of the injected sample plug is 2-3 orders of magnitude less than that of the background electrolyte, and sample stacking is expected under these conditions which provides a sharp sample front [29]. The

inlet of the capillary was then placed into a vial of BGE prior to separation. A voltage of -30 kV was applied to the capillary to drive the separation.

An EMASS-II (CMP Scientific, Brooklyn, NY) CZE-MS interface was employed to couple the CZE with a Thermo Fisher Scientific Orbitrap Elite mass spectrometer (Bremen, Germany) [35, 36, 48]. A separation capillary with a beveled outlet was nested inside a glass emitter sheath with a 0.75 mm inner diameter and a 30 µm tip orifice (CMP Scientific, Brooklyn, NY). The etched end of the capillary was positioned 0.3-0.5 mm from the tip of the sheath emitter orifice to create a mixing volume of ca. 1-5 nL and the emitter tip was filled with sheath liquid (SL) consisting of 25 mM ammonium acetate in 70 % methanol. An external power supply provided a voltage of -1.9 kV to the sheath liquid reservoir through a platinum wire, which produces electrospray at the emitter tip. MS detection was performed in negative ion mode. Prior to CZE-MS experiments, a semi-automatic optimization of source parameters was performed using sucrose octasulfate to improve sensitivity of sulfated GAGs and reduce sulfate decomposition during ion transfer prior to MS analysis. The Orbitrap Elite was scanned from m/z 150-2000 in negative ion mode for GAG oligosaccharides with a specified resolution of 120,000 for full MS and 60,000 for tandem MS experiments.

Fluoranthene radical cation produced by electron ionization was used as the reagent ion for NETD experiments. 110 ms activation times were used for doubly charged tetrasaccharides and triply charged hexasaccharides. 50 ms activation times were used for triply charged tetrasaccharides. Emission current was set to 75 µA and electron energy set to -70 V. Experiments were manually optimized. Preliminary CZE-MS was acquired to identify potential precursor ions, followed by individual NETD tandem experiments for each precursor, and then methods that split spectra acquisition evenly between MS1 and NETD MS2 of a single selected

precursor. A data dependent method was designed to apply NETD fragmentation to the two most intense m/z in the MS1 throughout the electropherogram, excluding the BGE peaks.

5.4 RESULTS AND DISCUSSION

With CZE, application of a strong electric field (ca. 30 kV) causes ions to migrate through an electrolyte solution. Small differences in mobility based on charge and molecular shape result in separation. This method is ideal for separating GAGs, which have a repeating disaccharide backbone structure with a high degree of charge arising from ionizable sulfo-modifications and carboxyl groups. CZE separations are rapid, with typical migration times less than 20-30 minutes (column lengths of 55 cm, and applied potential of 30 kV). Migration times vary too much to use this parameter to assign structures due to capillary heating effects, changes in the degree of modification of the interior wall of the separation capillary, and differences in capillary lengths between runs. Peaks in the electropherogram representing unique oligosaccharide structures are approximately 30 s wide. NETD activation is accomplished within 120 ms for low charge state precursors and 60 ms for higher charge state precursors and allows spectral averaging for a selected precursor ion or even for multiple co-migrating ions of different mass-to-charge. NETD operates near the speed of CID/HCD but with the informative ion activation of EDD. For an NETD experiment at a mass resolving power of 60,000 and a 110 ms activation time, 10-20 spectra can be recorded and averaged within a 30 s window corresponding to the peak width in CZE. NETD can also effectively fragment low charge state precursors without prior modification and produce fragmentation that provides sufficient information to assign sites of sulfo-modification to specific residues.

CZE has sufficient resolution to separate the enantiomeric iduronic acid (IdoA) and glucuronic acid (GlcA) residues, which differ only in the stereochemistry of C5. **Figure 5.1A** shows CZE separation of the synthetic tetrasaccharides GlcA-GlcNAc6S-IdoA-GlcNAc6S (GI) and GlcA-GlcNAc6S-GlcA-GlcNAc6S (GG), which both have two sulfo-modifications. A simple binary mixture of known tetrasaccharide epimers is a good test of CZE separation efficiency and NETD sequencing. **Figure 5.1B** shows the NETD fragmentation of $[M-2H]^{2-}$ precursor of GI, a tetrasaccharide with two sulfo-modifications on each of the 6-*O* positions of the glucosamine residues. Glycosidic bond fragment coverage is nearly complete across the GI ion with only B_1 and C_1 missing. The two sulfo-modifications can be confidently assigned to the glucosamine residues and cross-ring cleavages allow the assignment of the sulfo-modification on the reducing end at the 6-*O* position. The second sulfo-modification, assigned to the inner hexosamine residue cannot be differentiated between the 6-*O*- and 3-*O*- position; however, sulfo-modification of the 3-*O* position is rare [49]. **Figure 5.1C** is the NETD fragmentation of GG. The fragmentation patterns for both GG and GI are almost identical except for a $^{0,2}A_3$ peak present in GG and not in GI. This diagnostic ion has been shown previously to indicate the presence of glucuronic acid [50]. With this method it is possible to distinguish enantiomers as well as anomers. The latter often appear as a small peak of similar migration time to the dominant anomeric conformation, leading to the peak splitting observed in **Figure 5.1A**. Previous work using differential ion mobility gave similar results for resolving anomers [51]. The MS/MS spectra for the two structures can be differentiated by inspection in this case, though multivariate statistical approaches like principal component analysis are required for more highly sulfated HS tetramers [52, 53].

Table 4. The structure of four HS tetrasaccharide standards used for experiments are shown using symbol notation as defined in the table.

Sample 1	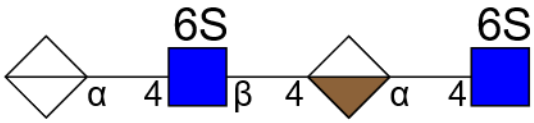
Sample 2	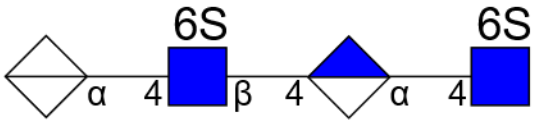
Sample 3	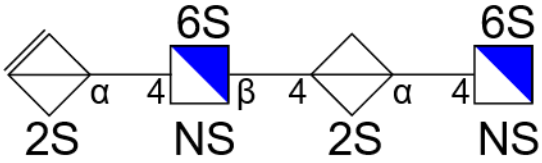
Sample 4	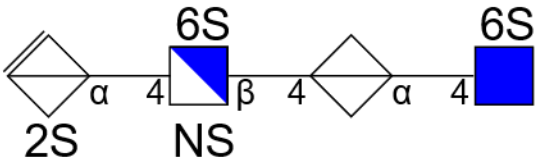

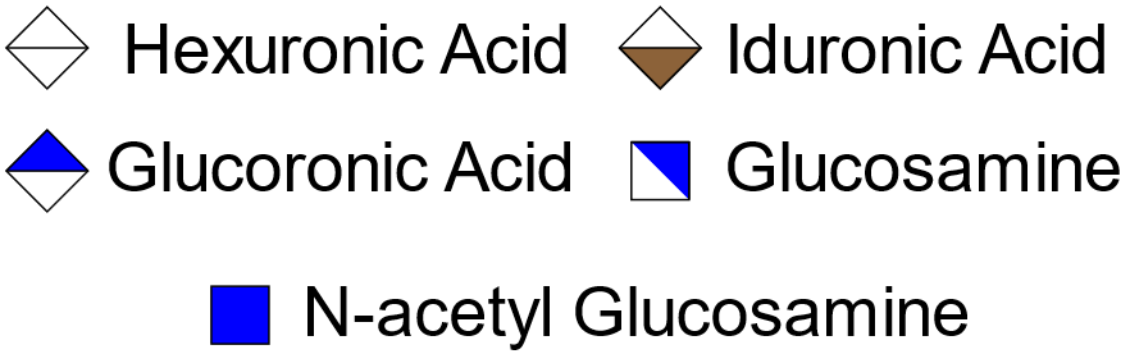

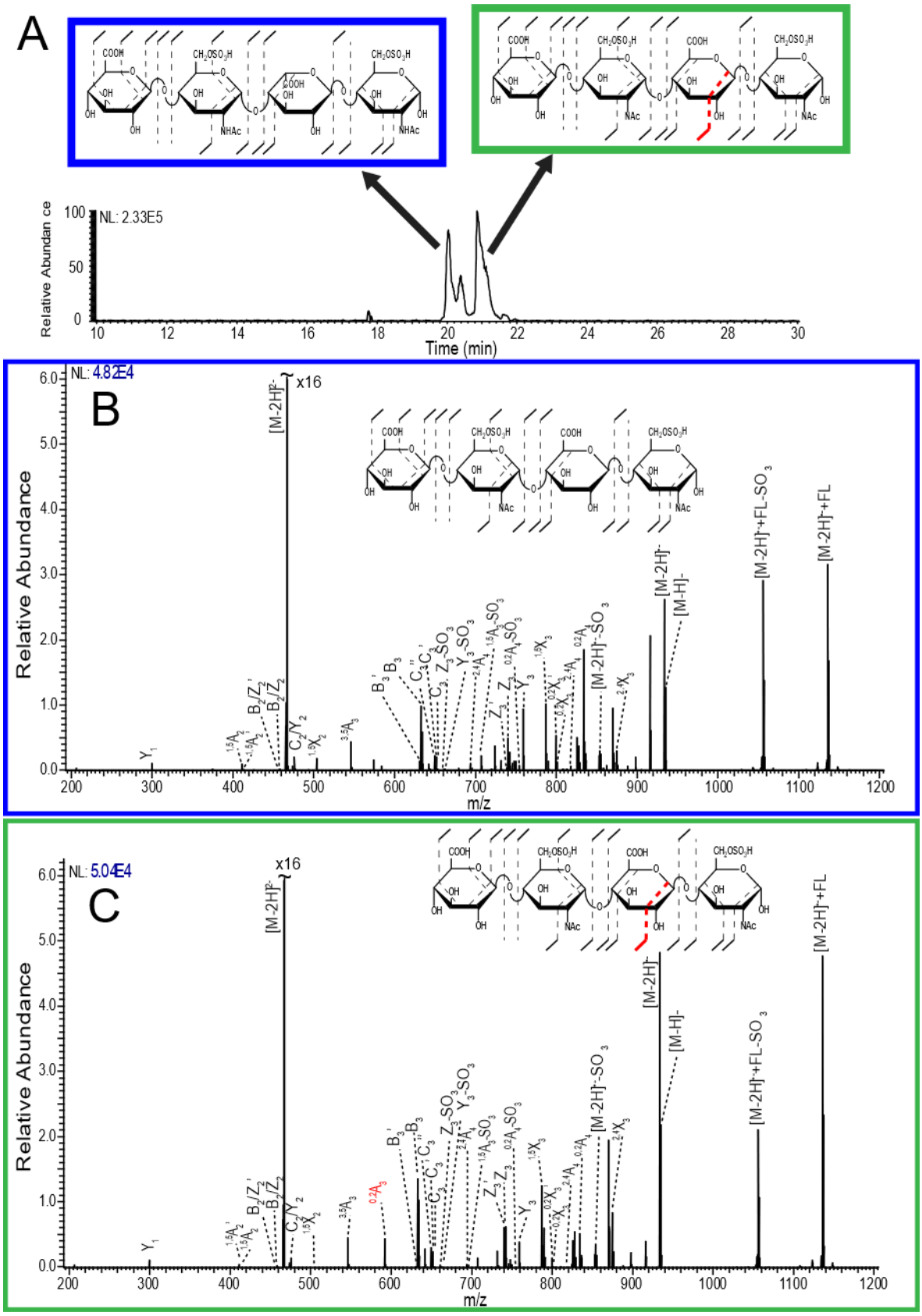
A
NL: 2.33E5
Relative Abundance
Time (min)
B
NL: 4.82E4
x16
[M-2H]2-
[M-2H]-
[M-H]-
[M-2H]-+FL-SO3
[M-2H]-+FL
Relative Abundance
m/z
C
NL: 5.04E4
x16
[M-2H]2-
[M-2H]-
[M-H]-
[M-2H]-+FL-SO3
[M-2H]-+FL
Relative Abundance
m/z

Figure 5.1. A) Capillary zone electrophoresis mass spectrometry (CZE-MS) separation and detection of a binary mixture of synthetically produced heparan sulfate (HS) tetrasaccharide epimers with two sulfo-modifications, with GlcA-GlcNAc6S-IdoA-GlcNAc6S (GI) on the left, and GlcA-GlcNAc6S-GlcA-GlcNAc6S (GG) on the right. B) The negative electron transfer dissociation (NETD) spectrum for the peak at 20 min in the CZE-MS electropherogram corresponding to GI, with structural assignments. C) The NETD spectrum for the peak at 21 min in the CZE-MS electropherogram corresponding to GG, with structural assignments.

The degree of sulfo-modification has an observable effect on the charge state distribution that impacts precursor selection. The difference in the CZE-MS spectra is demonstrated for a tetrasaccharide with two sulfo-modifications (**Figure 5.2A** top) compared to a tetrasaccharide with six sulfo-modifications (**Figure 5.2A** bottom). The tetrasaccharide with two sulfo-modifications generated only a 2- charge state peak, while the tetrasaccharide with six sulfo-modifications generated both 2- and a 3- charge state peak for precursor selection. By direct infusion, one would expect to see a larger difference in the charge state distributions for these two HS tetrasaccharides, but we find that the degree of ionization is lower with our CZE interface.

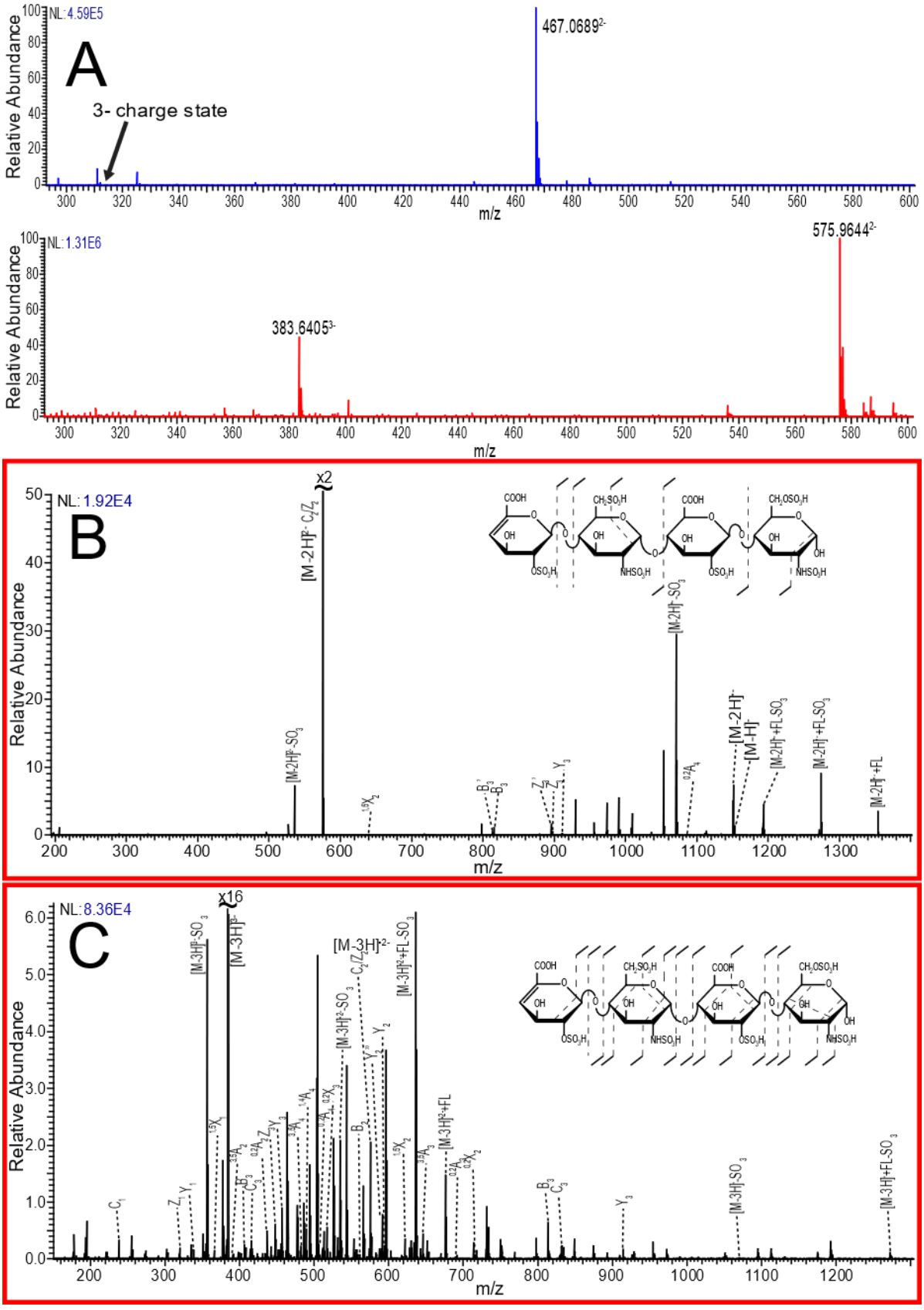
A
NL:4.59E5
467.0689²⁻
3- charge state
Relative Abundance
m/z
NL:1.31E6
575.9644²⁻
383.6405³⁻
B
NL:1.92E4
x2
[M-2H]²⁻-C₂/Z₂
[M-2H]²⁻-SO₃
[M-2H]⁻-SO₃
[M-2H]⁻
[M-H]⁻
[M-2H]⁻+FLSO₃
[M-2H]⁻+FL
C
NL:8.36E4
x16
[M-3H]³⁻
[M-3H]³⁻-SO₃
[M-3H]²⁻
[M-3H]²⁻-SO₃
[M-3H]²⁻+FL
[M-3H]²⁻+FL-SO₃
[M-3H]-SO₃
[M-3H]+FL-SO₃

Figure 5.2. A) Comparison of peak intensity measured for the 2- charge state and 3- charge state between a HS tetrasaccharide with two sulfo-modifications (top) and a tetrasaccharide with six sulfo-modifications (bottom). B) The NETD spectrum for the 2- charge state precursor of the six sulfo-modified HS tetrasaccharide, with structural assignments. C) The NETD spectrum for the 3- charge state precursor for the six-sulfo modified HS tetrasaccharide, with structural assignments.

The higher charge state enables more complete sequence information by NETD. **Figure 5.2B** shows the NETD fragmentation of the $[M-2H]^{2-}$ precursor for the tetrasaccharide (HS6) with six sulfo-modifications. The quality and coverage of NETD fragmentation has decreased compared to GI, due to the high degree of sulfo-modification on the low charge state precursor, but there is enough information to assign sulfo-modifications to each residue. The molecular weight of the molecule indicates that the amine group of both glucosamine residues are sulfated. The glycosidic cleavages also indicate that each uronic acid residue contains a sulfo-modification, which should be in the 2-*O* position, based on the known details of the biosynthesis of HS/Hp. This leaves a sulfate group on either the 6-*O* or 3-*O* position of each glucosamine residue, with the former occurring far more commonly than the latter.

In contrast, the NETD mass spectrum of the $[M-3H]^{3-}$ precursor for the same tetrasaccharide (HS6) is far more informative, as seen in **Figure 5.2C**. Glycosidic fragmentation coverage is nearly complete, with only the B_1 fragment missing, and all sulfo-modifications can be confidently assigned to specific residues. Cross-ring cleavage is sufficient to assign sites of modification, and the $^{3,5}A$ peak present on both glucosamine residues can be utilized to differentiate between 6-*O* and 3-*O* sulfo-modifications.

Unlike threshold activation techniques, such as CID or HCD, NETD does not require sodium replacement of protons to stabilize the labile sulfo-modifications. However, it has been shown that a certain degree of Na^+/H^+ exchange can improve electron based fragmentation [12]. **Figure 5.3** shows annotated structures for a 2- precursor series of a HS tetrasaccharide with four sulfo-modifications and A) $[M-2H]^{2-}$, B) $[M-4H+2Na]^{2-}$, and C) $[M-6H+4Na]^{2-}$. Overall, fragmentation for this tetrasaccharide is informative, with the production of large set of glycosidic and cross-ring fragments. Annotated spectra for the three tetrasaccharides are provided in the supplemental information (**Figures S1-S3**). The addition of two sodium adducts to the precursor has a minor effect; two glycosidic fragments are lost, C_1 and Y_2, while two cross-ring fragments are gained overall, though the observed cross-ring fragments are not entirely comparable. Fully ionizing the molecule by replacing all ionizable protons with sodium ions reduces overall fragmentation; few glycosidic bond fragments remain in comparison, and cross-ring fragmentation is shunted towards the outer residues with only two of the nine cross-ring fragments located on an inner residue. Adducting sodium to low charge state precursors presented by CZE-MS changes NETD fragmentation pathways and rearrangement options, and in some cases reduces the number of product ions once the molecule is fully ionized. In general, sodium adduction does not benefit NETD activation of heparin/HS after CZE separation.

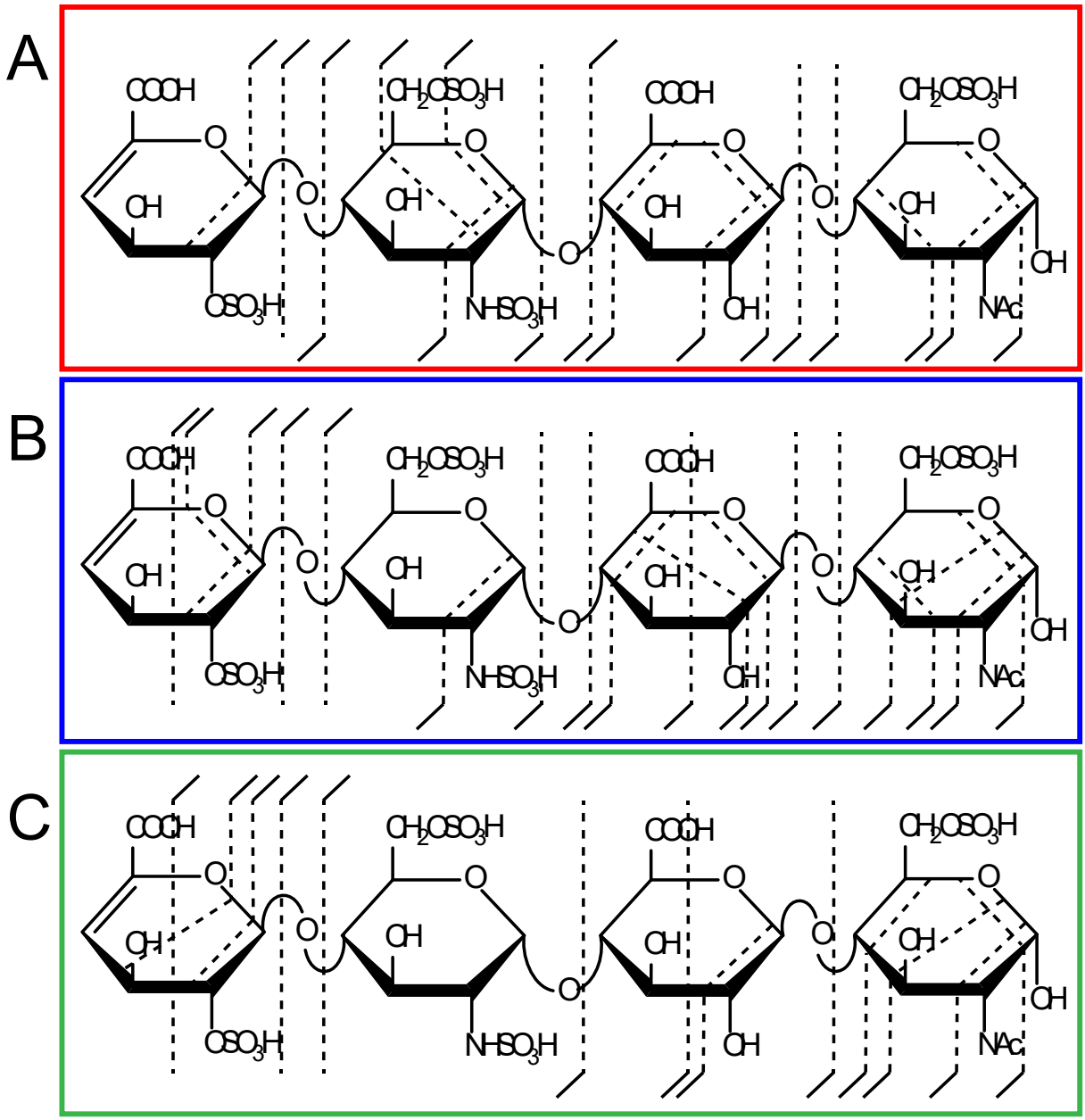

Figure 5.3. Comparison of NETD fragmentation patterns for different degrees of Na^+ stabilization of a four sulfo-modified HS tetrasaccharide. A) Two of six sites are ionized with no Na^+ adduction. B) Four of six sites are ionized with two Na^+ adductions. C) All six sites are ionized with 4 Na^+ adductions.

A more stringent test of the CZE-NETD MS/MS platform is the analysis of complex mixtures of GAGs. Enoxaparin, a low molecular weight heparin (LMWH) pharmaceutical, is a complex mixture derived from heparin polysaccharides that have been chemically digested to oligomers with up to 30 saccharide rings theoretically [54-56], and 3-12 saccharide rings observed with CZE-MS. We have examined this mixture by CZE-MS previously, and found that the components are detected within a 6 min wide window and present a series of well-defined peaks [28]. We have also identified compositions in enoxaparin with an extra water loss that is consistent with chemical digestion pathways that lead to a 1,6-anhydro bicyclic reducing end glucosamine residue [57, 58]. Here, we have integrated NETD with CZE-MS for the first time to assign structures to the components of enoxaparin. **Figure 5.4** shows the assignment of the top five most intense peaks found in the CZE separation of enoxaparin and characterized using NETD fragmentation. Mass lists of assigned peaks for all structures found in enoxaparin are in **supplemental tables 1-7** (**ST5.1-5.7**). The Orbitrap Elite was set to acquire data dependent MS/MS, selecting the two most intense peaks from the MS1 as a precursor to isolate and activate with NETD. The NETD spectra of the five most prominent masses were manually averaged and utilized to assign structure and sulfo-modification sites. The five prominent structures in enoxaparin are found to be highly sulfated, as one would expect for these heparin-derived fragments. Two of these five components, m/z 526.98^{2-} and 543.31^{3-}, are found to have a molecular weight that indicates the presence of a 1,6-anhydro bicyclic ring on the reducing end residue, which is an expected byproduct caused by the base-catalyzed digestion process used in the production of enoxaparin.

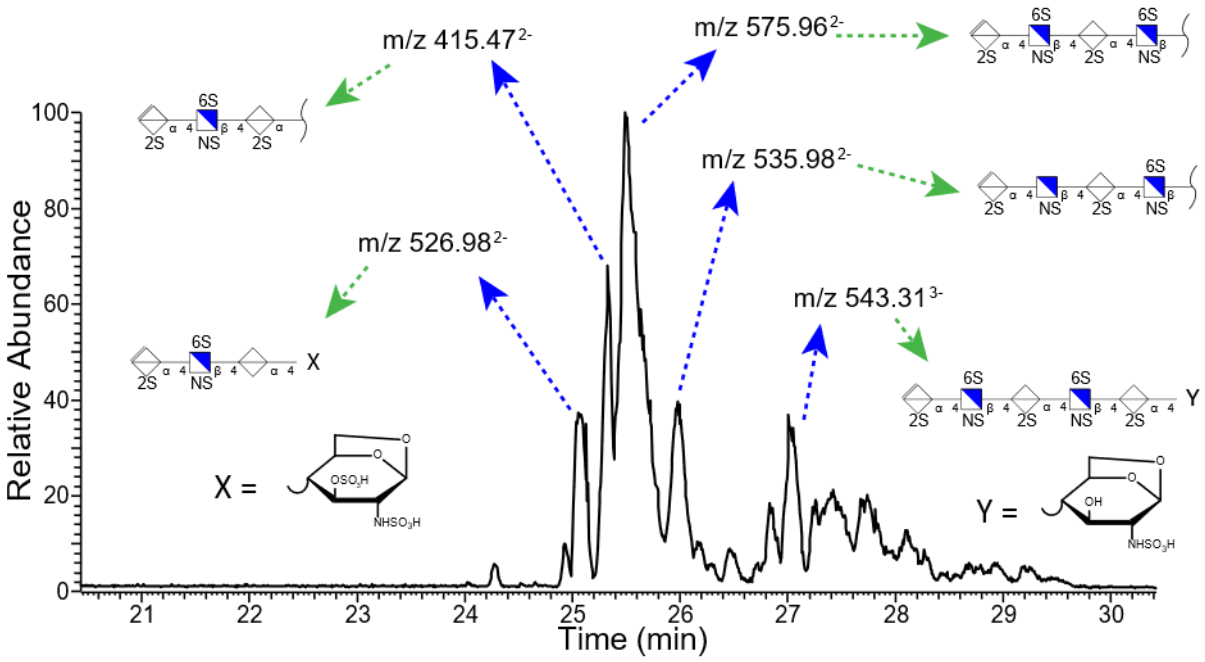

Figure 5.4. An electropherogram of the low molecular weight heparin pharmaceutical enoxaparin with structure assignments for the 5 most intense peaks determined by means of NETD activation.

Figure 5.5 shows extracted ion electropherograms for the five most prominent mass-to-charge values found in the CE separation of enoxaparin. Multiple peaks in the extracted ion electropherograms indicate that isomeric species exist for many of the prominent mass-to-charge values. These isomers can include GlcA/IdoA diastereomers as well as different combinations of sulfo-modification. NETD fragmentation was used to examine structural differences for these isomeric species. As an example, in **Figure 5.6A** more than five peaks were observed for m/z 535.98^{2-} throughout the electropherogram. These five peaks were selected for NETD analysis. **Figure 5.6B** shows the NETD spectra for the first peak in the grouping of three peaks from 23-24 min, which are partially resolved. Annotated NETD spectra and structural assignments for the three peaks in the grouping are in supplemental **Figure S4**. High intensity peaks in the spectra

that are unassigned are uninformative neutral losses and are detailed in the **supplemental tables**. The NETD spectra suggest a common pattern of sulfo-modification that differs from the peak that migrates at 25 min. The molecular structures in this grouping must differ by uronic acid stereochemistry (for the uronic acid residue closest to the reducing end) or by anomer state of the reducing end. NETD of the fourth peak at 25 min, **Figure 5.6C**, reveals a different pattern of sulfo-modification; on the 2-*O* position of the inner uronic acid residue instead of the 6-*O* position of the glucosamine observed for the previous three peaks, indicated by the red box in **Figure 5.6**. The fifth peak, 25.7 min, is too low in intensity to generate informative fragmentation with NETD. Multiple peaks indicating isomeric structures appear for many compositions found in Enoxaparin. **Figure 5.7A** shows that m/z 526 appears as only two main peaks in the electropherogram. Characterization of these two peaks with NETD reveals that they differ in sulfo-modification pattern. The annotated spectrum for the first peak at 24.53 min, **Figure 5.7B**, shows that the sulfo-modification is located on the reducing end glucosamine residue, and the 1,6-anhydro bicyclic ring structure of the reducing end glucosamine residue indicates that the sulfo-modification is most likely located on the rare 3-*O* position. The annotated spectrum for the second peak at 25.08 min, **Figure 5.7C**, shows that the sulfo-modification is located on the inner uronic acid residue, most likely at the 2-*O* position. NETD characterization of the two peaks for m/z 543, supplemental **Figure S5**, shows that the hexasaccharide has two different sites of sulfo-modification as well, with the late migrating peak most likely having a sulfo-modification in the rare 3-*O* position of the non-reducing end glucosamine due to the 1,6-anhydro bicyclic ring structure. Annotated spectra for the last remaining prominent mass-to-charge value m/z 415, a trisaccharide, as well as a separate low

intensity tetrassacharide, m/z 549, are provided in the supplemental information (**Figures S6 and S7**).

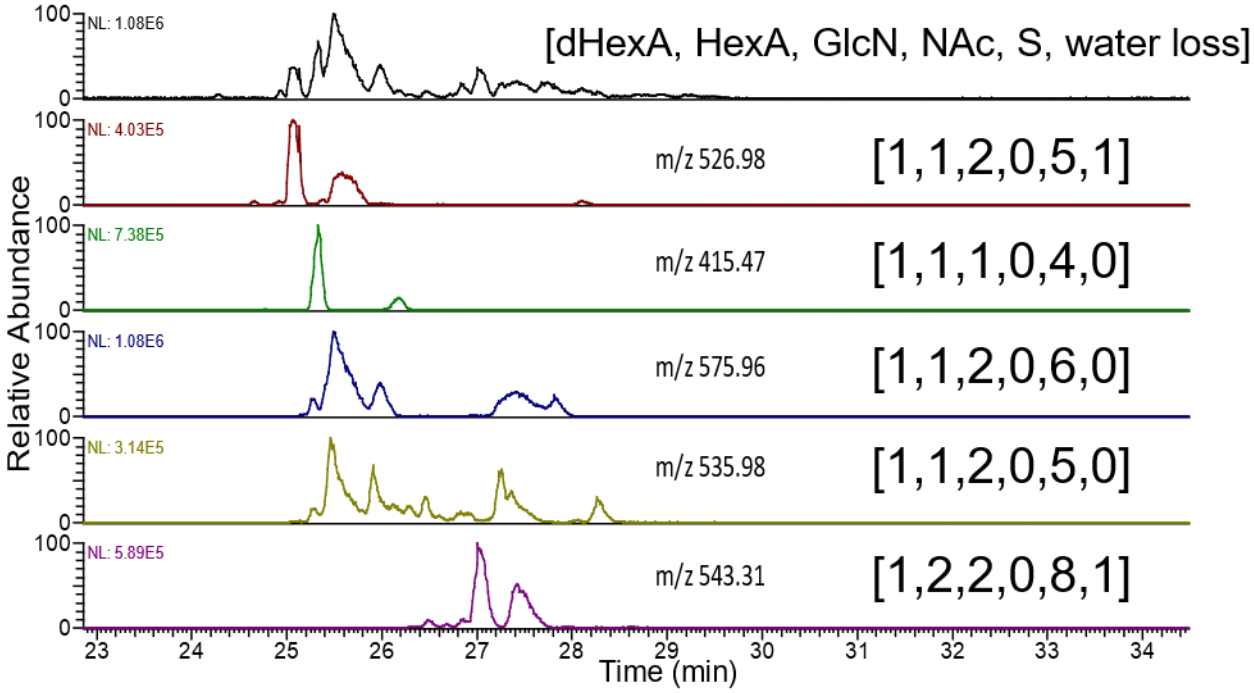

Figure 5.5. Extracted ion electropherograms with the mass-to-charge of the five most intense components found in enoxaparin, showing the presence of isomers at each of these m/z values. Composition assignments are represented as [dHexA, HexA, GlcN, NAc, S, water loss].

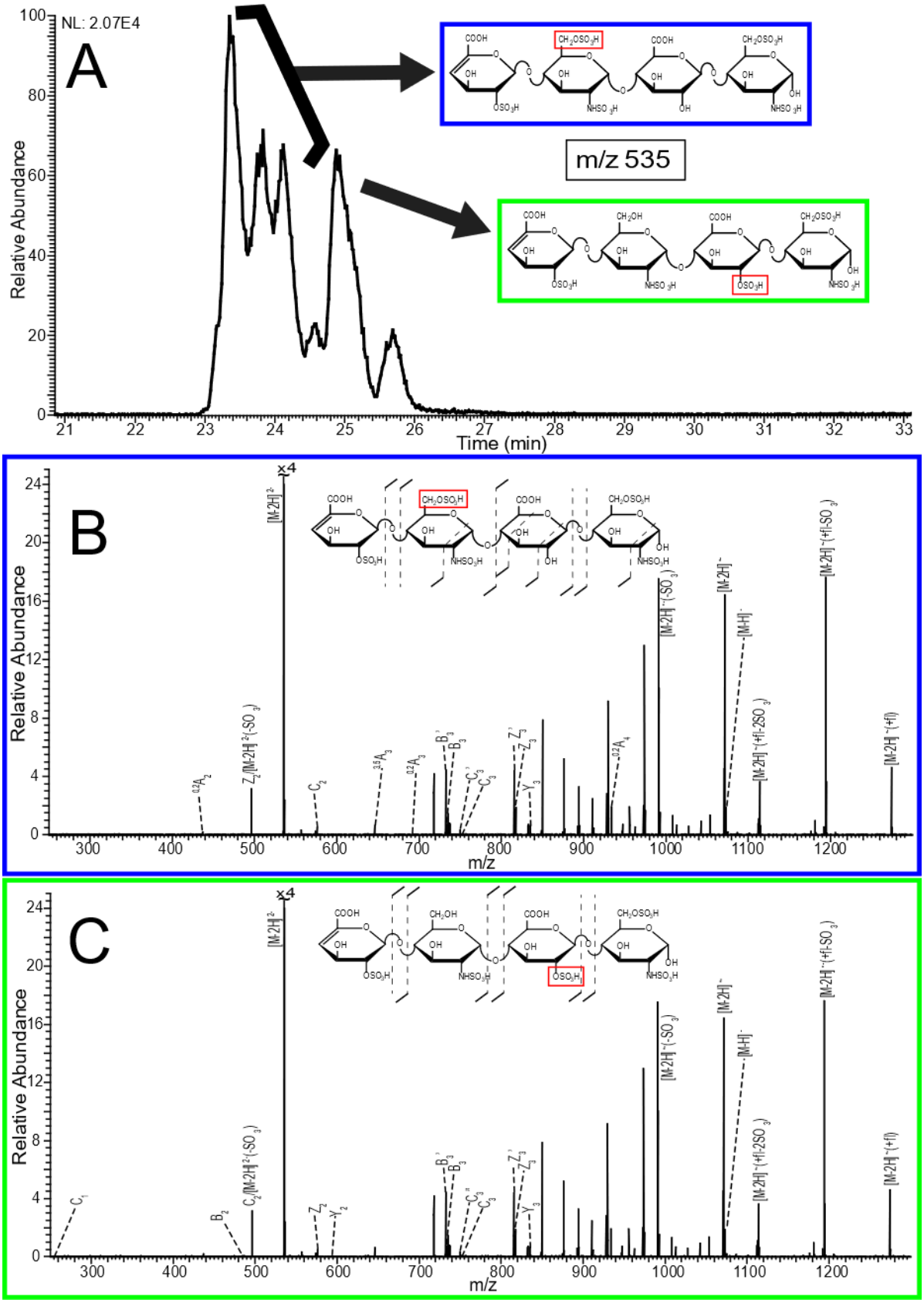
A
NL: 2.07E4
Relative Abundance
Time (min)
m/z 535
B
C
x4
m/z

Figure 5.6. Electropherogram for NETD activation of m/z 535.98^{2-} within enoxaparin, with structural assignment for the four most intense peaks. B) NETD spectrum for the first of three peaks (23-24 min) with annotations and structural assignments. C) NETD spectrum for the fourth peak (25 min) with annotation and structural assignments.

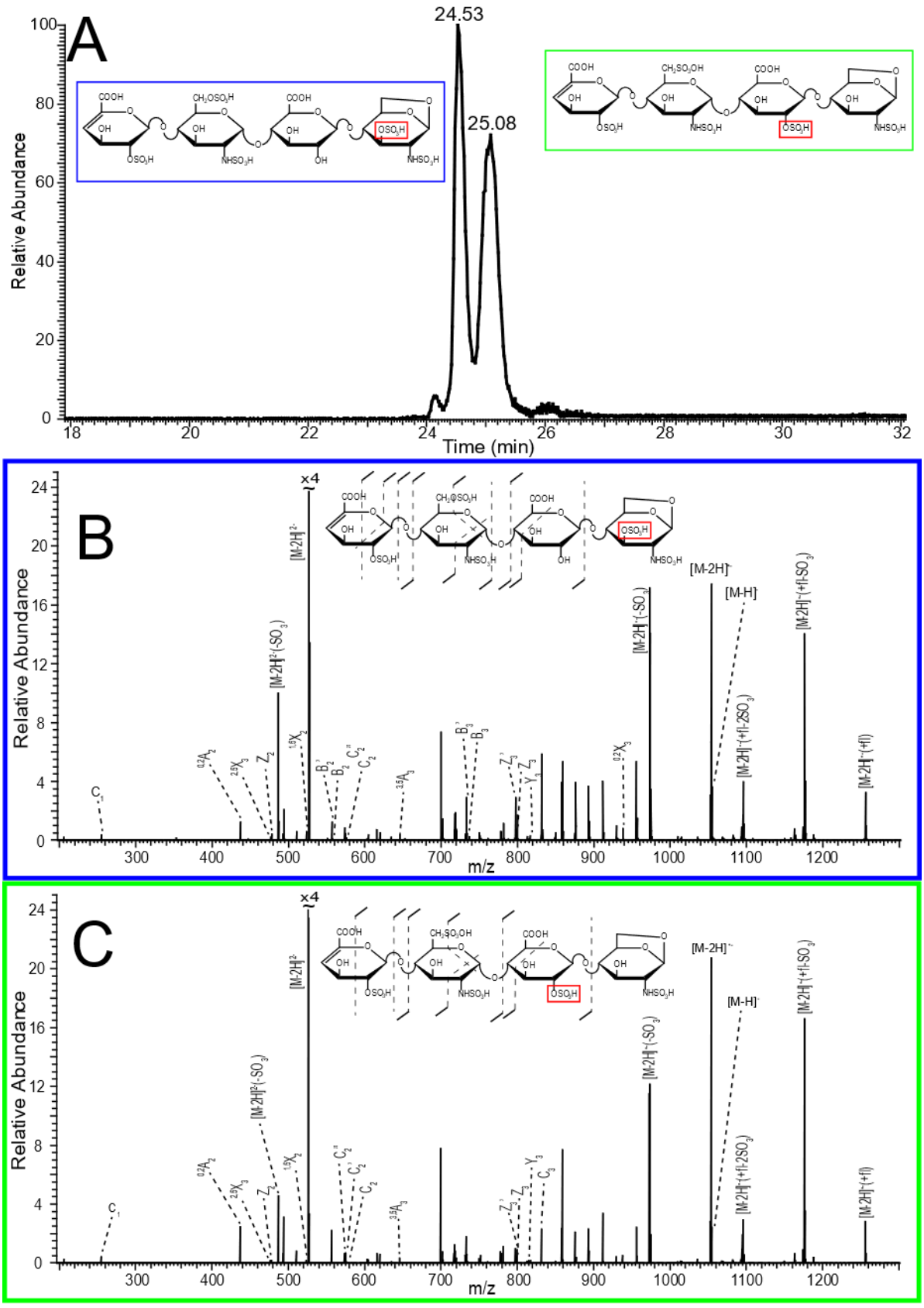
A
24.53
25.08
Relative Abundance
Time (min)
B
C
x4
[M-2H]2-
[M-2H]2-(-SO3)
[M-2H]-(-SO3)
[M-2H]-(+fl-SO3)
[M-2H]-(+fl-2SO3)
[M-2H]-(+fl)
[M-H]-
[M-2H]-
m/z

Figure 5.7. A) Isolated electropherogram of m/z 526.98^{2-} in enoxaparin. B) Annotated spectrum and structure for m/z 526.98^{2-} left peak (24.53 min). C) Annotated spectrum and structure for m/z 526.98^{2-} right peak (25.08 min).

5.5. CONCLUSIONS

CZE-NETD MS/MS provides a promising platform for analyzing complex GAG mixtures, to derive both chemical composition and structural information. GAG mixtures can be effectively separated by CZE. The speed of NETD activation (50-100 ms) is a good match for the CZE peak width (30 s), allowing improved signal-to-noise by signal averaging, and generating informative fragmentation spectra. In general, lower charge states are produced in the online CZE-MS experiment compared to direct infusion of GAGs. For this reason, CID is not a good match for CZE-MS sequencing of GAGs, as these lower charge states readily undergo sulfate decomposition. In contrast to CID, NETD of these lower charge state precursors produced by CZE separation generates fragmentation detail that is sufficient to assign sulfo-modification to specific GAG residues. Higher charge state precursors become more intense as the degree of sulfo-modifications increases and provides even more detailed fragmentation for the assignment of sulfo-modification to specific sites within GAG residues. With enough sulfo-modifications the higher charge state peak is sufficiently intense for NETD activation, and this provides near total coverage of the molecule. CZE-MS with NETD activation of complex mixtures like enoxaparin heparin results in structural assignment of multiple compositions. Isomeric compositions within enoxaparin are resolved by CZE and unique structures are assigned when there are differences in sulfo-modification. CZE is found to resolve diastereomers

resulting from differences in uronic acid stereochemistry, but their assignment by tandem mass spectrometry (IdoA versus GlcA) remains a challenge in most cases.

5.6. REFERENCES

1. Linhardt, R. J.; Toida, T., Role of Glycosaminoglycans in Cellular Communication. *Accounts of Chemical Research* **2004,** *37* (7), 431-438.

2. Aquino, R. S.; Park, P. W., Glycosaminoglycans and infection. *Frontiers in bioscience (Landmark edition)* **2016,** *21*, 1260-1277.

3. Iozzo, R. V.; Zoeller, J. J.; Nyström, A., Basement membrane proteoglycans: Modulators Par Excellence of cancer growth and angiogenesis. *Molecules and Cells* **2009,** *27* (5), 503-513.

4. Linhardt, R. J., 2003 Claude S. Hudson Award Address in Carbohydrate Chemistry. Heparin: Structure and Activity. *Journal of Medicinal Chemistry* **2003,** *46* (13), 2551-2564.

5. Xu, D.; Esko, J. D., Demystifying Heparan Sulfate–Protein Interactions. *Annual Review of Biochemistry* **2014,** *83* (1), 129-157.

6. Choay, J.; Petitou, M.; Lormeau, J. C.; Sinaÿ, P.; Casu, B.; Gatti, G., Structure-activity relationship in heparin: A synthetic pentasaccharide with high affinity for antithrombin III and eliciting high anti-factor Xa activity. *Biochemical and Biophysical Research Communications* **1983,** *116* (2), 492-499.

7. Jin, L.; Abrahams, J. P.; Skinner, R.; Petitou, M.; Pike, R. N.; Carrell, R. W., The anticoagulant activation of antithrombin by heparin. *Proceedings of the National Academy of Sciences* **1997,** *94* (26), 14683-14688.

8. Singh, A.; Kett, W. C.; Severin, I. C.; Agyekum, I.; Duan, J.; Amster, I. J.; Proudfoot, A. E. I.; Coombe, D. R.; Woods, R. J., The Interaction of Heparin Tetrasaccharides with Chemokine CCL5 Is Modulated by Sulfation Pattern and pH. *The Journal of Biological Chemistry* **2015,** *290* (25), 15421-15436.

9. Chen, Y.; Lin, L.; Agyekum, I.; Zhang, X.; St Ange, K.; Yu, Y.; Zhang, F.; Liu, J.; Amster, I. J.; Linhardt, R. J., Structural Analysis of Heparin-Derived 3-O-Sulfated Tetrasaccharides: Antithrombin Binding Site Variants. *Journal of pharmaceutical sciences* **2017,** *106* (4), 973-981.

10. Casu, B.; Naggi, A.; Torri, G., Re-visiting the structure of heparin. *Carbohydrate Research* **2015,** *403*, 60-68.

11. Laremore, T. N.; Ly, M.; Solakyildirim, K.; Zagorevski, D. V.; Linhardt, R. J., High-resolution preparative separation of glycosaminoglycan oligosaccharides by polyacrylamide gel electrophoresis. *Analytical Biochemistry* **2010,** *401* (2), 236-241.

12. Kailemia, M. J.; Li, L.; Ly, M.; Linhardt, R. J.; Amster, I. J., Complete Mass Spectral Characterization of a Synthetic Ultralow-Molecular-Weight Heparin Using Collision-Induced Dissociation. *Analytical Chemistry* **2012,** *84* (13), 5475-5478.

13. Wolff, J. J.; Chi, L.; Linhardt, R. J.; Amster, I. J., Electron Detachment Dissociation of Gycosaminoglycan Tetrasaccharides. *Journal of the American Society for Mass Spectrometry* **2007,** *18* (2), 234-244.

14. Ly, M.; Leach Iii, F. E.; Laremore, T. N.; Toida, T.; Amster, I. J.; Linhardt, R. J., The proteoglycan bikunin has a defined sequence. *Nature Chemical Biology* **2011,** *7*, 827.

15. Lin, L.; Liu, X.; Zhang, F.; Chi, L.; Amster, I. J.; Leach, F. E.; Xia, Q.; Linhardt, R. J., Analysis of heparin oligosaccharides by capillary electrophoresis-negative-ion electrospray ionization mass spectrometry. *Anal. Bioanal. Chem.* **2017,** *409* (2), 411-420.

16. Zaia, J., Glycosaminoglycan Glycomics Using Mass Spectrometry. *Molecular & Cellular Proteomics : MCP* **2013,** *12* (4), 885-892.

17. Gill, V. L.; Aich, U.; Rao, S.; Pohl, C.; Zaia, J., Disaccharide Analysis of Glycosaminoglycans Using Hydrophilic Interaction Chromatography and Mass Spectrometry. *Analytical Chemistry* **2013,** *85* (2), 1138-1145.

18. Hitchcock, A. M.; Bowman, M. J.; Staples, G. O.; Zaia, J., Improved Workup for Glycosaminoglycan Disaccharide Analysis using Capillary Electrophoresis with Laser-Induced Fluorescence Detection. *Electrophoresis* **2008,** *29* (22), 4538-4548.

19. Yang, B.; Weyers, A.; Baik, J. Y.; Sterner, E.; Sharfstein, S.; Mousa, S. A.; Zhang, F.; Dordick, J. S.; Linhardt, R. J., Ultra-performance ion-pairing liquid chromatography with on-line electrospray ion trap mass spectrometry for heparin disaccharide analysis. *Analytical Biochemistry* **2011,** *415* (1), 59-66.

20. Zaia, J., On-line separations combined with MS for analysis of glycosaminoglycans. *Mass Spectrometry Reviews* **2009,** *28* (2), 254-272.

21. Staples, G. O.; Zaia, J., Analysis of Glycosaminoglycans Using Mass Spectrometry. *Current proteomics* **2011,** *8* (4), 325-336.

22. Wang, Z.; Li, D.; Sun, X.; Bai, X.; Jin, L.; Chi, L., Liquid chromatography–diode array detection–mass spectrometry for compositional analysis of low molecular weight heparins. *Analytical Biochemistry* **2014,** *451*, 35-41.

23. Yang, B.; Chang, Y.; Weyers, A. M.; Sterner, E.; Linhardt, R. J., Disaccharide analysis of glycosaminoglycan mixtures by ultra-high-performance liquid chromatography-mass spectrometry. *J Chromatogr A* **2012,** *1225*, 91-98.

24. Jones, C. J.; Beni, S.; Larive, C. K., Understanding the Effect of the Counterion on the Reverse-Phase Ion-Pair High-Performance Liquid Chromatography (RPIP-HPLC) Resolution of Heparin-Related Saccharide Anomers. *Analytical Chemistry* **2011,** *83* (17), 6762-6769.

25. Fasciano, J. M.; Danielson, N. D., Ion chromatography for the separation of heparin and structurally related glycoaminoglycans: A review. *Journal of Separation Science* **2016,** *39* (6), 1118-1129.

26. Ruhaak, L. R.; Zauner, G.; Huhn, C.; Bruggink, C.; Deelder, A. M.; Wuhrer, M., Glycan labeling strategies and their use in identification and quantification. *Analytical and Bioanalytical Chemistry* **2010,** *397* (8), 3457-3481.

27. Wuhrer, M.; de Boer, A. R.; Deelder, A. M., Structural glycomics using hydrophilic interaction chromatography (HILIC) with mass spectrometry. *Mass Spectrometry Reviews* **2009,** *28* (2), 192-206.

28. Sanderson, P.; Stickney, M.; Leach, F. E.; Xia, Q.; Yu, Y.; Zhang, F.; Linhardt, R. J.; Amster, I. J., Heparin/heparan sulfate analysis by covalently modified reverse polarity capillary zone electrophoresis-mass spectrometry. *Journal of Chromatography A* **2018,** *1545*, 75-83.

29. Whatley, H., Basic Principles and Modes of Capillary Electrophoresis. In *Clinical and Forensic Applications of Capillary Electrophoresis*, Petersen, J. R.; Mohammad, A. A., Eds. Humana Press: Totowa, NJ, 2001; pp 21-58.

30. Albin, M.; Grossman, P. D.; Moring, S. E., Sensitivity enhancement for capillary electrophoresis. *Analytical Chemistry* **1993,** *65* (10), 489A-497A.

31. Smith, R. D.; Olivares, J. A.; Nguyen, N. T.; Udseth, H. R., Capillary zone electrophoresis-mass spectrometry using an electrospray ionization interface. *Analytical Chemistry* **1988,** *60* (5), 436-441.

32. Ruiz-Calero, V.; Moyano, E.; Puignou, L.; Galceran, M. T., Pressure-assisted capillary electrophoresis–electrospray ion trap mass spectrometry for the analysis of heparin depolymerised disaccharides. *Journal of Chromatography A* **2001,** *914* (1), 277-291.

33. Zaia, J., Capillary electrophoresis-mass spectrometry of carbohydrates. *Methods in molecular biology (Clifton, N.J.)* **2013,** *984*, 13-25.

34. Ucakturk, E.; Cai, C.; Li, L.; Li, G.; Zhang, F.; Linhardt, R. J., Capillary electrophoresis for total glycosaminoglycan analysis. *Analytical and Bioanalytical Chemistry* **2014,** *406* (19), 4617-4626.

35. Sun, L.; Zhu, G.; Zhang, Z.; Mou, S.; Dovichi, N. J., A third-generation electrokinetically pumped sheath flow nanospray interface with improved stability and sensitivity for automated capillary zone electrophoresis-mass spectrometry analysis of complex proteome digests. *Journal of proteome research* **2015,** *14* (5), 2312-2321.

36. Lin, L.; Liu, X.; Zhang, F.; Chi, L.; Amster, I. J.; Leach, F. E.; Xia, Q.; Linhardt, R. J., Analysis of heparin oligosaccharides by capillary electrophoresis-negative-ion electrospray ionization mass spectrometry. *Analytical and bioanalytical chemistry* **2017,** *409* (2), 411-420.

37. Wolff, J. J.; Laremore, T. N.; Aslam, H.; Linhardt, R. J.; Amster, I. J., Electron-Induced Dissociation of Glycosaminoglycan Tetrasaccharides. *Journal of the American Society for Mass Spectrometry* **2008,** *19* (10), 1449-1458.

38. Oh, H. B.; Leach, F. E.; Arungundram, S.; Al-Mafraji, K.; Venot, A.; Boons, G.-J.; Amster, I. J., Multivariate Analysis of Electron Detachment Dissociation and Infrared Multiphoton Dissociation Mass Spectra of Heparan Sulfate Tetrasaccharides Differing Only in Hexuronic acid Stereochemistry. *Journal of The American Society for Mass Spectrometry* **2011,** *22* (3), 582-590.

39. Leach, F. E.; Ly, M.; Laremore, T. N.; Wolff, J. J.; Perlow, J.; Linhardt, R. J.; Amster, I. J., Hexuronic Acid Stereochemistry Determination in Chondroitin Sulfate Glycosaminoglycan Oligosaccharides by Electron Detachment Dissociation. *Journal of The American Society for Mass Spectrometry* **2012,** *23* (9), 1488-1497.

40. McLuckey, S. A.; Stephenson, J. L.; O'Hair, R. A. J., Decompositions of odd- and even-electron anions derived from deoxy-polyadenylates. *Journal of the American Society for Mass Spectrometry* **1997,** *8* (2), 148-154.

41. Syka, J. E. P.; Coon, J. J.; Schroeder, M. J.; Shabanowitz, J.; Hunt, D. F., Peptide and protein sequence analysis by electron transfer dissociation mass spectrometry. *Proceedings of the National Academy of Sciences of the United States of America* **2004,** *101* (26), 9528-9533.

42. Coon, J. J.; Shabanowitz, J.; Hunt, D. F.; Syka, J. E. P., Electron transfer dissociation of peptide anions. *Journal of the American Society for Mass Spectrometry* **2005,** *16* (6), 880-882.

43. Wolff, J. J.; Leach, F. E.; Laremore, T. N.; Kaplan, D. A.; Easterling, M. L.; Linhardt, R. J.; Amster, I. J., Negative electron transfer dissociation of glycosaminoglycans. *Analytical chemistry* **2010,** *82* (9), 3460-3466.

44. Leach, F. E.; Wolff, J. J.; Xiao, Z.; Ly, M.; Laremore, T. N.; Arungundram, S.; Al-Mafraji, K.; Venot, A.; Boons, G.-J.; Linhardt, R. J.; Amster, I. J., Negative electron transfer dissociation Fourier transform mass spectrometry of glycosaminoglycan carbohydrates. *European Journal of Mass Spectrometry (Chichester, England)* **2011,** *17* (2), 167-176.

45. Leach, F. E.; Riley, N. M.; Westphall, M. S.; Coon, J. J.; Amster, I. J., Negative Electron Transfer Dissociation Sequencing of Increasingly Sulfated Glycosaminoglycan

Oligosaccharides on an Orbitrap Mass Spectrometer. *Journal of The American Society for Mass Spectrometry* **2017,** *28* (9), 1844-1854.

46. Wu, J.; Wei, J.; Hogan, J. D.; Chopra, P.; Joshi, A.; Lu, W.; Klein, J.; Boons, G.-J.; Lin, C.; Zaia, J., Negative Electron Transfer Dissociation Sequencing of 3-O-Sulfation-Containing Heparan Sulfate Oligosaccharides. *Journal of The American Society for Mass Spectrometry* **2018,** *29* (6), 1262-1272.

47. Arungundram, S.; Al-Mafraji, K.; Asong, J.; Leach, F. E.; Amster, I. J.; Venot, A.; Turnbull, J. E.; Boons, G.-J., Modular Synthesis of Heparan Sulfate Oligosaccharides for Structure−Activity Relationship Studies. *Journal of the American Chemical Society* **2009,** *131* (47), 17394-17405.

48. Sun, L.; Zhu, G.; Zhao, Y.; Yan, X.; Mou, S.; Dovichi, N. J., Ultrasensitive and Fast Bottom-up Analysis of Femtogram Amounts of Complex Proteome Digests. *Angewandte Chemie International Edition* **2013,** *52* (51), 13661-13664.

49. Thacker, B. E.; Xu, D.; Lawrence, R.; Esko, J. D., Heparan sulfate 3-O-sulfation: a rare modification in search of a function. *Matrix biology : journal of the International Society for Matrix Biology* **2014,** *35*, 60-72.

50. Wolff, J. J.; Chi, L.; Linhardt, R. J.; Amster, I. J., Distinguishing glucuronic from iduronic acid in glycosaminoglycan tetrasaccharides by using electron detachment dissociation. *Analytical chemistry* **2007,** *79* (5), 2015-2022.

51. Kailemia, M. J.; Park, M.; Kaplan, D. A.; Venot, A.; Boons, G.-J.; Li, L.; Linhardt, R. J.; Amster, I. J., High-field asymmetric-waveform ion mobility spectrometry and electron detachment dissociation of isobaric mixtures of glycosaminoglycans. *Journal of The American Society for Mass Spectrometry* **2014,** *25* (2), 258-268.

52. Agyekum, I.; Patel, A. B.; Zong, C.; Boons, G.-J.; Amster, I. J., Assignment of hexuronic acid stereochemistry in synthetic heparan sulfate tetrasaccharides with 2-O-sulfo uronic acids using electron detachment dissociation. *International Journal of Mass Spectrometry* **2015,** *390*, 163-169.

53. Agyekum, I.; Zong, C.; Boons, G.-J.; Amster, I. J., Single Stage Tandem Mass Spectrometry Assignment of the C-5 Uronic Acid Stereochemistry in Heparan Sulfate Tetrasaccharides using Electron Detachment Dissociation. *Journal of The American Society for Mass Spectrometry* **2017,** *28* (9), 1741-1750.

54. Mourier, P. A. J.; Agut, C.; Souaifi-Amara, H.; Herman, F.; Viskov, C., Analytical and statistical comparability of generic enoxaparins from the US market with the originator product. *Journal of Pharmaceutical and Biomedical Analysis* **2015,** *115*, 431-442.

55. Guerrini, M.; Rudd, T. R.; Mauri, L.; Macchi, E.; Fareed, J.; Yates, E. A.; Naggi, A.; Torri, G., Differentiation of Generic Enoxaparins Marketed in the United States by Employing NMR and Multivariate Analysis. *Analytical Chemistry* **2015,** *87* (16), 8275-8283.

56. Zaia, J.; Khatri, K.; Klein, J.; Shao, C.; Sheng, Y.; Viner, R., Complete Molecular Weight Profiling of Low-Molecular Weight Heparins Using Size Exclusion Chromatography-Ion Suppressor-High-Resolution Mass Spectrometry. *Analytical Chemistry* **2016,** *88* (21), 10654-10660.

57. Mascellani, G.; Guerrini, M.; Torri, G.; Liverani, L.; Spelta, F.; Bianchini, P., *Characterization of di- and monosulfated, unsaturated heparin disaccharides with terminal N-sulfated 1,6-anhydro-beta-D-glucosamine or N-sulfated 1,6-anhydro-beta-D-mannosamine residues*. 2007; Vol. 342, p 835-42.

58. Li, D.; Chi, L.; Jin, L.; Xu, X.; Du, X.; Ji, S.; Chi, L., Mapping of low molecular weight heparins using reversed phase ion pair liquid chromatography–mass spectrometry. *Carbohydr. Polym.* **2014,** *99*, 339-344.

5.7 SUPPLEMENTAL DATA

ST5.1. Mass lists for the NETD tandem mass spectra of the two peaks of m/z 526.98^{2-} in enoxaparin shown in Figure 7; A) peak at 24.53 min and B) peak at 25.08 min.

A

m/z	%I	Assignment
254.9799	0.35	C_1
436.9701	1.2	$^{0,2}A_2$
476.9657	0.19	$^{2,5}X_3$
477.9973	0.36	Z_2
487.0024	9.99	$[M-2H]^{2-}$-SO_3
496.0076	0.03	Y_2
524.0032	0.54	$^{1,5}X_2$
526.9813	100	$[M-2H]^{2-}$
557.9504	0.08	B_2
575.9636	0.18	C_2
645.9691	0.38	$^{3,5}A_3$
700.0014	7.18	Z3'-SO3-H2O
701.0055	0.59	Z3-SO3-H2O
718.0117	1.76	Z3'-SO3
719.0196	1.79	Z_3-SO_3
733.9808	0.46	B_3
737.0304	0.22	Y_3-SO_3
779.0501	0.56	$^{0,2}X_3$-$2SO_3$
797.9689	2.86	Z_3'
798.9762	0.75	Z_3
816.9875	0.28	Y_3
832.0439	5.69	$[M-2H]^{\cdot-}$-$2SO_3$-H_2O-CO_2
859.0076	5.18	$^{0,2}X_3$-SO_3
876.0342	3.83	$[M-2H]^{\cdot-}$-$2SO_3$-H_2O
893.0369	3.6	$[M-3H]^-$-$2SO_3$
894.0433	1.21	$[M-2H]^{\cdot-}$-$2SO_3$
895.0504	0.22	$[M-H]^-$-$2SO_3$
912.0009	3.96	$[M-2H]^{\cdot-}$-SO_3-H_2O-CO_2
938.9516	0.09	$^{0,2}X_3$
955.9908	5.2	$[M-2H]^{\cdot-}$-SO_3-H_2O
972.9934	16.92	$[M-3H]^-$-SO_3
974.0006	14.11	$[M-2H]^{\cdot-}$-SO_3
975.0073	3.5	$[M-H]^-$-SO_3
1053.9587	17.43	$[M-2H]^{\cdot-}$
1054.964	3.87	$[M-H]^-$

B

m/z	%I	Assignment
254.9799	0.4	C_1
436.97	2.43	$^{0,2}A_2$
476.9659	0.13	$^{2,5}X_3$
477.997	0.13	Z_2
487.0021	4.54	$[M-2H]^{2-}$-SO_3
524.0033	0.15	$^{1,5}X_2$
526.9813	100	$[M-2H]^{2-}$
575.9643	0.06	C_2
645.9693	0.29	$^{3,5}A_3$
700.0016	7.45	Z_3'-SO_3-H_2O
701.0062	0.07	Z_3-SO_3-H_2O
718.0122	1.18	Z_3'-SO_3
719.0198	0.75	Z_3-SO_3
733.9831	0.56	C3-SO3-H2O
751.9942	0.47	C_3-SO_3
797.9691	0.93	Z_3'
798.9776	0.39	Z_3
816.9869	0.14	Y_3
831.9509	1.31	C_3
832.0439	2.23	$[M-2H]^{\cdot-}$-$2SO_3$-H_2O-CO_2
857.9902	2.27	$[M-2H]^{\cdot-}$-$2SO_3$-$2H_2O$
876.0342	2.07	$[M-2H]^{\cdot-}$-$2SO_3$-H_2O
893.0367	2.22	$[M-3H]^-$-$2SO_3$
894.0441	0.78	$[M-2H]^{\cdot-}$-$2SO_3$
912.0009	3.26	$[M-2H]^{\cdot-}$-SO_3-H_2O-CO_2
955.9909	2.32	$[M-2H]^{\cdot-}$-SO_3-H_2O
972.9935	11.18	$[M-3H]^-$-SO_3
974.0014	11.91	$[M-2H]^{\cdot-}$-SO_3
975.0083	1.8	$[M-H]^-$-SO_3
1053.9589	20.25	$[M-2H]^{\cdot-}$
1054.966	2.37	$[M-H]^-$

ST5.2. Mass list for the NETD tandem mass spectrum of the peak m/z 415.47^{2-} in enoxaparin, shown in Figure 5 at 25.33 min.

m/z	%I	Assignment
254.9799	0.13	C_1/Z_1
300.9854	0.21	$^{1,5}X_1$
335.516	0.19	$[M-2H]^{2-}-2SO_3$
375.4935	3.13	$[M-2H]^{2-}-SO_3$
390.9647	0.04	$^{3,5}A_2$
415.4723	100	$[M-2H]^{2-}$
436.9702	1.01	$^{0,2}A_2$
476.9895	4.66	$C_2'/Z_2'-SO_3-H_2O$
556.9457	1.03	$C_2'/Z_2'-H_2O$
574.9564	2.35	C_2'/Z_2'
575.9641	1	C_2/Z_2
591.9593	0.28	Y_2''
593.975	0.67	Y_2
609.0305	1.41	$[M-2H]^{\cdot-}-2SO_3-H_2O-CO_2$
634.9769	7.01	$[M-2H]^{\cdot-}-2SO_3-2H_2O$
645.9688	0.2	$^{3,5}A_3$
653.0206	3.89	$[M-2H]^{\cdot-}-2SO_3-H_2O$
670.0232	2.93	$[M-3H]^{-}-2SO_3$
691.9732	0.27	$^{0,2}A_3$
732.9758	8.47	$[M-2H]^{\cdot-}-SO_3-H_2O$
749.9782	7.42	$[M-3H]^{-}-SO_3$
750.9858	3	$[M-2H]^{\cdot-}-SO_3$
829.936	0.81	$[M-3H]^{-}$
830.9434	0.89	$[M-2H]^{\cdot-}$
831.9511	0.52	$[M-H]^{-}$

ST5.3. Mass list for the NETD tandem mass spectrum of the peak m/z 575.96^{2-} in enoxaparin, shown in Figure 5 at 25.50 min.

m/z	%I	Assignment
486.9943	0.14	$[M-2H]^{2-}-2SO_3-H_2O$
526.9824	1.57	$[M-2H]^{2-}-SO_3-H_2O$
535.9878	8	$[M-2H]^{2-}-SO_3$
566.96	0.06	$[M-2H]^{2-}-H_2O$
575.9654	100	C_2/Z_2
575.9654	100	$[M-2H]^{2-}$
621.9712	0.06	$^{1,5}X_2$
733.9835	0.08	B_3-SO_3
797.9697	1.57	$Z_3'-SO_3-H_2O$
813.9405	0.47	B_3
816.9875	0.77	Z_3-SO_3
835.0008	0.19	Y_3-SO_3
895.9375	1.45	Z_3'
896.9439	0.82	Z_3
914.9566	0.27	Y_3
930.0123	5.27	$[M-2H]^{2-}-2SO_3-H_2O-CO_2$
955.959	1.73	$[M-2H]^{2-}-2SO_3-2H_2O$
974.0025	4.71	$[M-2H]^{2-}-2SO_3-H_2O$
975.0102	3.66	$[M-H]^{-}-2SO_3-H_2O$
991.0051	5.62	$[M-3H]^{2-}-2SO_3$
993.0211	0.59	$[M-H]^{-}-2SO_3$
1009.97	3.07	$[M-2H]^{2-}-SO_3-H_2O-CO_2$
1013.942	0.14	$^{0,2}A_4$
1053.96	12.4	$[M-2H]^{2-}-SO_3-H_2O$
1054.967	7.41	$[M-H]^{-}-SO_3-H_2O$
1070.963	29.75	$[M-3H]^{2-}-SO_3$
1071.97	11.15	$[M-2H]^{2-}-SO_3$
1072.978	8.46	$[M-H]^{-}-SO_3$
1134.924	0.16	$[M-H]^{-}-H_2O$
1150.92	4.95	$[M-3H]^{2-}$
1151.928	7.46	$[M-2H]^{2-}$
1152.935	5.95	$[M-H]^{-}$

ST5.4. Mass list for the NETD tandem mass spectrum of the peak m/z 383.64^{3-} in enoxaparin, which is the 3- charge state precursor for m/z 575.96^{2-} shown in Figure 5 at 25.50 min.

m/z	%I	Assignment
254.9773	2.14	C_1
319.9699	0.8	Z_1
337.9805	0.57	Y_1
356.9752	0.35	$^{0,2}X_2$
356.9828	4.11	$[M-3H]^{3-}-SO_3$
365.9753	0.5	$^{1,5}X_1$
377.6311	0.95	$[M-3H]^{3-}-H_2O$
383.6351	100	$[M-3H]^{3-}$
406.4619	0.68	B_3
415.467	0.36	C_3
436.9649	2.94	$^{0,2}A_2$
447.9641	2.5	Z_3
456.9695	4.61	Y_3
463.994	11.16	$[M-4H]^{2-}-2SO_3-H_2O$
504.4761	20.74	$[M-3H]^{2-}-SO_3-H_2O-CO_2$
506.4611	0.56	$^{0,2}A_4$
517.9526	0.42	$^{0,2}X_3$
525.9671	8.7	$[M-4H]^{2-}-SO_3-H_2O$
534.9724	9.52	$[M-4H]^{2-}-SO_3$
543.4467	13.91	
566.4489	5.65	$[M-3H]^{2-}-H_2O$
566.9499	1.57	$[M-2H]^{2-}-H_2O$
575.4536	2.16	$[M-3H]^{2-}$
575.9581	8.29	$C_2/Z_2/[M-2H]^{2-}$
593.9681	1.46	Y_2
596.5362	11.49	$[M-3H]^{2-}+fl-2SO_3$
621.9628	2.13	$^{1,5}X_2$
636.5139	24.83	$[M-3H]^{2-}+fl-SO_3$
645.9624	3.03	$^{3,5}A_3$
676.4917	5.49	$[M-3H]^{2-}+fl$
691.9664	0.25	$^{0,2}A_3$
731.9621	4.53	
733.9776	4	$[M-3H]^{-}-4SO_3-H_2O$
813.9336	4.73	$[M-3H]^{-}-3SO_3-H_2O$
813.9337	4.53	B_3
831.9438	1.21	C_3
849.0392	6.01	$[M-3H]^{-}-2SO_3-H_2O-CO_2$
893.0289	2.11	$[M-3H]^{-}-2SO_3-H_2O$
914.9475	0.98	Y_3
928.9957	2.82	$[M-3H]^{-}-SO_3-H_2O-CO_2$
972.9848	2.76	$[M-3H]^{-}-SO_3-H_2O$
1051.116	1.98	$[M-3H]^{-}+fl-3SO_3-H_2O-CO_2$
1052.942	0.89	$[M-3H]^{-}-H_2O$
1070.951	0.4	$[M-3H]^{-}$
1095.105	3.54	$[M-3H]^{-}+fl-3SO_3-H_2O$
1113.115	3.85	$[M-3H]^{-}+fl-3SO_3$
1175.062	2.53	$[M-3H]^{-}+fl-2SO_3-H_2O$
1193.071	8.42	$[M-3H]^{-}+fl-2SO_3$
1273.027	3.86	$[M-3H]^{-}+fl-SO_3$
485.9887	4.25	$[M-4H]^{2-}-2SO_3-H_2O$

ST5.5. Mass lists for the NETD tandem mass spectra of the two structures found for m/z 535.98^{2-} in enoxaparin, shown in Figure 6; A) peak at 23.30 min and B) peak at 24.95 min.

A

m/z	%I	Assignment
436.9701	0.04	$^{0,2}A_2$
487.0022	0.42	$[M-2H]^{2-}$-SO_3-H_2O
496.0076	6.8	Z_2/[M-2H]2--SO3
526.9807	0.03	$[M-2H]^{2-}$-H_2O
535.9867	100	$[M-2H]^{2-}$
575.964	0.42	C_2
645.9683	0.75	$^{3,5}A_3$
691.9731	0.21	$^{0,2}A_3$
718.0119	2.71	Z_3'-SO_3-H_2O
732.9756	2.7	B_3'
733.9835	0.32	B_3
737.0309	0.57	Z_3-SO_3
750.9867	0.39	C_3'
751.9942	0.25	C_3
755.0422	0.14	Y_3-SO_3
815.9799	2.45	Z_3'
816.9876	0.81	Z_3
834.9986	0.39	Y_3
850.0549	4.18	$[M-2H]^{\cdot-}$-2SO_3-H_2O-CO_2
854.027	0.09	$^{0,2}A_4$-SO_3
877.0173	0.11	$^{0,2}X_3$-SO_3
894.0447	1.28	$[M-2H]^{\cdot-}$-2SO_3-H_2O
895.0526	0.4	$[M-H]^-$-2SO_3-H_2O
911.0472	1.39	$[M-3H]^-$-2SO_3
930.116	4.51	$[M-2H]^{\cdot-}$-SO_3-H_2O-CO_2
933.9831	1.19	$^{0,2}A_4$
974.0019	4.36	$[M-2H]^{\cdot-}$-SO_3-H_2O
975.0105	0.99	$[M-H]^-$-SO_3-H_2O
991.0046	8.33	$[M-3H]^-$-SO_3
992.0127	4.52	$[M-2H]^{\cdot-}$-SO_3
993.0206	1.13	$[M-H]^-$-SO_3
993.0206	1.13	$[M-H]^-$-SO_3
1070.962	2.13	$[M-3H]^-$
1071.97	6.36	$[M-2H]^{\cdot-}$
1072.978	1.53	$[M-H]^-$

B

m/z	%I	Assignment
254.9799	0.11	C_1
477.9975	0.03	B_2
487.0024	0.12	$[M-2H]^{2-}$-SO_3-H_2O
496.0078	6.11	C_2/[M-2H]2--SO3
526.982	0.05	$[M-2H]^{2-}$-H_2O
535.9868	100	$[M-2H]^{2-}$
575.9642	0.04	Z_2
593.9751	0.12	Y_2
654.0275	0.06	B_3-SO_3
718.0125	3.8	Z_3'-SO_3-H_2O
732.9758	3.88	B_3'
733.985	0.88	B_3
737.0307	0.33	Z_3-SO_3
750.9864	0.34	C_3'
751.9945	0.03	C_3
815.9799	3.04	Z_3'
816.988	0.51	Z_3
834.9989	0.03	Y_3
850.0549	1.38	$[M-2H]^{\cdot-}$-2SO_3-H_2O-CO_2
894.0449	1.41	$[M-2H]^{\cdot-}$-2SO_3-H_2O
895.0527	0.23	$[M-H]^-$-2SO_3-H_2O
911.0472	1.8	$[M-3H]^-$-2SO_3
930.0118	1.26	$[M-2H]^{\cdot-}$-SO_3-H_2O-CO_2
974.0019	8.59	$[M-2H]^{\cdot-}$-SO_3-H_2O
975.0096	0.38	$[M-H]^-$-SO_3-H_2O
991.0046	14.43	$[M-3H]^-$-SO_3
992.0126	5.81	$[M-2H]^{\cdot-}$-SO_3
993.0206	1.32	$[M-H]^-$-SO_3
993.0206	1.32	$[M-H]^-$-SO_3
1070.962	4.37	$[M-3H]^-$
1071.97	8.45	$[M-2H]^{\cdot-}$
1072.978	1.36	$[M-H]^-$

ST5.6. Mass lists for the NETD tandem mass spectra of the two peaks of m/z 543.31^{3-} in enoxaparin shown in Figure 5; A) peak at 27.01 min and B) peak at 27.42 min.

A

m/z	%I	Assignment
254.98	0.09	C_1
436.9701	0.77	$^{0,2}A_2$
490.0033	0.43	$[M-3H]^{3-}$-$2SO_3$
496.0077	0.54	Y_2
496.0077	0.54	C_2-SO_3
496.0077	0.54	Y_4-SO_3
496.0077	0.54	C_4-$2SO_3$
516.6567	10.34	$[M-2H]^{2-}$-SO_3
543.309	100	$[M-3H]^{3-}$
575.964	1.12	C_2/C_4
645.969	0.31	$^{3,5}A_3$
646.9882	0.57	$^{0,3}X_2$
647.4908	0.5	Z_5-SO_3
656.4975	0.5	Y_5-SO_3
676.9989	1.48	$^{2,4}X_2$-SO_3
677.5049	1.37	$^{0,2}X_5$-$2SO_3$
686.9651	2.66	Z_5'
687.4676	0.86	Z_5
696.4746	1.03	Y_5
703.9571	0.1	C_5
704.0024	16.54	$[M-3H]^{2-}$-$2SO_3$-H_2O-CO_2
717.4834	6.29	$^{0,2}X_5$-SO_3
725.9974	6.74	$[M-3H]^{2-}$-$2SO_3$-H_2O
734.4988	7.35	$[M-4H]^{2-}$-$2SO_3$
735.5054	0.71	$[M-2H]^{2-}$-$2SO_3$
743.9807	18.17	$[M-3H]^{2-}$-SO_3-H_2O-CO_2
756.9732	1.98	$^{2,4}X_2$
757.4711	0.47	$^{0,2}X_5$
765.976	17	$[M-3H]^{2-}$-SO_3-H_2O
774.4773	19.38	$[M-4H]^{2-}$-SO_3
774.9802	12.88	$[M-3H]^{2-}$-SO_3
775.4839	3.86	$[M-2H]^{2-}$-SO_3
814.9598	8.38	$[M-3H]^{2-}$
815.4624	4.35	$[M-2H]^{2-}$
816.9876	0.05	Y_3
831.952	0.39	C_3
836.0416	3.84	$[M-3H]^{2-}$+fl-$2SO_3$
876.0203	9.32	$[M-3H]^{2-}$+fl-SO_3
915.999	5.11	$[M-3H]^{2-}$+fl
1013.941	0.22	$^{0,2}A_4$
1070.962	0.49	Y_4"
1072.977	0.17	Y_4
1072.977	0.17	C_4-SO_3
1100.975	0.13	$^{1,5}X_4$

B

m/z	%I	Assignment
436.9705	0.21	$^{0,2}A_2$
490.002	0.27	$[M-3H]^{3-}$-$2SO_3$
516.6566	11.43	$[M-3H]^{3-}$-SO_3
543.3089	100	$[M-3H]^{3-}$
575.9646	1.51	C_2/Y_2
647.4912	0.28	Z_5-SO_3
647.997	0.21	$^{1,4}X_2$
654.9751	0.22	B_5
656.4985	0.53	Y_5-SO_3
663.9799	1.32	C_5
676.9988	1.61	$^{2,4}X_2$-SO_3
677.5049	0.77	$^{0,2}X_5$-$2SO_3$
687.4684	0.4	Z_5
696.4751	1.18	Y_5
704.0025	20.16	$[M-3H]^{2-}$-$2SO_3$-H_2O-CO_2
717.4833	4.46	$^{0,2}X_5$-SO_3
725.9974	5.59	$[M-3H]^{2-}$-$2SO_3$-H_2O
734.4988	6.7	$[M-4H]^{2-}$-$2SO_3$
735.5058	0.66	$[M-2H]^{2-}$-$2SO_3$
743.9809	12.8	$[M-3H]^{2-}$-SO_3-H_2O-CO_2
756.9544	0.81	$^{2,4}X_2$
757.4678	0.12	$^{0,2}X_5$
765.4658	1.2	$^{2,5}X_5$
765.976	14.49	$[M-3H]^{2-}$-SO_3-H_2O
774.4773	14.23	$[M-4H]^{2-}$-SO_3
774.9808	20.54	$[M-3H]^{2-}$-SO_3
775.4832	5.77	$[M-2H]^{2-}$-SO_3
814.9597	12.41	$[M-3H]^{2-}$
815.4622	5.07	$[M-2H]^{2-}$
836.042	3.71	$[M-3H]^{2-}$+fl-$2SO_3$
876.0205	11.91	$[M-3H]^{2-}$+fl-SO_3
915.9993	5.7	$[M-3H]^{2-}$+fl
1072.979	0.25	C_4/Y_4

ST5.7. Mass lists for the NETD tandem mass spectrum of the middle peak of m/z 549.31^{2-} at 30.88 min in enoxaparin shown in Figure S7.

m/z	%I	Assignment
436.9659	1.01	$^{0,2}A_2$
522.6541	6.23	$[M-3H]^{3-}$-SO_3
549.3061	100	$[M-3H]^{3-}$
575.9579	0.64	C_2/Z_2
654.4639	1.16	B_5'
654.9667	0.22	B_5
656.4904	0.11	Z_5-SO_3
663.9726	0.22	C_5
665.4966	0.21	Y_5-SO_3
696.4684	0.63	Z_5
705.4745	1.4	Y_5
713.0027	7.43	$[M-3H]^{2-}$-$2SO_3$-H_2O-CO_2
714.9883	0.19	$^{0,2}A_6$-SO_3
725.976	5.75	$[M-4H]^{2-}$-$2SO_3$-H_2O
726.4785	0.87	$^{0,2}X_5$-SO_3
734.4935	1.15	$^{2,5}X_5$-SO_3
734.9973	5.64	$[M-3H]^{2-}$-$2SO_3$-H_2O
735.4993	2.16	$[M-2H]^{2-}$-$2SO_3$-H_20
743.4987	3.11	$[M-4H]^{2-}$-$2SO_3$
752.9806	15.49	$[M-3H]^{2-}$-SO_3-H_2O-CO_2
754.9659	1.99	$^{0,2}A_6$
766.4562	0.39	$^{0,2}X_5$
774.4712	2.6	$^{2,5}X_5$
774.9752	17.51	$[M-3H]^{2-}$-SO_3-H_2O
775.4774	5.89	$[M-2H]^{2-}$-SO_3-H_2O
783.4767	8.9	$[M-4H]^{2-}$-SO_3
783.9792	5.55	$[M-3H]^{2-}$-SO_3
784.4832	1.73	$[M-2H]^{2-}$-SO_3
801.9637	0.83	$[M-3H]^{2-}$-CO_2
814.9534	3.17	$[M-3H]^{2-}$-H_2O
815.4548	0.85	$[M-2H]^{2-}$-H_2O
823.9585	5.95	$[M-3H]^{2-}$
824.461	3.38	$[M-2H]^{2-}$
845.04	2.39	$[M-3H]^{2-}$+fl-2SO3
885.0185	11.32	$[M-3H]^{2-}$+fl-SO3
924.9966	6.99	$[M-3H]^{2-}$+fl
1090.977	0.34	Y_4
1118.971	0.1	$^{1,5}X_4$
1390.039	0.31	$^{2,5}X_5$-$2SO_3$
1469.994	0.5	$^{2,5}X_5$-SO_3

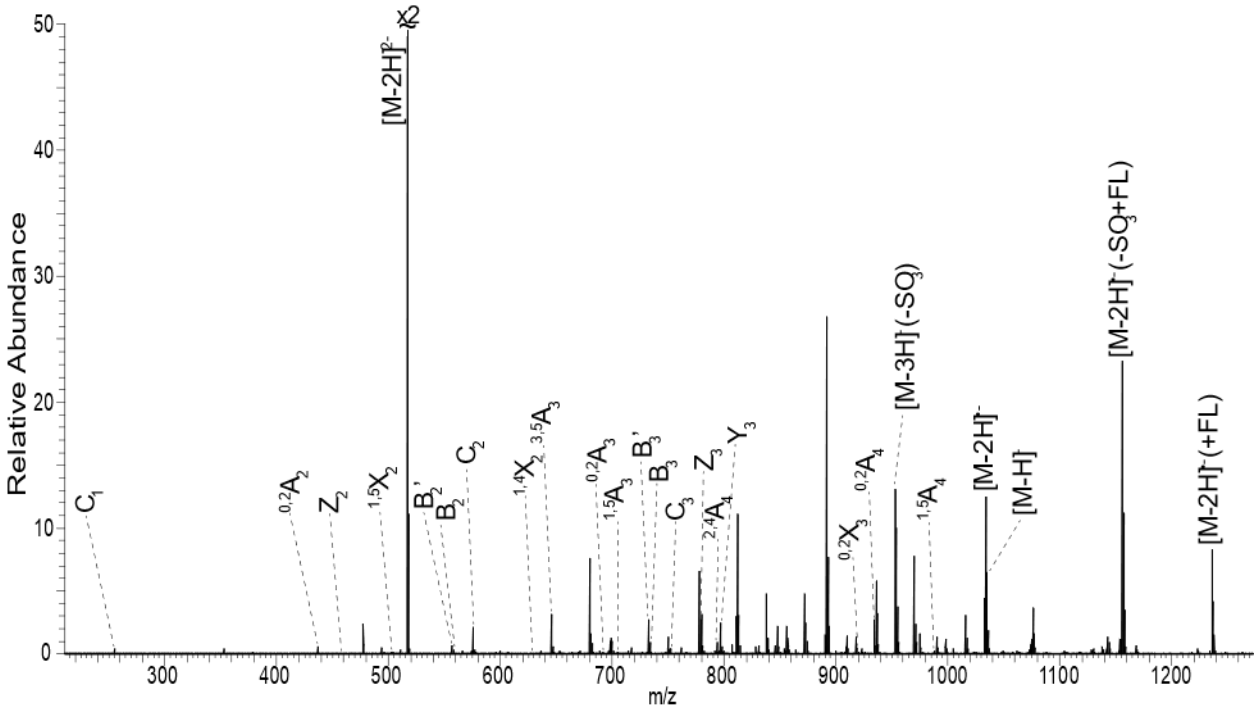

S5.1. Annotated NETD spectrum of HS tetrasaccharide with 4S and 0 Na adduction (2/6 sites ionized), m/z 517.01^{2-}, from Figure 3A.

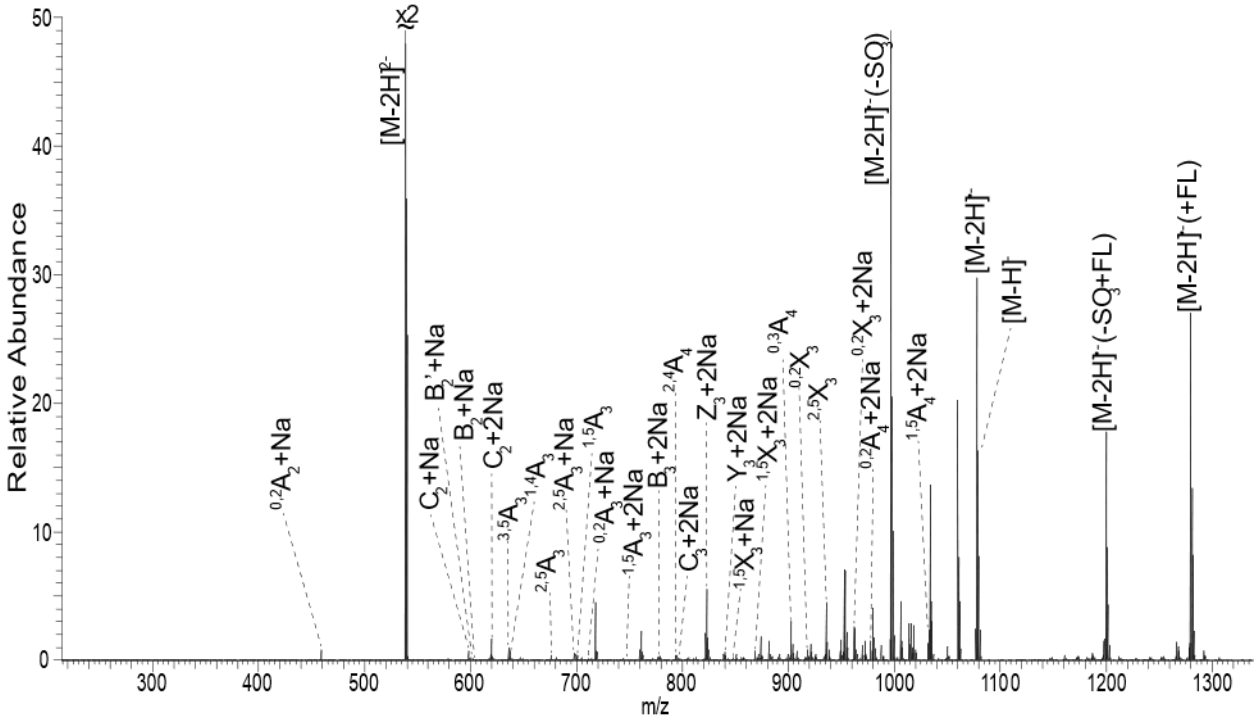

S5.2. Annotated NETD spectrum of HS tetrasaccharide with 4S and 2 Na adduction (4/6 sites ionized), m/z 538.99^{2-}, from Figure 3B.

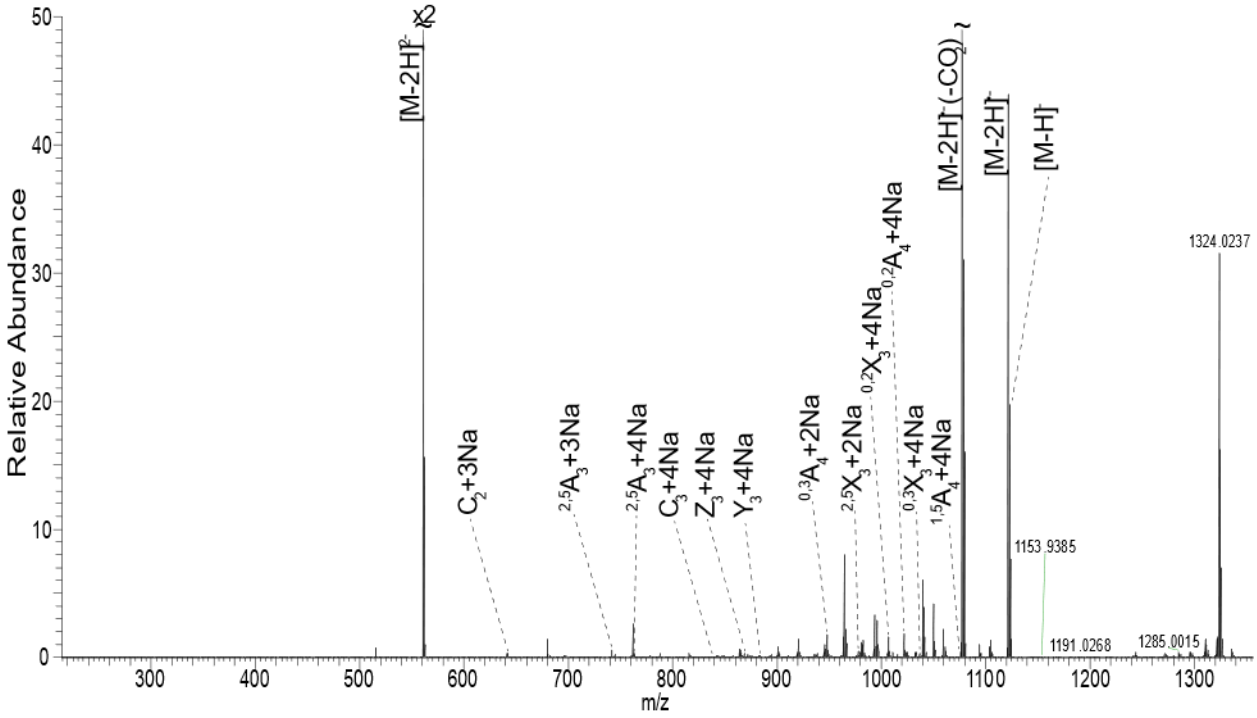

S5.3. Annotated NETD spectrum of HS tetrasaccharide with 4S and 4 Na adduction (6/6 sites ionized), m/z 560.97^{2-}, from Figure 3C.

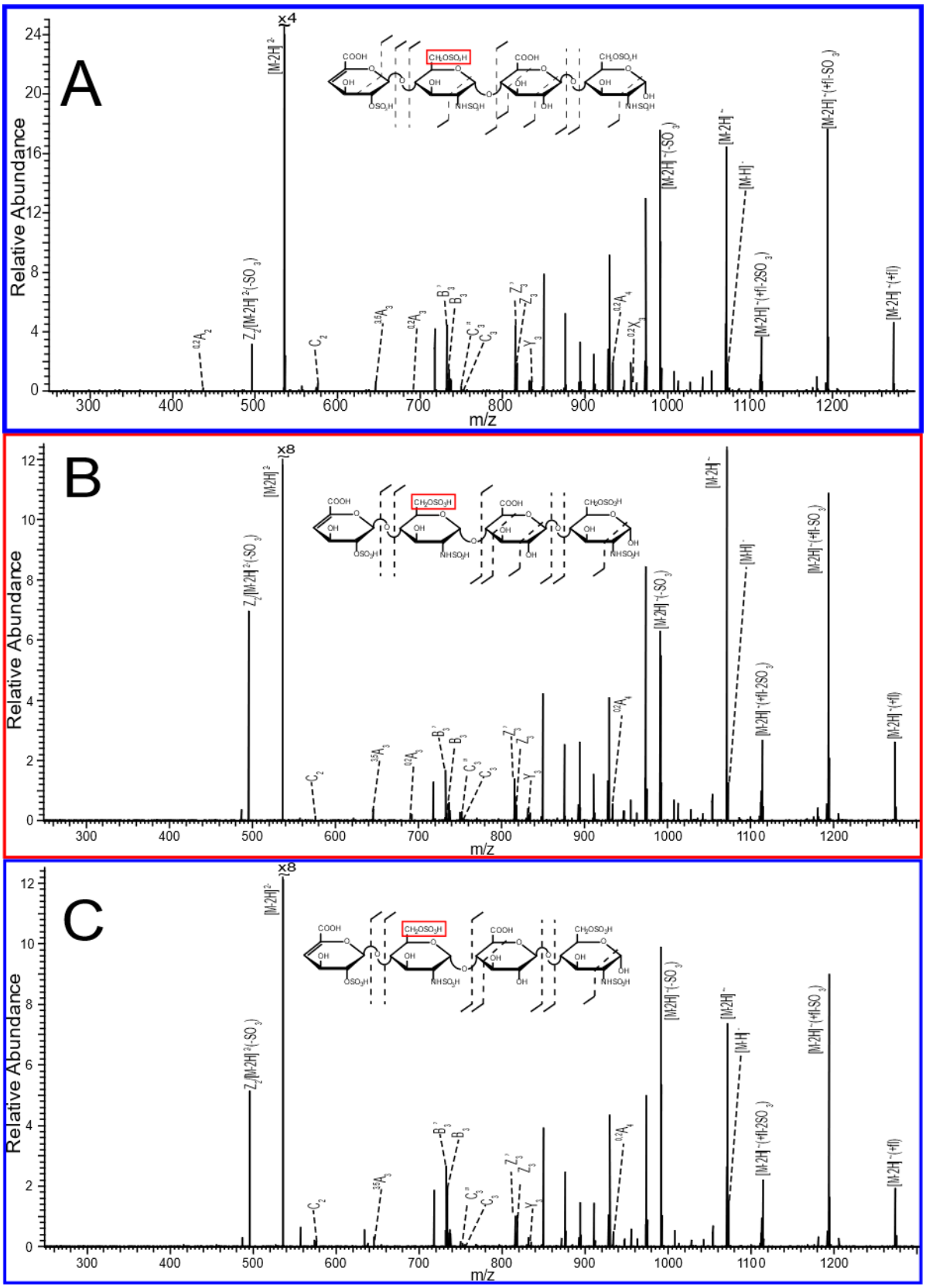
A
B
C
Relative Abundance
m/z
x4
x8
x8
[M-2H]2-
[M-H]-
[M-2H]-(+H)
[M-2H]-(+H-SO3)
[M-2H]-(+H-2SO3)
[M-2H]-(-SO3)
[M-2H]2-(-SO3)
CH2OSO3H
COOH
NHSO3H
OSO3H

S5.4. Annotated NETD spectra of m/z 535.98^{2-} in Figure 6 and assigned structures for (A) peak 1 (23.35min), (B) peak 2 (23.84 min), and (C) peak 3 (24.13 min).

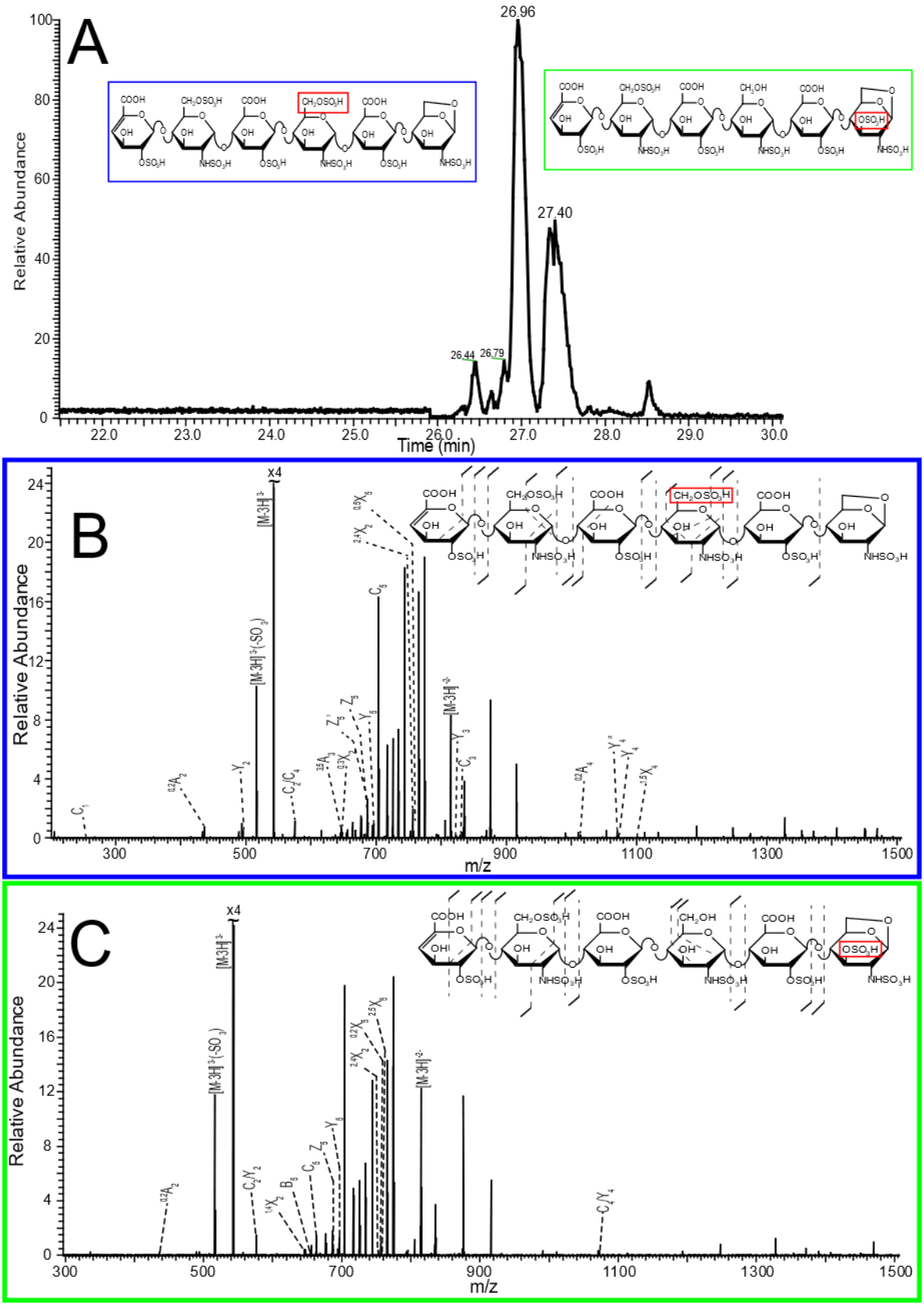
A
26.96
27.40
26.44
26.79
Relative Abundance
Time (min)
B
x4
[M-3H]-3
[M-3H]-3(-SO3)
[M-3H]-2
m/z
Relative Abundance
C
x4
[M-3H]-3
[M-3H]-3(-SO3)
[M-3H]-2
m/z
Relative Abundance

S5.5. A) Isolated electropherogram of m/z 543.31^{3-} in Enoxaparin, shown in Figure 5. Annotated NETD spectra and structures of m/z 543.31^{3-} for (B) the left peak (26.96 min), and for (C) the right peak (27.40 min).

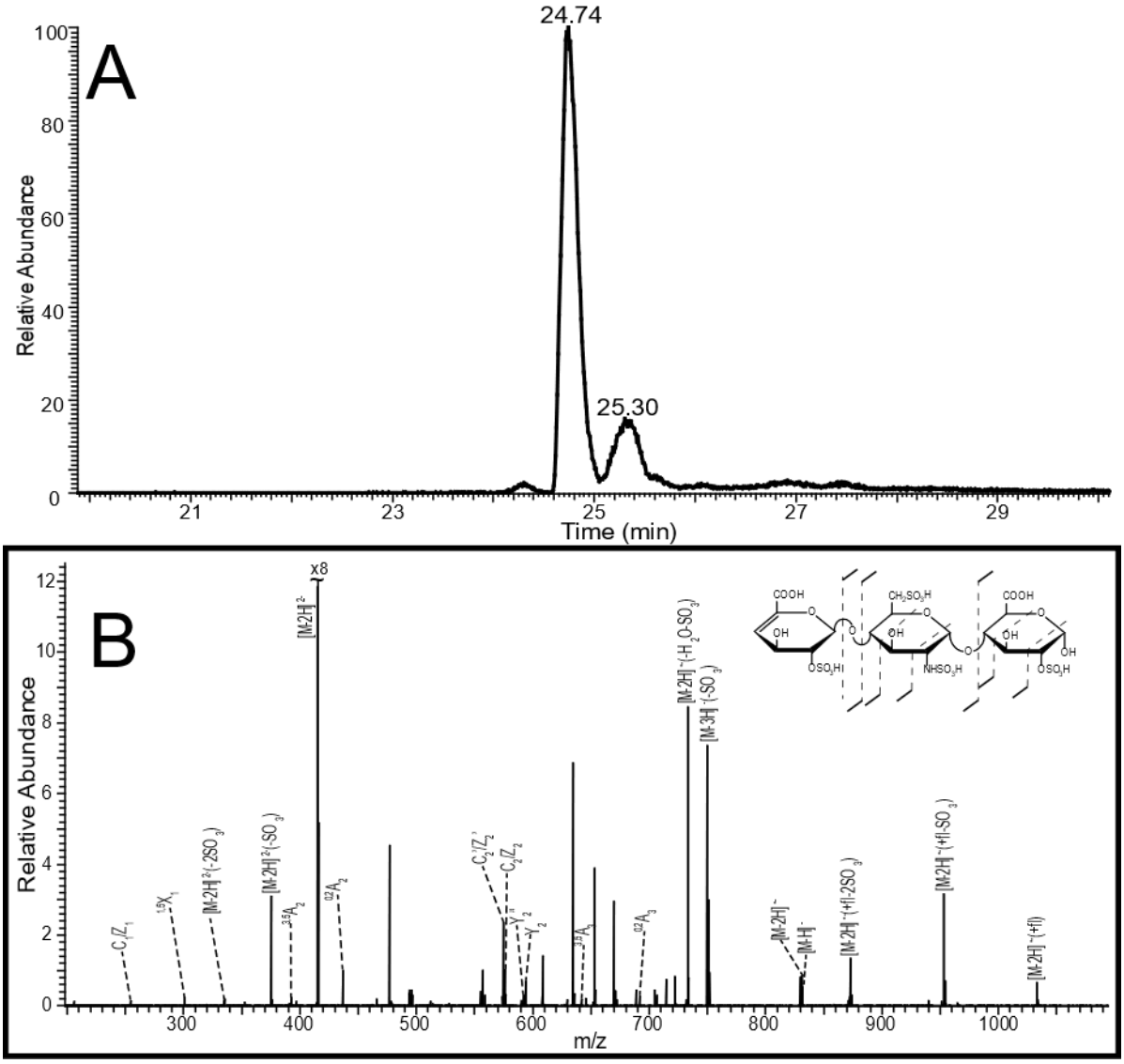

S5.6. Annotated NETD spectrum and structure for m/z 415.47^{2-} in Enoxaparin, shown in Figure 5 at 25.3 min.

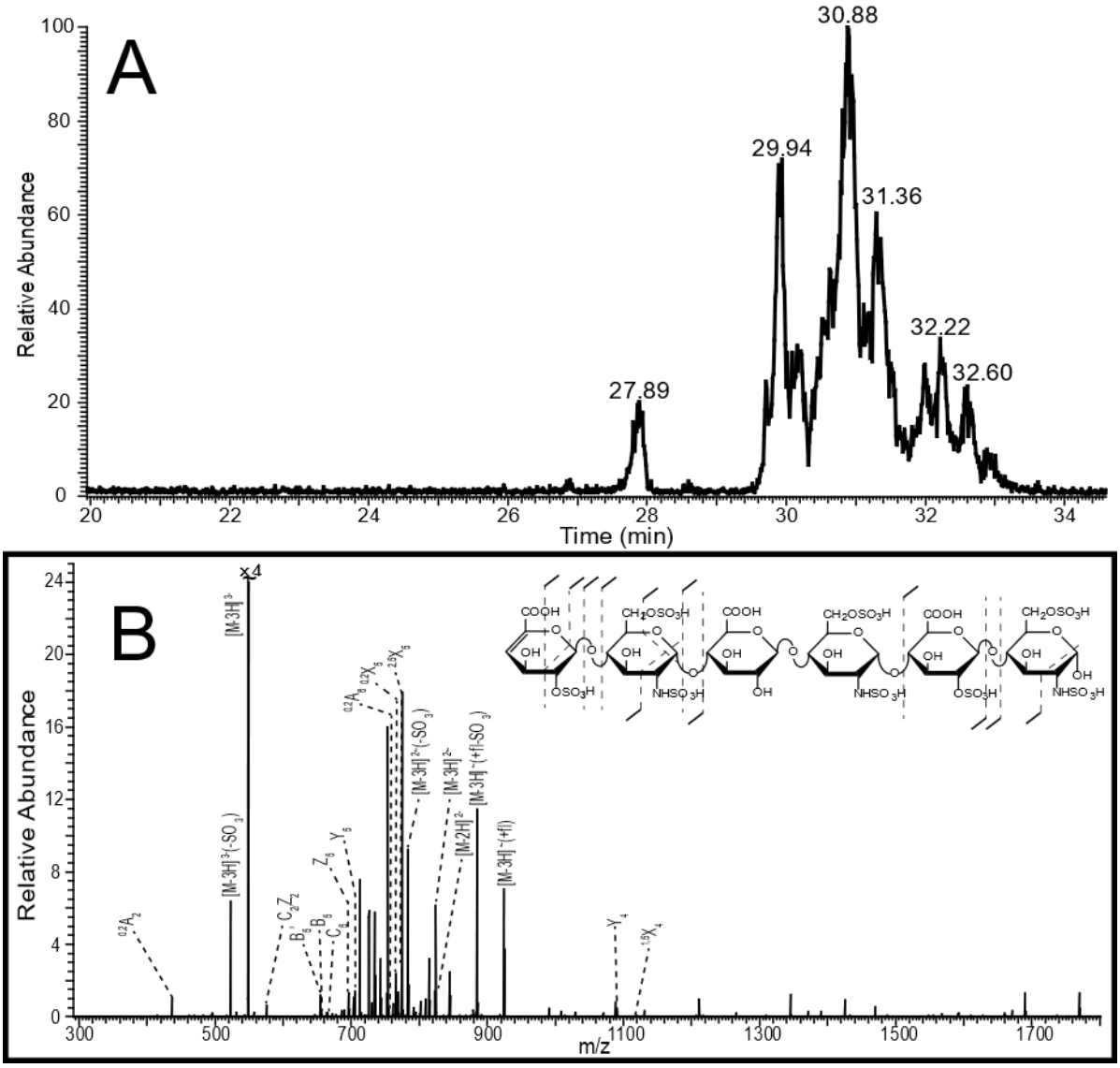

S5.7. A) Selected ion electropherogram of m/z 549.31^{2-} in Enoxaparin. B) Annotated NETD spectrum and structure for m/z 549.31 component at 30.88 min.

CHAPTER 6

CONCLUSION AND FUTURE DIRECTIONS

6.1. CONCLUDING REMARKS

Complex biological mixtures of glycosaminoglycans can be separated and characterized with a simple CZE-MS/MS platform. CZE is ideal for separating highly anionic GAGs based on their charge and size. A basic coating of the inner surface of the separation capillary is highly beneficial to sample throughput. No coating is necessary for the emitter of the interface where electrospray forces are dominant. NETD is an adequate fragmentation method for the low charge state precursors and the relatively narrow migration times generated by CZE-MS. NETD provides enough glycosidic and cross-ring fragmentation to narrow down sulfo-modification sites to specific sugar rings, and under the right conditions, specific carbons within the ring.

6.2. FUTURE DIRECTIONS

The ultimate goal is to make a platform that is relatively cheap and easy to use so that GAG analysis can become more accessible and thus commonplace. The CZE-MS/MS platform is currently reliant on NETD technology that is proprietary on the orbitrap mass spectrometer. Work will need to be done by our collaborators to ensure that NETD becomes a stable and normal component on orbitraps. Alternatively, the manufacturer of the CZE-MS interface is currently working on an interface for connecting CZE to Bruker's Solarix FTICR which already

has NETD capabilities. Furthermore, it would be interesting to see how much more effective the CZE-MS/MS platform can be with the high sensitivity and resolving power of an FTICR system.

As good an ion activation technique as NETD is there is always room for improvement; ultra-violet photon dissociation (UVPD) has shown great promise for GAG fragmentation in initial trials and may be even better suited for the low charge state precursors and short fragmentation windows presented by CZE separation.

So far CZE-MS/MS of GAG chains up to hexasaccharide length has been demonstrated, but that is the bare minimum chain length for binding motifs. Experimentation on CZE-MS of longer chains has already begun, and separation results thus far are promising, but CZE-MS/MS analysis of longer chain lengths must be shown to prove that this system can identify biologically relevant GAGs.

Protein pulldown experiments must be performed. The effectiveness and ease of CZE-MS/MS analysis to identify binding motifs must be established on protein-GAG interactions that are already well understood. Identification of GAG binding motifs for proteins can really take off once that groundwork has been laid.

Establish simple and reproducible methods for CZE-MS/MS analysis of GAGs. Integrate automated data interpretation for quick and easy structural characterization of GAGs after CZE-MS/MS analysis. These two things will lower the barrier of entry to GAG analysis and make it a more common experiment for biological inquiry.

APPENDIX A:

TUNING FRONT END OPTICS OF ORBITRAP MASS SPECTROMETERS FOR ANALYSIS OF GLYCOSAMINOGLYCANS

GAGs are generally more fragile than proteins and peptides due to the sulfo-modifications. Some special considerations should be taken when analyzing GAGs on mass spectrometers, like the orbitrap, which are designed for streamlined peptide analysis. A few simple adjustments to the front-end optics of the orbitrap can make it much more accommodating to GAG analysis.

The suite of optics on the front-end of the orbitrap, (MP00, Lens 0, MP0, Lens 1, MP1, and the front lens) are essential for creating soft introduction conditions for GAGs. These optics are used to create a potential gradient for ions to roll down into the analyzer. For GAGs the hill should be even gentler than for proteins/peptides, especially MP00 and Lens 0, to avoid drastic loss of ion intensity. It is important to tune the optics settings on fragile GAG samples like sucrose octasulfate (SOS) or de-salted Arixtra after calibration of the instrument.

The most important front-end optic on orbitraps for GAGs is the S-Lens. The S-Lens is a series of RF controlled focusing lenses immediately following the inlet capillary of the instrument. The intensity of the RF voltages applied to the S-Lens plates is controlled by a percentage input. The S-Lens is designed to run at around 50-75% intensity, which is optimal for proteomics but far too harsh for GAGs and such high intensity causes sulfate loss peaks to

appear for GAG samples. Most likely, rapidly forcing injected ions into a narrow volume causes sulfate loss peaks which are generated by a process similar to threshold activation.

Sulfate loss peaks can complicate already complex spectra of biological mixtures and cause lower intensity peaks to be lost due to space charge effects. For MS1 of GAGs it is beneficial to set the S-Lens intensity to ~20% as this prevents most sulfate loss without loss of intensity from fully intact peaks. Initial MS1 experiments are useful for identifying real peaks from the sample that can be investigated further with tandem MS (MS2).

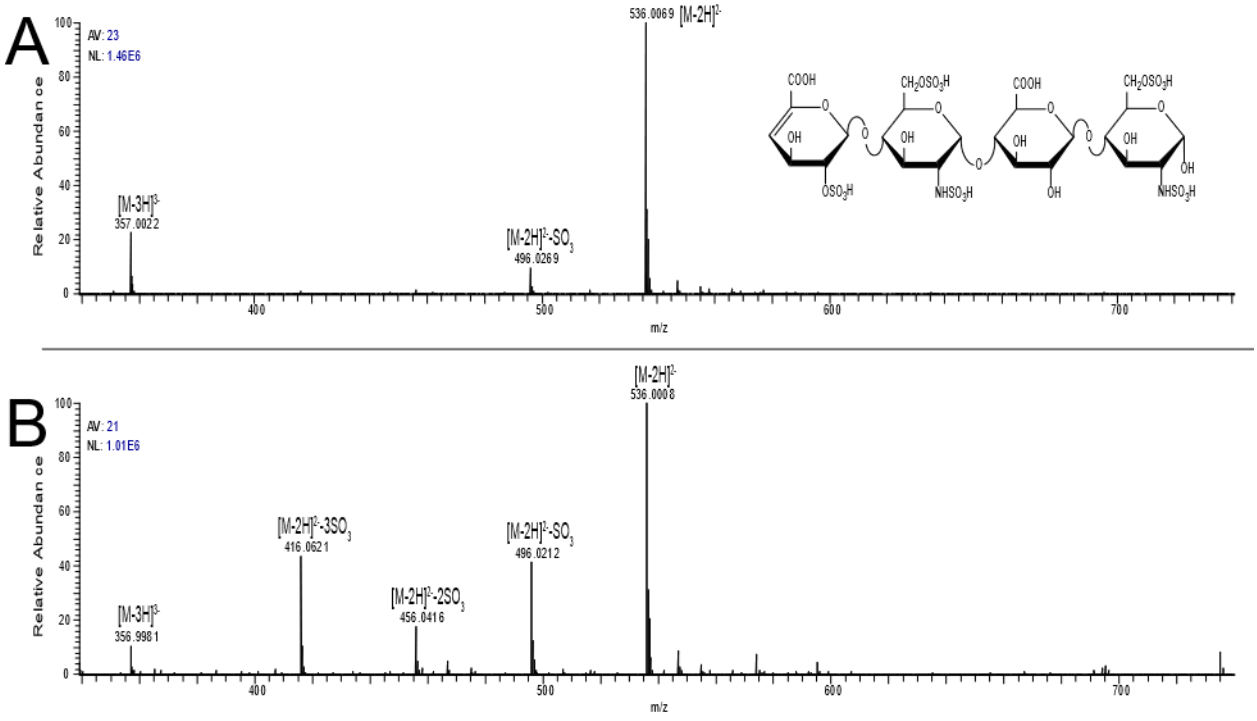

Figure A1. A) Mass spectrum of a standard tetrasaccharide analyzed by an orbitrap with the S-Lens set to 20%. B) Mass spectrum of a standard tetrasaccharide analyzed by an orbitrap with the S-Lens set to 55%. Sulfate loss peaks are much more abundant when the S-Lens is 55%.

For MS2 higher S-Lens intensities, in the 55% range, will stabilize the selected precursor and focus the ion beam/packet in the analyzer cell making fragmentation methods more effective. A low S-Lens intensity, 20%, will produce NETD fragmentation of an abundant precursor with low intensity informative fragments that are lost in the noise. A higher S-Lens intensity, 55%, will produce NETD fragmentation from an abundant precursor where the low intensity informative fragments are well above the noise. Increasing the S-Lens intensity drastically increases the signal-to-noise of the spectra which is hugely beneficial for fragmentation techniques like NETD that produce mainly low intensity informative fragments.

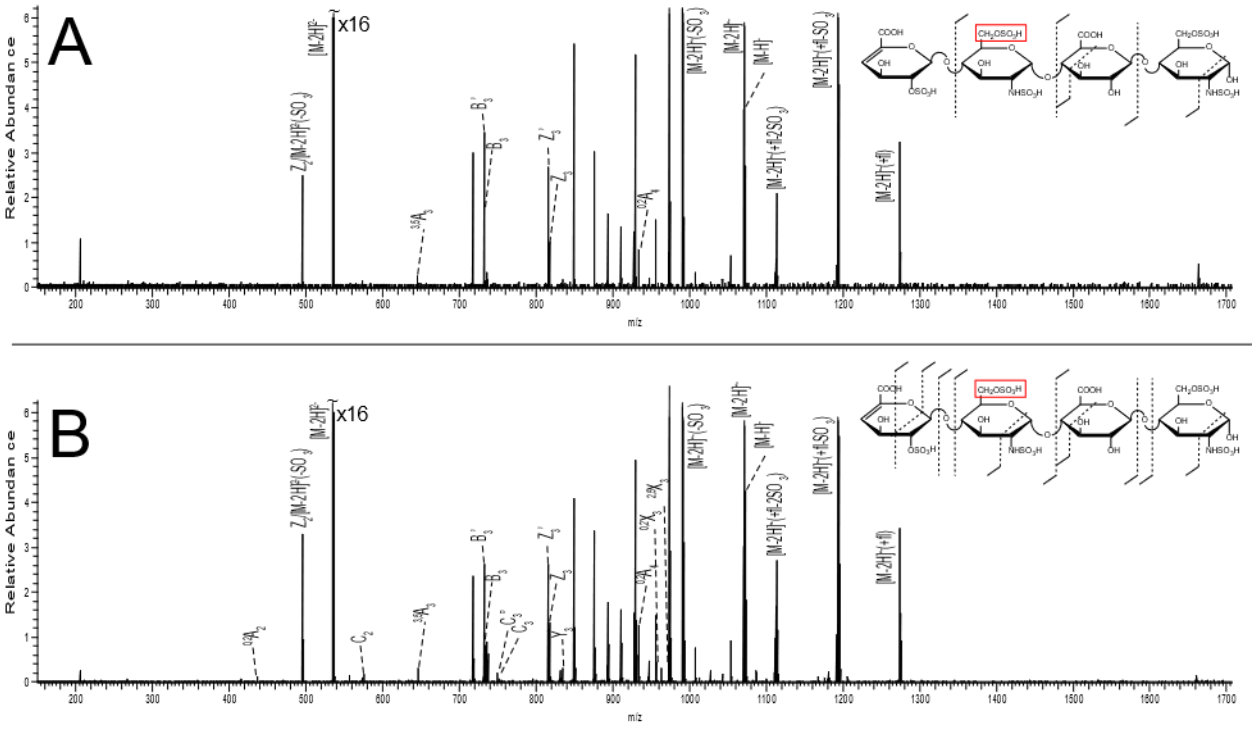

Figure A2. A) NETD fragmentation mass spectrum of a tetrassacharide standard on an orbitrap with S-Lens set to 20%. B) NETD fragmentation mass spectrum of a tetrassacharide standard on

an orbitrap with S-Lens set to 55%. Informative low intensity fragments emerge from the noise with higher S-Lens values.

An important flaw in running the orbitrap at 55% S-Lens is that the creation of intense sulfate loss peaks can be misidentified as real natural species. Experimentation so far would suggest that NETD of sulfate loss peaks resulting from higher S-Lens presents a precursor ion with no isotope peaks. This could help determine if an artificial species was selected as a precursor accidently. Careful precursor selection using an initial MS1 experiment at lower 20% S-Lens intensity can help prevent NETD of false sulfate loss peaks.

A more difficult problem resulting from higher s-lens intensity is when two real species that differ by the mass of one sulfo-modification overlap in the electropherogram. This situation can result in NETD fragmentation that shows a mixture of structures is present.

A two-stage experiment is recommended for fragmentation analysis of GAGs with an orbitrap mass spectrometer. The first stage should be MS1 run at low S-Lens intensities to identify real precursors, and the second stage should be a MS2 run at high S-Lens intensities to improve signal to noise for fragment ion peaks.